Identification of Size and Location of a Single Crack in Marine Propeller Shaft Using Strain and Displacement

by

©Ridwan Hossain

A thesis submitted to the School of Graduate Studies in partial fulfillment of the requirement for the degree of

Master of Engineering

Faculty of Engineering and Applied Science

Memorial University of Newfoundland

May, 2014

St. John's Newfoundland

Abstract

The presence of cracks in any type of structure is undesirable as they often lead to fracture or failure of the structure. Marine propeller shaft is a key component in marine propulsion systems; moreover due to the strenuous working conditions, to which it is subjected during its marine operation, it is prone to develop crack(s). The presently available crack detection methods, either require disassembly of the shaft substructure for visual inspection or require external excitation of the relevant portion of the shaft for subsequent dynamic analyses; consequently these methods are quite complex and time consuming.

In this study a simpler crack detection method is proposed for crack detection in rotating marine propeller shafts. The crack detection method is based on simple strain and displacement measurements at identified locations and hence easy to execute. The study was carried out using Finite Element Analysis through ABAQUS, a well-known commercial finite element package. The analysis was carried out both for the existence of single bending crack and single circumferential crack, on the body of the rotating shaft component, and the proposed method was able to identify both types of cracks at quite early stages of their growth and development. It was found that if measured at the proper locations, the percentage changes and slopes of percentage changes for these parameters (strain and displacement) changed more rapidly than frequencies, due to the presence of a

crack. Only two measurements were required to get such identification which could be directly related to crack location and size. Based on the computed and analyzed numerical results, a simple but effective crack detection method has been proposed which would eliminate the complexities present in the currently available crack detection methods for such structures.

Acknowledgement

First, I would like to express my profound gratitude to my supervisor Dr. Swamidas for his outstanding support and guidance throughout this work. I would also like to thank my co-supervisor Dr. Seshadri who financially supported this research and gave his valuable comments regarding this work.

I would like to specially thank my wife for her constant encouragement and also my parents for their enormous support throughout my whole career. Without their support it would be almost impossible for me to come this far. Finally, I would like to thank all my friends in St. John's who made this place home to me.

Table of Contents

List of Tables

List of Figures

List of Notation and Abbreviation

s	Tensile Fracture Strength of the Material
E	Young's Modulus of Elasticity
a	Crack Length
G	Strain Energy Release Rate
G_c	Critical Fracture Toughness Criterion
d_p	Size of Plastic Zone
S_y	Yield Strength
K	Stress Intensity Factor
N	Number of Cycles
C,m	Material Constant
γ	surface energy
NDT	Non-Destructive Technique
SHM	Structural Health Monitoring
LEFM	Linear Elastic Fracture Mechanics
CTOD	Crack Tip Opening Displacement
PSB	Persistent Slip Band
FEM	Finite Element Method
FRF	Frequency Response Function
MAC	Modal Assurance Criterion
COMAC	Co-ordinate Modal Assurance Criterion
LDV	Laser Doppler Vibrometer
CDF	Curvature Damage Factor
SEM	Scanning Electron Microscope
SCC	Stress Corrosion Cracking

TPS	Thermal Protection System
DDA	Damage Detection Algorithm
ANN	Artificial Neural Network
CMAES	Covariance Matrix Adaptation Evolutionary Strategy
IGA	Improved Genetic Algorithm
CAD	Computer Aided Design
TLS	Terrestrial Laser Scanner
GUI	Graphical User Interface

Chapter 1

Introduction

Travelling through the ocean to experience the unseen has always been of great interest to curious human nature. But such experience often came with great price as numerous incidents of ship sinking can be found throughout the history of human civilization. Therefore, human civilization has always tried to develop the safest marine vehicle possible which requires the assurance of safety for each and every component of the ship. Propeller shaft is a key element in marine propelling systems and is one of the few components of the ship structure, working under the most strenuous loading conditions, caused by the start-up/shutting-down, encounter of propellers with floating/submerged debri or broken ice and the speed-and-course maintenance during an unexpected stormy ocean scenario. Failure of the propeller shaft would lead to a stoppage of the vessel motion, leading to exorbitant operation costs, and perhaps to loss of vessel/human lives; therefore safety of the propeller shaft operation requires continuous supervision and maintenance. Fractures and failures are often originated by cracks that initiate and propagate during the continuous cyclical bending and rotational loading exerted on the propeller shaft; hence the development of an effective early crack detection method for propeller shaft is a must for the safe operation marine vehicles.

1.1 General Overview & Motivation

Marine propeller shaft is a key component of the marine propulsion system. The main purpose of propeller shaft is to transfer the engine torque to the propeller and the consequent axial forces to the thrust bearing. Figure 1.1 represents a typical marine propulsion system showing the propeller shaft.

Figure 1.1: Marine Propulsion System

Due to the rotating bending nature and continuous transfer of dynamic loads, the shaft is always at great risk of failure due to crack growth and propagation. Also tribological wear, caused by the continuous abrasion of the shaft on the sealing components, presents an ever present danger to initiate cracking. Moreover, the presence of small cracks might not lead to imminent fracture or failure of the shaft, but it will affect the overall dynamic behavior and the performance of propulsion system. Hence early crack detection in marine propeller shaft is very important for ship performance and safety. Most

conventional NDT's such as visual inspection or eddy-current method requires disassembly of the whole system which is cumbersome. Dynamic analysis such as vibration or frequency measurement provides large amount of data which is difficult to interpret sometimes. Hence, a simpler and easy-to-execute crack detection method is required for early identification of cracks in such shafts.

Crack detection considering static parameters such as strain, displacement and bending moments are much simpler to use but has not received much attention so far. A few research studies have been carried out based on theoretical modeling but no one has proposed a complete crack identification method which could be further extended to practice (see section 2.3.2 for details). An effective crack detection method based on such simple strain and displacement measurements would reduce the complexity and time spent during periodical maintenance operations and hence it becomes essential and necessary to seek for one. The study presented in this thesis is one such effort.

1.2 Objective

The main goal of this study is to propose an effective crack identification method for overhanging propeller shafts based on strain and displacement measurements. Such crack identification method in practice would facilitate the technicians to identify cracks in different types of overhanging shafts more conveniently. The initial goal is to model the propeller shaft properly for finite element analysis; this exact numerical modeling would be required to identify the possibility of cracking under its own weight.

The next objective is to identify the optimum locations both for strain and displacement measurements, where significant variations would occur due to the presence of the crack for most of the possible crack locations. For both bending and circumferential cracks these locations would be kept unchanged to differentiate between these two. The identification of optimum locations would reduce the number of sensors required for identifying the cracks or damages under actual load scenarios.

The final objective is to use the measurement to calculate the percentage difference and slope of percentage difference for both strain and displacement and propose a crack detection method which would be able to identify both crack location and size along the whole beam. From a theoretical viewpoint, since crack location and size are the two parameters to be identified, at least two sensors would be required and the measured data will be used to identify the crack location and size.

1.3 Novelty and Contribution

The novelty and contribution of this thesis can be summarized as follows:

- The study has shown that the use of two sensors is sufficient to locate the position of a single crack present in a rotating shaft, and as well to determine the size of the crack.

- The study found out that in overhanging shafts having a load (propeller weight) at the end, strain and displacement show higher percentage change than frequency due to the presence of crack.
- The study found out that near the point of contra-flexure strains show higher percentage change, whereas displacement is more sensitive at the free end.
- It was found that slope of percentage change is much higher than the percentage change for both strain and displacement and can be used as an effective crack detection tool.
- The study has also shown that it is possible to have cracking in marine propeller shaft under the weight of its propeller.
- Based on the findings, a crack detection method is proposed which has successfully identified both bending and circumferential helical cracks in such shafts.

1.3 Thesis Outline

The thesis is written in manuscript format. The outline of the thesis is given below:

Chapter 1: A brief introduction to marine propeller shaft and crack detection along with the motivation and objective of the research is discussed.

Chapter 2: An extensive literature review of the mechanics of cracking and crack detection methods were presented

Chapter 3 introduces the procedure used for strain and displacement for crack detection, using the finite element method. Thereafter it develops the method used for the identification of optimum locations for measurement of strain and displacement. This chapter has been presented in *International Workshop on Smart Materials, Structures and SHM in Conjunction with NDT in Canada 2013 Conference and NDT for the Energy Industry, Calgary, Alberta, CANADA, 2013.*

Chapter 4 discusses about the possibility of cracking in marine propeller shafts due to the weight of the propeller and also uses the method described in chapter 3 to identify a single bending crack in such systems. This chapter has been accepted for publication in *International Journal of Engineering, Science and Management* for publication.

Chapter 5 discusses a possibility of circumferential helical crack development in marine propeller shafts along with the limitation of current dynamic methods to identify such cracks and proposes a complete identification method for crack location and size. A version of this chapter has been prepared for submission in *International Journal of Engineering, Science and Management.*

Chapter 6 concludes the thesis with a summary, findings, conclusions and relevant areas for further extension of this study.

Chapter 2

Literature Review

2.1 Introduction

As most fractures are initiated by cracks, early detection of crack can often minimize the risk of sudden collapse. Hence researchers have sought for an effective early crack detection method for decades. Although not much work has been done for crack detection considering marine propeller shafts yet it poses the same risks to floating ship and other marine structures as for other cracked structures and shafts. The overhanging nature of the shaft having a static load (propeller) at the end makes it prone mainly to surface cracks; also any delay in crack detection may cause sudden collapse since large cracks have been observed only at the very late stage of its total life. To develop an effective crack detection method the mechanism of cracking including crack initiation and propagation must be understood. Therefore, in this chapter, the mechanism of cracking and some of the popular and often-used crack detection methods have been discussed. In the first section, the basic mechanism of cracking including types of cracks, linear elastic fracture mechanics, elasto-plastic fracture mechanics is discussed. It is followed by a brief discussion of crack initiation and propagation. The second section discusses some of the recently developed crack detection methods including frequency change and mode

shapes. Although not much work can be found related to the use of static response as a tool of crack detection, some of the related articles have also been reviewed.

2.2 Mechanics of Cracking

Cracking might be referred to as the separation of two adjacent surfaces under the application of load. Depending on the types of applied load crack can be mainly classified in three categories:

Mode I Cracking or Opening: Mode I cracking or opening is caused by the application of tensile stresses normal to the plane of crack, as shown in Figure 2.1 (a).

Mode II Cracking or Sliding: Mode II cracking or sliding is caused by the application of shear stress acting parallel to the plane of crack and perpendicular to crack front [see Figure 2.1 (b)].

Mode III Cracking or Tearing: Mode III cracking or tearing occurs when a shear stress is acting parallel to the plane of crack and parallel to the crack front [see Figure 2.1 (c)].

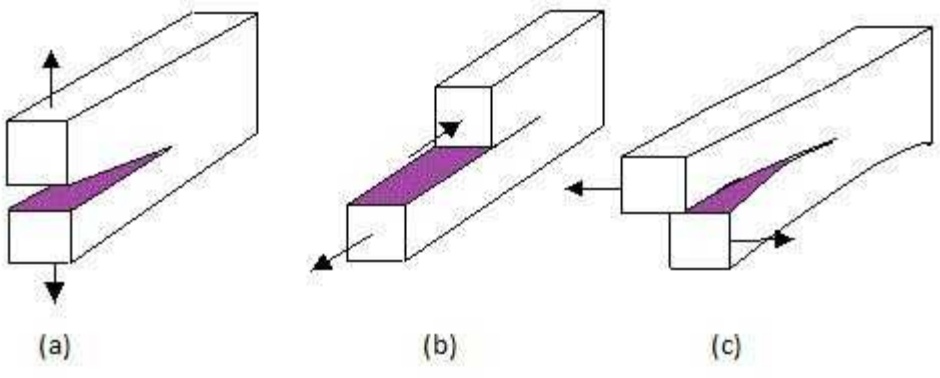

Figure 2.1: Different types of Crack modes; (a) Mode I or Opening; (b) Mode II or Sliding; (c) Mode III or Tearing

2.2.1 Early Works on Crack Mechanism

The very first work related to crack development and fracture was probably done by Inglis [1]. He researched on the stress in a plate due to the presence of the crack. He considered a plate with an elliptical hole under stress and tried to find out the stress concentration around the hole. Later, he proposed how it might be used to calculate fracture strength. However, his proposed solution posed a mathematical difficulty since for a sharp crack, the stress approaches infinity at the crack tip. This was not very practical as it suggested that even for a small applied load the stress at crack tip would become infinite and the material bond will rupture. Weighardt [2] had earlier refused this possibility by finding out a paradox that the stresses at crack tip of a sharp crack at elastic body is infinite no matter how small the loads are. Therefore, he proposed that rupture

does not occur when the stress at a point exceeds some critical value but only when the average stress over a small region exceeds the critical value.

Griffith [3, 4] was the first one to come up with a valid postulate which laid the basis of modern fracture mechanics. Rather than focusing on the crack tip stresses directly, Griffith considered an energy-balance approach which eventually became one of the famous contributions in material science. He proposed that, a certain amount of energy was required to produce a fracture which was later known as free surface energy for pure elastic material. Due to the fact that this type of system is conservative, he concluded that fracture problem is just an extension of the elastic theory of minimum potential energy considering the potential surface energy and other potential energies as well. He assumed that under tensile loading crack extension and fracture would occur when the loss of stress field energy per crack increment becomes greater than the gain of surface energy. The relationship was expressed as:

$$s = \sqrt{\frac{2E\gamma}{\pi a}} \qquad (2.1)$$

where, γ = surface energy, s = tensile fracture strength of the material, E = Young's modulus of elasticity and a = crack length. However, in his later studies, Griffith himself noted that this equation is only valid for glass and other types of brittle materials.

2.2.2 Development of Linear Elastic Fracture Mechanics (LEFM)

Until 1940, Griffith's work [3, 4] did not get much attention as his theory was applicable to only glass and other highly brittle materials which had little to do with the engineering application. It was the work of Orowan [5] which led the Griffith's theory applicable to less brittle materials. Using X-ray scattering, Orowan [5] studied the depth of plastic strain below cleavage facets in low carbon steel. Based on his work, Irwin [6] noted that the fracture energy in low carbon steel at 0^0C is 2000 times higher than the surface energy. Therefore, Griffith's theory could be applicable to ductile materials if the surface energy is replaced by the work causing plastic strains around the crack tip. He defined this as strain energy release rate, G, and showed that it could be determined using the stress and displacement field around the crack tip. Although his initial development of LEFM was based on energy, later Growan [7] established a critical fracture toughness criterion (G_c), specifying that fracture occurs when G equals to G_c.

2.2.3 Development of Elasto-plastic fracture mechanics

As the LEFM predicts infinite stress at the crack tip, so there must be a zone where the elastic solution breaks down. Irwin [8] proposed the size of the plastic zone d_p, at a crack tip, for a material of yield strength S_Y to be:

$$d_p = \frac{1}{2\pi}\left(\frac{K}{S_Y}\right)^2 \qquad (2.2)$$

When d_p is smaller, compared to the object dimension which causes the stress intensity K-field to dominate outside the plastic zone, LEFM can be applied to model the crack tip deformation. He also suggested that the plastic-zone size under plane strain condition can be obtained if the tensile stress for plastic yielding caused by plane-strain elastic constraint is considered. Under these conditions, the yield strength is estimated to increase by a factor of $\sqrt{3}$ and hence the size of the plastic zone becomes:

$$d_p = \frac{1}{6\pi}\left(\frac{K}{S_Y}\right)^2 \tag{2.3}$$

The advantage of LEFM is that it only depends upon the state of stress and not its history. But plastic deformation is path dependent and therefore it is not possible to have a simple one parameter model.

In 1961, Wells [9] proposed that fracture behavior, in the vicinity of the crack tip, can model opening of the notch faces as crack opening displacement (COD), later known as crack tip opening displacement (CTOD). He used the slip line theory and the rotation of arms to obtain CTOD of a deep notch bending specimen for complete yielding. Dugdale [10] proposed a strip yield model analysis and showed that it is possible to relate the CTOD to the applied stress and crack length. Based on his analysis a more exact expression for CTOD was obtained by Burdekin and Stone [11] and expressed as:

$$\delta = 8\,\frac{\sigma_{ys}a}{\pi E}\ln sec\left(\frac{\pi}{2}\,\frac{\sigma}{\sigma_{ys}}\right) \tag{2.4}$$

where, σ_{ys} = yield strength of the material, ksi

a = half of the real crack length, in.

s = nominal stress, ksi

2.2.4 Fatigue Crack Initiation

The fatigue life of a structure may be considered to be composed of three stages: (1) fatigue crack initiation; (2) fatigue crack propagation and (3) fracture. The final fracture stage represents the terminal condition and is not considered in this work; hence we will be focusing on the first two stages only. The contribution of these two stages to the fatigue life depends upon the intended application. For example, components containing stress concentration or initial defects may be determined primarily by the characteristics of fatigue crack propagation. On the other hand, the fatigue life of structural components intended for infinite-life application, i.e., crack propagation under decreasing stress field may be governed by fatigue crack initiation or propagation or by both. The main principle to design structural components subjected to fluctuating loads is based on a design fatigue curve which represents the basic un-notched fatigue properties as well as the fatigue-strength-reduction factor. The design fatigue curves are based on the prediction of cyclic life from data on nominal stress (or strain) versus elapsed cycles to failure, also known as S-N curves.

In metals, the plastic deformation is caused at the dislocation level (atomic scale) which is accomplished via slip of the lattice. As slip accumulates during the cyclic loading, plastic deformation causes strain localization leading to crack initiation. The slips, introduced during the forward loading cycle, are not fully recovered in the reverse loading causing slip irreversibility. The main reasons behind this are developments in material science including arrangement of edges in low energy level, point defects, difference in dislocation back stresses etc. After a large number of cycles, dislocations pile up and form structures named persistent slip bands (PSB). These PSBs either rise up or fall below the original level surface due to the movement of grains of the material. These up and down movements leave tiny steps in the surface where stress concentrations occur. This localized stress concentrations may cause the localized region of the component, in that neighborhood, to undergo plastic deformation. As the nominal stresses in most structures are elastic, the plastic zone in the vicinity of stress concentration is surrounded by an elastic-stress field. The deformations of the plastic zone are therefore governed by the elastic displacement of the surrounding elastic-stress field causing a micro-crack to become a visible one.

2.2.5 Fatigue Crack Propagation

Figure 2.2 shows a schematic log-log plot of da/dN vs. ΔK which illustrates typical fatigue growth behavior in most metals; ΔK is the stress intensity range. The curve contains three distinct regions. At the lower end, i.e. region I is the threshold region

where the crack does not grow. The crack starts to propagate when ΔK value exceeds the threshold limit, which is represented as the region II, and the curve is linear in that region. The relationship of this region can be described by the following power law:

$$\frac{da}{dN} = C\Delta K^m \tag{2.5}$$

in which C and m are material constants. This is also known as Paris' Law.

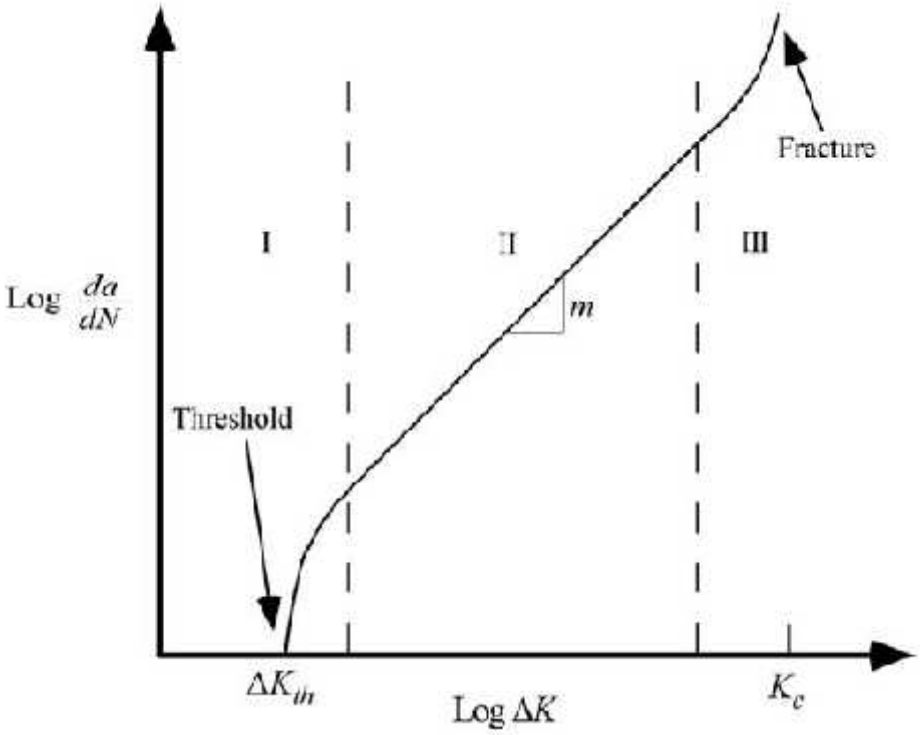

Figure 2.2: Typical Fatigue Growth Behavior in Metal

Paris and Erdogan [12] were probably the first ones to propose this relationship. According to their experimental data, they proposed the value of the exponent m as 4.

However, later studies showed that m can range from 2 to 4. A number of researchers had tried to develop an equation to model for all or part of the *da/dN* vs. Δ*K* relationship, most of which were empirical. Forman [13] proposed that the following equation can be used in both region II and III:

$$\frac{da}{dN} = \frac{C\Delta K^m}{(1-R)K_c - \Delta K} \tag{2.6}$$

where $R = \frac{\sigma_{min}}{\sigma_{max}}$; K_c = fracture toughness

The equation can also be re-written as:

$$\frac{da}{dN} = \frac{C\Delta K^{m-1}}{\frac{K_c}{K_{max}} - 1} \tag{2.7}$$

This equation is based on the assumption that region III behavior is influenced by fracture and fatigue rather than plastic zone effect. Thus crack growth rate becomes infinite when K_{max} approaches to K_c. Also this equation does not have the same material constants as proposed by Paris and Erdogan [12].

Klesnil and Lucas [14] modified the equation (2.5) for the threshold as follows:

$$\frac{da}{dN} = C(\Delta K^m - \Delta K_{th}^m) \tag{2.8}$$

Donahue [15] suggested a similar type of equation with the exponent m applied to the bracketed terms, $(\Delta K - \Delta K_{th})$. One problem with this equation is ΔK_{th} depends on the *R* ratio.

The most common expression that describes the relationship in all three regions was developed by the scientists at NASA and was first published by Forman and Mettu [16] and the simplified form is as follows:

$$\frac{da}{dN} = C(\Delta K)^m \frac{\left(1-\frac{\Delta K_{th}}{\Delta K}\right)^p}{\left(1-\frac{K_{max}}{K_C}\right)^q} \tag{2.9}$$

where *C, m, p* and *q* are material constants. At intermediate ΔK values where $\Delta K >> \Delta K_{th}$ and $K_{max} << K_c$ this equation reduces to the equation (2.5) therefore the material constants are equivalent. Dowling and Begley [17] applied the *J* integral to fatigue crack growth under large scale yielding for which *K* is no longer valid. The equation they developed was in terms of ΔJ but followed the same power law expression:

$$\frac{da}{dN} = C(\Delta J)^m \tag{2.10}$$

However, in later studies it was found that *J* integral has lots of theoretical in-justifications and limitations for modelling fatigue crack growth.

2.3 Types of Crack Detection

Hundreds of papers have been published considering crack/damage detection in a number of engineering disciplines. Current crack detection methods include visual inspection, eddy-current method, ultrasonic method, radiography etc. However, all of these methods are effective if the crack location is priory known or it has been localized (discussed in the literature review). Therefore, researchers have sought for an alternative solution, wherein crack location and size can be determined simultaneously, and modal testing and analyses have been given the highest attention in this regard. So far, a number of studies have been done for early crack detection which have been applied for shafts in various sectors. Most of these crack detection methods are based on the dynamic behavior of the structure and therefore researchers have been working on the dynamics of the cracked structure for decades [18-20]. In this section, a brief review has been presented regarding modal testing due to their extensive use in cracked shaft systems. Some of the other analogous crack detection methods using static measurements have also been reviewed here although the number of studies in that area is extremely limited.

2.3.1 Crack Detection Using Modal Testing

The modal testing became popular as the parameters (frequency, mode shapes, modal damping) measured are direct functions of the physical properties (mass, stiffness, damping) of the structure. So, as the presence of cracks causes reduction in stiffness, it

directly affects the modal parameters. Also, due to the technological advancement, it became easier to measure the modal parameters instead of measuring the physical properties directly. Among the different parameters of modal testing, frequency and mode shapes have received the most attentions due to their ease of measurement and this literature review will be focused on those only. The attention given to the modal testing and analyses methodologies is primarily due to the fact that most of the experimental/analytical methods are based on the concepts of measured/analyzed outputs obtained from the given inputs to the system; thus modal procedures have been successively used in vibration, acoustic intensity scanning, Laser Doppler Vibrometer scanning, 3-D vision based measurements and in other areas.

2.3.1.1 Frequency Change

Frequency measurement for damage detection has gained greater attention because of its simplicity in measurement than mode shapes. It was earlier found that the presence of a crack or multiple cracks directly affects the natural frequencies of a structure because the resonant frequencies directly depend on the geometrical and the physical properties of the structure (such as spatial profiles and stiffness) under consideration. Besides, they are less seriously affected by experimental errors. The amount of literatures published on damage detection using natural frequencies is quite large. A brief description of those can be found in the literature reviews of Salawu [21] and Doebling et al [22]. In this study, however, only major contributions will be discussed in this field.

Lifshitz and Rotem [23] were probably the first to discuss about damage detection using vibration measurement. Their method involves vibration testing and continuous measurement of audio frequency, dynamic modulus and damping for specimen under tensile loading. They introduced a term called dynamic modulus which can be related to frequency shift and was sensitive to stress induced structural changes. Three composite specimens were used in their test and the effect of tension induced structural changes on dynamic moduli and damping, were reported.

However, the analytical procedure to use the natural frequencies of a structure as a diagnostic tool for damage detection was started to get attention when Adams et al [24] introduced it for structural integrity. In an earlier work, Adams et al [25] had observed that in fibre-reinforced plastics, a reduction in stiffness and increase in damping occur due to the presence of a damage. This phenomenon occurs both for localized (single crack) and distributed damages (many micro-cracks). Changes in stiffness for both the cases have direct effect on frequency changes and thus frequency measurement can be regarded as an essential parameter for damage detection. Adams et al [24] carried out their experiment for one dimensional bar under axial excitation only. They modeled the damage as a massless axial spring where the stiffness, expressed as a function of receptance (inverse of stiffness), defined the damage severity. An analytical formulation was developed for change in natural frequencies because of the induced damage. A plot superimposing this relationship for two different modes provided the possible damage location. To use this formulation as a generalized condition, they developed a functional

relationship by differentiating the summation of the receptances of the undamaged section on both sides of the crack in two different modes with respect to the corresponding natural frequency. A universally applicable chart was obtained by plotting the ratio of this function against x/ℓ, where 'x' was the location of the damage and 'ℓ' the length of the bar. This method is applicable to all bars if the receptance can be expressed as a function of position 'x'. Adams et al [24] carried out experiments based on this theory on: (i) An Aluminium bar with a saw cut; (ii) An Aluminum beam with different types of damage; (iii) A tapered bar; and (iv) A camshaft. This method provided identifiable results except for the case of severe damages where the presence of non-uniform stress distribution made it impossible to define a single resonant frequency. In these studies, the assumption of a single axial massless spring to represent the effects for all the possible axial frequencies seems to be questionable.

Rizos et al [26] used measurement amplitudes at two different locations in a beam vibrating at one of its natural frequencies and an analytical solution for dynamic response. But this method was only limited to one dimensional beam or bar type structure. Hearn et al [27] performed modal analysis for vibration response of welded steel frames and wire ropes. Natural frequency changes were derived from a perturbation of the equations of motion and by suitably interpreting this frequency change, damage location was identified. The presence of damage was found to influence the natural frequencies and modal damping in a predictable manner. The required modal parameters of the structures were obtained from the free vibration response of the structure.

Friswell et al. [28] tried to identify damage through measurement of small change in natural frequency based on the priory known likely damaged scenarios. He considered a theoretical model of the damaged structure and calculated the frequency shifts of the first several modes for the undamaged structure and the presumed damaged structures. However, the accuracy of the method depended upon the accuracy of the model and in his case it was assumed that the model was highly accurate. By comparing the frequency shift ratios for the model and the candidate structure, a power-law fit was proposed and it was postulated that if the damage is of the same class it would produce a fit that is a line with unity slope. Narkis [29] proposed an analytical solution for computing the natural frequencies of a simply supported beam having a crack, considering both the cases of transverse and axial vibrations. He considered the beam as two separate beams connected together by a bending spring. Combining the earlier work of Shen and Pierre [30] and Haisty and Springer [31], he was able to formulate a relationship between structural flexibility and frequency parameter. For different crack depths, the results showed similarity in behavior with the work of Shen and Pierre [30] who used Fourier analysis and Finite element method.

However, the solution of the inverse problem, i.e., identification of damage parameters (crack location and/or size) based on frequency shifts (as it is dependent on both crack location and depth) would have been a better procedure for crack detection. Vestroni and Capecchi [32] adopted a different approach to identify damage detection as the inverse problem did not have a straight forward unique solution. They proposed that as the

damage was located in a few sections it was therefore more convenient to focus the identification on those specific sections rather than the whole model. In this regard they used a finite element model to solve this problem for a simply supported beam. By discretizing the whole model into a number of elements it was possible to locate the crack in a much less number of elements. The proposed method suggested that the change in stiffness in those elements only should provide the information regarding the severity of the damage. But this method required the cracks to be located on the identified number of elements for which an objective function was proposed. The objective function was defined as the square of the experimental eigenvalues and the function that furnished the analytical quantities through a finite element code. The minimization of this objective function was done by standard minimization methods rather than using derivatives (to avoid cumbersome iteration) and a computer code IDEFEM (Capecchi et al [33]) was used for this purpose. By assigning the cracks to localized zones only, they reduced the number of parameters required to obtain the severity parameter for the crack. In fact in different cases they showed that if crack was defined in k distinct elements, only k+1 parameters are required to identify the crack. Thus they were able to overcome the indeterminacy of the problem by proposing a minimum norm solution. Nikolakopoulos et al [34] examined an experimental single storey frame and were able to identify a single crack from shifts in the first three natural frequencies. Using FEM, the dependency of first two eigen-frequencies on crack size was represented by a contour graph. The location and depth of the crack were found out by identifying the intersection of the

contour plots for all variations of location and depth against change in the natural frequencies.

Perchard and Swamidas [35] presented a finite element analysis and experimental study for crack detection in a cantilever plate having notched crack. The first 20 mode shapes and natural frequencies were considered for the finite element analysis but the primary foci were kept to the bending modes having frequencies in between 0 to 1000 Hz due to the comparison with experimental analysis. Changes in the displacement and rotation mode shapes for the cracked model from their corresponding un-cracked model were computed and plotted; it was found that for lower modes the discontinuity of the plot of rotation mode shape difference around the notch was significantly larger than any other location in the plate and it increased with the increase of crack depth. The experimental study was carried out using two methods: (a) accelerometers as transducers and (b) strain gauges as transducers. The FRF's obtained from accelerometers showed that comparison of off-the-peak amplitudes showed a clear downward trend indicating the existence of crack; however the trend was not as smooth as the one obtained through finite element analysis. For the strain gauges, the peak magnitudes of the resulting FRF's were found to be more sensitive to cracking than off-the-peak amplitudes; however, location of the strain gauge had to be near to the crack.

Nwosu et al [36] used finite element analysis of tubular T-joints to find out the existence of cracks in their welded joint intersections. The joint was modelled with 8-node

degenerate shell elements having 5 degrees of freedom per node. The exact crack configuration was achieved through a mapping function which allowed the cracks to be mapped on the surface of the tube. The lowest natural frequency showed only a very small change of 4.82 percent change for an 83 percent chord crack depth; however, dynamic bending moments near crack vicinity showed a 97 percent changes for an eighty-three percent chord thickness crack. The dynamic bending moments showed 34.15 to 78 percent changes even for a location far away from crack location as well. Hence it was proposed that combining the change in natural frequencies with the change in bending moments or curvatures (using strain gauges as sensors) could be an effective tool for crack detection. Li et al [37] presented a crack detection method based on acoustical modal response (using acoustic pressure intensity functions) for submerged structure. The analysis was carried out for a cantilever plate under cyclic bending load. The effect of submergence depth was also taken into account. Instead of considering the added masses as constants, they were considered as functions of the in-vacuo natural frequencies. The results showed a good agreement in natural frequency and damping ratios obtained from acoustic pressure intensity and vibrational modal responses. When the crack area was 33% of the cross-section, the first bending frequency showed 3.5% decrease and the damping ratio increased by 62% when the crack area was 40% of total cross-section. The effect submergence depth and air bubble on modal responses were also discussed.

Cheng et al [38] presented an experimental and numerical analysis of cracks in intermediate scale tubular T-joints; the experimental study on fatigue crack initiation and

growth simulated the loading scenarios of the tubular T-joints used for offshore platforms. The crack locations and profiles were recorded and fractographic examinations were carried out to reveal the mechanisms of crack initiation, growth, and crack closure. Strain gages were used as the main response measurement transducers. Strain response function was particularly analyzed to indicate the presence of cracking at the tubular joint intersections. Analyses of the response functions also showed the presence anti-resonance shifts, quasi-static phenomenon and nonlinearity, even at a normalized crack size (the ratio of cracking area to load-bearing area) as small as 0.07. A finite element analysis was also carried out to validate the results and to present cracked and un-cracked mode shapes. Parametric equations were developed to relate the fatigue life of the tubular specimen to the strains/frequencies measured at the various strain gauge locations. In addition equations were also developed to relate the crack size to the strains/frequencies measured at various locations. These equations could be utilized to predict the remaining life of the joint as well as the probable crack size at the critical location near the gauge.

Owolabi et al [39] carried out experiments on one set of fixed beams (seven in each set) and another set of simply supported beams, made of aluminum. They investigated the effects of cracks on the first three modes of vibrating beams and proposed a simple method to identify the size and location of the crack based on the changes in natural frequencies and amplitudes of the frequency response functions (FRF). To detect the crack, the changes in frequency ratios were plotted against crack location and crack depth and it was proposed that the point of intersection of the three contour plots for three

different modes will provide the location and size of the crack. The same method was applied for amplitude ratios as well and the results were compare with the theoretical results obtained earlier by Yang et al [40] and was found to be in good agreement. A possible method for identifying multiple cracks was also discussed.

Yang et al [40] proposed an identification method of cracks in vibrating beam using energy method. The strain energy for a cracked beam was calculated first for a dead load condition and the bending stiffness of the system was determined. The equation of transverse vibration was formulated using Galerkin's method for beams containing one or two cracks. The results available from an experimental study carried out earlier for a simply supported beam, were compared with those obtained from the developed theory and were found to be in good agreement. It was found that the presence of a crack (both its location and size) has a direct influence on the obtained frequencies. Based on these measurements and computations, a crack identification procedure was proposed based on calculating the first four frequencies and mode shapes of the structure. As the existing crack belonged to a particular frequency or mode shape contour of the beam, it was proposed that by plotting the contours of different frequency or mode shape, the intersection will give the location and size of the crack. Yang et. al. [41] also considered the vertical bending and the coupled bending-torsion of a hydro-elastic ship model, modeled as a free-free beam supported on an elastic foundation (water); the model also included the effect of added water mass in the vertical and transverse directions. Coupled and uncoupled vibration equations were solved using Hamilton’s principle and Galerkin’s

procedure. Analysis of coupled vibrations, along with the vertical vibration, provides a thorough theoretical dynamic analysis for the model, and provided a good verification for the test results. In addition to these, a crack identification procedure was also developed by considering the frequency contours that had the same normalized frequency on the contour line as that obtained for the cracked beam. The contours from the first four modes were plotted together, and the intersection point gave the crack location as well as the crack depth.

Chaudhari & Maiti [42] adopted Frobenius method to study the transverse vibrations of for stepped slender Euler-Bernouli beams (simply supported and cantilever beams were considered). They considered both the cracked and un-cracked conditions and divided the beam into two segments, one of which had a linearly varying depth and the other one was uniform. They expressed displacement of the two sections in terms of mode shapes and used Frobenius method to obtain the solution of the differential equation. For the cracked beam, the beam was divided into three segments considering the crack as a bending spring. Chinchalkar [43] modelled the crack as a rotational spring for a beam with varying cross-section and obtained the first three natural frequencies by finite element approach. At first, the crack was modelled as a rotational spring and graphs of spring stiffness versus crack location were plotted for each natural frequency. Having known the first three frequencies of the varying depth beam, the location of the crack and its depth was modelled as an inverse problem of finding the spring stiffness, given the natural frequency. The method was shown to be related to the problem of a rank-one

modification of an eigenvalue problem. Examples outlining the accuracy and ease of using this method were also shown.

Morassi [44] found that variations of the nth frequency and 2nth frequency uniquely determined the position parameter. When n = 1, this work agreed with Narkis [29] who earlier developed that the localization of crack can be determined by the variation of first two natural frequencies. Based on this result, he proposed that by increasing the number of frequencies the stiffness parameter can also be determined. Although the problem was ill-posed, he found that a careful choice of data based on the work of Vestroni and Capecchi [32] could reduce the non-uniqueness of the solution for several cases. Armon et al [45] used rank ordering of the modes according to reduction in natural frequency to locate slots and cracks in a beam. It was found that rank ordering of the eigen-frequency shift is a function of damage location. However, their work also showed it does not depend on the damage magnitude for small cracks. Lee and Chung [46] found the first four natural frequencies by FEM and then applied Armon's rank ordering scheme [45] to approximate the location of the crack. An appropriate model was then developed by FEM based on the crack location range. The crack depth was identified by FEM program which was modified to carry out do-loops so that the natural frequency equaled the measured value. The accurate location of the crack was then estimated by Newton-Raphson iteration method using Gudmundson's [47] equation.

However, the success rate for multiple damage identification using frequency shift is not very common as there are very few studies concerning this. Choy et al [48] used natural frequency change to model a beam on elastic foundation and to identify damage. Damage was expressed in terms of reduction in Young's modulus of a beam element and change in stiffness. The elastic foundation was modelled as a Winkler spring, with some damping associated with it. Due to the presence of a single fault the change in each element was calculated iteratively and was matched with the shift in natural frequency. For two possible damages, all possible combinations were calculated in a similar manner which best matched the shift in first two natural frequencies. The intersection of these solution sets provided the damage location and severity. The third natural frequency was then determined based on the solution and the closest match deemed the true solution. A caution needs to be exercised in modelling the crack/damage as a single spring constant, since the structure executes a number of modal vibrations as it vibrates. The single spring constant cannot properly model all the modal vibratory effects at that specific location; moreover at each location, theoretically there are six spring constants that need to be used. Hence the spring constant used can only model the dominant effect visualized for a particular mode at that particular location. A continuous finite element model eliminates all these approximations present in the study.

2.3.1.2 Mode Shapes

Another popular method for damage detection is based on mode shapes. The mode shapes are generally measured using a single excitation point and many sensors or by a roving exciter having one or more fixed sensors [49]. Generally, damage is identified by direct measurement of the mode shapes or mode shape curvature [50]. Commonly to compare the two sets of mode shapes, two types of methods are used. One is Modal Assurance Criterion (MAC) [51] and the other is Co-ordinate Modal Assurance Criterion (COMAC) [52]. The MAC values are numbered from 0 to 1 between two modal shapes. The MAC value 1 means complete similarity while MAC value 0 means complete dissimilarity. Thus variation of MAC value (between 0.0 and 1.0) can be used as a damage identification criterion. COMAC measures the difference of two mode shapes based on each point. And similar to the MAC method a low COMAC value indicates the possibility of damage. Messina et al [53] proposed a method called Multiple Damage Location Assurance Criterion (MDLAC) to localize damage. This method was formulated on the same basis as MAC. Shi et al [54] extended Messina et al.'s method [53] of using frequency only for incomplete (measured at a few locations only, along the modal shape) mode shapes for the location of damage. The damage locations were initially localized using initial mode shape measurement. The true damage locations were then identified using more accurate modal frequencies. A significant advantage of this method is neither the expansion of incomplete measurement set nor the reduction of

simulated stiffness or mass matrices is required. The method was applied to a 2-D planar truss and found to produce more accurate results than Messina et al.'s [53] frequency shift method. The algorithm was further improved by optimization of the sensor placement for the measurement of incomplete mode shapes. Khan et al [55] used Laser Doppler Vibrometer (LDV) to measure mode shapes in (i) a steel cantilever beam; (ii) a steel cantilever plate and (iii) a concrete beam. LDV allowed a dense grid of measurement which facilitated measurement of modal displacements in a large number of locations required for mode shape analysis. The local mode shape discontinuities indicated the presence of the crack. But for thick metals it was found that damage having a depth less than half the thickness of the structure was not detectable. An algorithm based on the original condition of mode shape sensitivities were developed by Araujo dos Santos et al [56]. The algorithm was applied to a laminated rectangular plate, free in space, which was discretized using first order shear deformation finite element (Soares et al [57]). The results obtained by this procedure showed greater accuracy, than the ones found by using mode shapes only.

Rathcliffe and Bagaria [58] were able to identify the delamination in a composite beam based on gapped smoothing method. Using Laplace's difference equation, the displacement mode shape was converted into curvature shape. The curvature shape was then smoothed using a gapped polynomial at every point. A term, damage index, was introduced which was defined by the curvature polynomial at each point. The largest damage index (identifying the separation of faces) indicated the position of delamination.

Wahab and De Roeck [59] applied a curvature based method to damage detection for a real life structure. They considered the Z24 bridge of Switzerland and obtained satisfactory results with their method. They introduced a term called Curvature Damage Factor (CDF) to indicate damage. CDF was defined as the difference of curvature before and after the damage and averaged over a number of modes. Modal curvature has also been used with other measured data and found to improve the identification assessment. Oh and Jung [60] used both dynamic and static data on a bowstring truss. They found that best results were achieved when static displacements and mode shape curvatures were used in combination.

2.3.2 Crack Detection Using Static Behavior

The dynamic analysis of damage detection always provides large amount of information and sometimes it is not feasible to measure all the responses at critical locations. Static analysis procedure on the other hand, is easily executable and provides easily measurable information for many types of structure. Furthermore static analysis contains less theoretical underpinnings and hence provides easily comprehensible results and conditions pertaining to damage detection. Compared to dynamic analysis, little attention has been paid to the use of static analysis in damage detection so far; this was perhaps due to the fact that the magnitudes of static displacements or strains would be very small and hence needed very sensitive static deformation sensors.

The static measurements are based on the resistance to deformation provided by the structure when subjected to forces whereas the frequency and acoustic measurements require excitation of the structure. All that a static method requires is a parameter estimation algorithm as they use analytical models of the structure to interpret the data. Due to the noise and sparse nature of data most of the early algorithms were not successful. To overcome this problem Hjelmstad and Shin [61] proposed an adaptive parameter grouping scheme technique to eliminate the effect of sparsity of data and a data perturbation scheme to distinguish the damage response from noise. Their proposed algorithm was based on the property change of the structure and, to identify the properties and assess the change in the properties, they used a parameterized finite element model along with the measurement obtained from a static test. Hence, there were two basic requirements, viz. one is the parameterized description of the structure and the second is a method to estimate the parameter. In the development of this technique, they used the estimation method developed by Banan et al [62]. The governing equation for static equilibrium was not satisfied exactly; consequently an output error was defined which was a function of inverse of the stiffness matrix and displacements using the finite element model and a Boolean matrix. An objective function was formulated using the output error vector and minimizing this objective function, the unknown parameters were obtained. The number of unknown parameters was minimized by parameter grouping where similar parameters were grouped without modification of data. If a member of the group was damaged, it had very small effect; but if few parameters of a group were

damaged, the combined effect became noticeable enough. The main goal was to determine a parameter grouping distinguishing the damaged members from the undamaged ones. The adaptive grouping parameter was then introduced where the parameter groups were divided into sequential manner starting from a known parameter estimation obtained from measured data. The group whose estimated parameter differed from its baseline value was subdivided. The subdivision was done repeatedly until the model reached interpolating data with zero error. However measurements were never free from error and the presence of noise affected the group behavior of data. In order to eliminate this problem, a data perturbation scheme was proposed which was able to distinguish the damage from noise for baseline structure and to compute damage indices in damaged structure. For both the cases of single and multiple damages they were able to assess damage in spite of the presence of noisy and sparse data. However, due to the perturbation trials many times, over and over again, the algorithm required a great deal of computational time.

Di Paola [63] showed that applying a convenient set of parameters dependent on superimposed strains on a reference structure, the variation in the structural parameters can always be defined typically due to the temperature variation based on stress distribution. Using this concept Di Paola and Bilello [64] proposed a damage identification procedure for Euler-Bernouli beams. The governing equation for damaged structure was reduced to a Fredholm integral of second kind in terms of bending moment. The proposed method suggested that the integral can be solved by an iterative manner or

in exact form using the properties of its kernel. The solution will therefore depend explicitly on the variation of stiffness parameter caused by the presence of damage and hence it can be used in damage identification procedure by comparing the theoretical and measured response from the damaged and undamaged beams. They employed this method for an Euler-Bernoulli beam and expressed the change of the response in terms of the variation of the bending stiffness. In case of non-redundant beams the variation in the stiffness due to the presence of the damage was modeled as a superimposed curvature. The original damaged beam was then divided into two beams: a principle beam which was subjected to external loads and an auxiliary beam which was subjected to superimposed curvature. By applying the superposition principle the case of a simply supported beam was analyzed. The equations were solved by breaking the problem into two sub-problems and a closed form solution was obtained for the original beam. However, in case of redundant beams an explicit dependence of the beam response on the variation of stiffness parameter could not be obtained. Unlike the previous case of the superimposed curvature, in this case the curvature depended on actual bending moment distribution in the beam, which was unknown. To solve this problem, the bending moment distribution was expressed as an integral function of superimposed curvature and bending moment distribution of the auxiliary beam named as curvature Green's function. Applying the boundary conditions, a Fredholm integral of second kind was then obtained. Solving the kernels an equation providing the analytical relation between the bending moment distribution and damage parameter were developed. Using the superposition

relationship, the equations for deflection, slope and shear force were also calculated. These two equations provided exact solution for the Euler-Bernouli beams having an arbitrary bending stiffness variation. By minimizing the objective function expressed in terms of the theoretical and experimental variations a damage identification procedure was proposed. The identification algorithm was then formulated as a non-linear constrained minimization problem. An optimization method used earlier by Vestroni and Capecchi [32, 65] and Cerri and Vestroni [66] was adopted to solve this problem.

Buda and Caddemi [67] tried to identify concentrated damage in Euler-Bernouli beams using static response and the linear behaviour of the beam. Due to the presence of a crack there existed an 'ineffective' zone adjacent to the crack. This ineffective zone, due to its low stress level reduces the flexural stiffness in case of straight beams. By avoiding closure or propagation of cracks, i.e., assuming the behavior of the beam to be linear, they modeled the flexural stiffness as an internal hinge restrained by rotational spring whose 'equivalent' stiffness was dependent on damage extent at the crack location. The combination of the equilibrium, compatibility and constitutive equations generated a fourth order differential equation in terms of deflection parameter. The presence of the damage was defined as a slope discontinuity at x_0 and the moment of inertia was defined as a distribution, considering the singularity at the crack location as a Dirac delta function. A new parameter named level of damage α was introduced which was directly related to damage intensity. The equation for deflection function was then developed for single and multiple damages. The optimization was done by defining the error function as

the square of the difference between deflection of the Euler-Bernouli beam model and the experimental deflection measurements for different cross-section and load conditions. The solution procedure developed earlier by Vestroni and Capecchi [32, 65] and Cerri and Vestroni [66] was carried out by two phases; i) Minimization of the error function for fixed values of x_0 with respect to α_i only and leading to reduced error function; and ii) minimization of the error function with respect to x_0. But the inverse identification problem requires that the number of measurements required must be equal or greater than the number of the parameters to be identified and hence the study was limited to identification of single and double crack problems only.

Caddemi and Morassi [68] applied this principle (damage induced variation) to identify crack in straight elastic beams. Their aim was to look for an explicit expression in static deflection measurement which indicated the position and severity in case of beam bending. They also focused their attention on finding sufficient analytical conditions to formulate a rigorous identification of damage. By measuring the damage-induced variation for both undamaged and damaged beam under the same load condition, a procedure to solve the inverse identification was proposed. Also to identify the damage location and severity as explicit closed form solution, in terms of deflection measurement, sufficient conditions were obtained. The crack was modeled as a linear elastic rotational spring. By restraining the ends of the beam with translational and rotational springs, boundary conditions were set. Applying the jump condition, the bending moment equation at the cross section where the crack was present was obtained

in terms of transverse displacement and bending stiffness of the beam. A new term called angular distortion was then introduced and damage-induced variation was obtained as the product of angular distortion and bending moment of the undamaged beams. Finally it was possible to express the damage-induced variation in terms of the both bending moment and the stiffness of the rotational spring. The method was applied for several types of beams and the expression of the damage location was obtained by the above mentioned relationship. To calculate the severity of the damage, numerical calculations were adopted and for a number of cases satisfactory results were obtained

Umesha et al [69] proposed a new method for locating and quantifying damage by using the static deflection profile as an input signal for wavelet (Symlet) analysis. This method emphasized on measuring the deflection at a particular point, since in real life it is often very difficult to measure deflection at several points due to the requirement of large amount of instrumentation. They used a fixed beam with single damage to demonstrate the method. The damage was modeled as a reduced stiffness element in finite element analysis. Based on the work of Poudel et al [70], the stiffness of the damaged beam was modeled and an equation of deflection for concentrated load on that beam was obtained. The measured or calculated deflections were then treated as spatial distributed signal in wavelet analysis. For that signal, the continuous wavelet transform was obtained and wavelet coefficient was computed. When the wavelet coefficient was plotted against the length the curve, it showed a sudden change or peak at the locations of the damage, location of the sensor and supports. By eliminating the location of the sensor and support,

the location of the damage was determined. A generalized curve was then plotted with all maximum wavelet coefficients of the deflection response at the damaged point. The severity of the damage was then obtained by mapping the calculated wavelet co-efficient in the generalized curve. They also carried out a parametric case study by varying the damage, location of damage, intensity of load, flexural stiffness and length of the beam. It was observed that wavelet coefficient was directly related to the above mentioned factors.

2.3.3 Crack detection in Rotor Shafts

The technical bulletin of Bently-Nevada [71] reported at least 28 incidents of shaft failure over last 10 years and according to the manufacturers it was a partial list only. According to an EPRI report mentioned in that bulletin, one utility paid $6.2 million to replace power alone during an outage caused by shaft crack on turbine. The replacement cost was $100,000; hence crack detection on shafts has received large attention over the decades. Moreover, it was also reported in that bulletin that under an especial context, the presence of a helical crack was noted only when it was already greater than 90% in crack depth.

The success of modal testing in different structures encouraged researchers to apply this method in crack detection for rotor shafts as well. The earlier focus was to study the dynamics of the cracked rotor and hence papers have been found as early as 1944 related to this topic [18]. Based on the dynamics and other studies crack detection and diagnostic methods have been formulated.

Collins et al [72] investigated the excitation of a rotating Timshenko shaft having a single crack by applying a single and periodic compressive axial impulse at one end. By applying the periodic impulse, they found that the vertical motion in un-cracked shaft decayed with time and the vibration spectrum had a single frequency component Ω, whereas in the cracked shaft the vertical motion did not decay and the vibration spectrum had two additional components of the exciting frequency. They stated that this coupling mechanism can be used to identify cracks. Gounaris and Papadopoulos [73] presented a crack detection method by applying radial excitation at one end and measuring displacement at the other. The crack was considered as a transverse crack on a rotating circular shaft. The crack was modeled using local compliance matrix and for each case they used three sets of excitation frequencies and shaft rotational speed. A 3D contour plot was developed by plotting the response against crack location and crack depth and they mentioned that by measuring the axial response at each run, the location and size of the crack can be determined graphically.

Prabhakar et al [74] analyzed the influence of an open and breathing crack on the mechanical impedance of a rotor bearing system using FEM. Impedance was defined as the ratio of the magnitude of an exciting force to the velocity response. By applying an impulse at different locations the impedance was measured. They observed substantial change in the normalized mechanical impedance due to the presence of the crack and identified a definite trend depending upon the location and size of the crack. Also, they found a breathing crack to be more sensitive than an open crack. Thus, he identified

mechanical impedance as a potential parameter for crack detection in such systems. Brooks et al [75] patented a collar attachment system having facilities for mounting multiple vibration responsive transducers which allows for simultaneous measurement of vibrational responses. Radial, torsional and other exciters can also be mounted on the collar and can be fixed at any angular position.

Sekhar and Srinivas [76] used a commercial finite element analysis package NASTRAN and FEMAP to model hollow cracked composite shafts, fabricated using stacking sequences of boron-epoxy, carbon-epoxy and graphite-epoxy materials. The finite element formulation was based on first order shear deformation theory. They created a crack on the shaft by using Boolean operations. Spring elements were used to represent the effects of the bearings. They have stated that the stacking sequences such as 90/0/90/0 and 90//90/0/0 produced a higher frequency than other sequences of stacking. They also found that for all the three materials used in their study, the eigen-frequencies decreased with increases in crack depth. Kisa and Gurel [77] used a combination of finite element analysis and synthesis method (substructure technique) for non-propagating cracks in beams with circular cross section. The substructure technique was first proposed by Hurty [78] to facilitate the study of large structures. However, they used it to reduce the non-linearity of the structure by splitting the beam into components at the cracked sections or substructures having linear behavior. They discussed three scenarios viz. (i) a cantilever beam with single crack; (ii) a cantilever beam with three cracks of same depth and (iii) a simply supported beam with three cracks of same depth and concluded that by

using this model a relationship between the magnitude of the frequency and form of mode shapes with the location and depth of the cracks can be formulated.

Lissenden et al. [79] tried to model crack propagation and determined natural frequencies and mode shapes for a line shaft system using experimental and numerical methods. They considered both straight and semi-elliptical surface cracks under quasi static and dynamic bending loads. They created the 3D model using finite element analysis and represented the crack by decoupling the joined nodes. In their experimental study, they found no significant change in torsional stiffness for quasi-static loading while a gradual decrease in torsional stiffness and natural frequency for occurred for dynamic loading. The numerical analysis also showed the change in first torsional natural frequency to be directly proportional to the extent of crack growth.

The studies on crack detection in marine propeller shafts, so far, are extremely limited. Arisoy et al [80] inspected a failed 17-4 stainless steel sailboat propeller shaft visually and macroscopically. The analysis included chemical analysis on part of the shafts, hardness measurement, scanning electron microscope (SEM) analyses and X-ray dispersive analysis. It was found that deformation due to press fitting led to surface deformation tracks, which assisted in crack occurrence. The cracks were propagated mainly due to stress corrosion cracking (SCC) and torsional fatigue. Bielawski [81] proposed a diagnostic method of marine propeller shafts based on measurement of shaft journal trajectory. He mentioned that the available methods for condition monitoring and

diagnostic method of propeller shafts were insufficient. One of the common failures occurring in such shafts was tribiological wear when the sealing between the propeller and the bearing breaks, causing the water to leak inside the sealing. The condition monitoring in this case consists of measurement of journal center trajectory, position of the journal center inside the circle and changes of clearance circle. The physical model used in the experiment was built in a test stand ROTOR KIT OIL WHIRL/WHIP OPTION from Bently Nevada. The tests were carried out in the range of 0 - 2500 rev/min and the trajectory examined using eddy-current sensors and a digital real-time oscilloscope TDS 210. A relationship was obtained between the tightness of the sealing, eccentricity of the journal center trajectory and eccentricity of reaction force. It was proposed that this relationship can be used to identify sealing condition and hence shaft system condition. Tlaisi et al [82] carried out experimental measurements (for impedance measurement) and numerical studies, using finite element procedure, to examine the crack development in rotating shafts. The experimental study was carried out using a modal analysis software, LMS test lab, and the numerical study was carried out using ANSYS software. Impedance and velocity frequency functions were used for crack detection and they were measured in the vertical direction for resonant and anti-resonant frequencies. These parameters showed significant variation for crack depths greater than 0.2 and 0.25 hence it was proposed as a tool for crack detection in such shafts.

2.4 Sensor Placement Optimization

Since an efficient methodology required to detect/predict crack/damage detection needs to know the location of the damage/crack and its size, one needs to look at the optimum placement of sensors (or the minimum number of locations at which measurements need to be made or computed) to identify the damage. Consequently, a brief literature review is given here on earlier efforts made to optimize the sensor placement on structures.

The problem of optimal number of sensors and their placements has been first addressed probably by control engineers [83]. However, their concern was identification and control of distributed electrical parameter systems. The majority of the recent studies on sensor placement are in the field of structural dynamics and although a handful of those are concerned with fault detection in different structural components, yet they share the same common goals. Guratzsch and Mahadevan [84] discussed a methodology for optimum sensor placement under uncertainty conditions. The methodology included four major steps: (a) Structural simulation and model validation; (b) Probabilistic Analysis; (c) Damage Detection; and (d) Sensor Placement Optimization. The structure considered was a simplified Thermal Protection System (TPS), consisting of a plate and four fastener locations, and was modelled using the known finite element software package, ANSYS. The load considered was a dynamic mechanical load consisting of sinusoidal frequency sweep and the structure was considered to be excited from 0 to 1500 Hz in approximately 2.0 seconds. This excitation was used as the auxiliary input to the damage detection

algorithm used. Four sensors were placed one of which acted as the point of input excitation and was stationary. The other three were points of sensing and their locations were variable and the damage considered in this study was located at any of the four fasteners placed at the four corners of the plate. A probabilistic finite element model was used to generate statistical information on stress, strain or deformation at each possible sensor location. Each node of the FEM model was considered as the possible sensor location. From the pool of probabilistic outputs consisting of temporal data, a set of 300 measurements of von Mises stress from sensors 2, 3 and 4 were utilized. A state classification was then done using Bayes theory to reduce the classification error. State classification was continued by generating a discriminant function and the consequent evaluation of each data set. The state was assigned according to the discriminant function having the smallest value. A classification matrix was then developed corresponding to a given sensor layout which can be used to estimate the probability of damage detection and probability of false alarm as well. Repeating the above calculations for different sensor layouts will allow the optimization of damage detection with respect to the position of sensor. The authors stated that for the given thermal protection system, sensor placement optimization was achieved in this study. Worden and Burrows [85] proposed a damage identification method using a neural network, and discussed its effectiveness compared to a number of methods, used for optimal sensor placement. The subject structure was a cantilever plate and the adopted methods for sensor distribution were: (a) Iterative insertion/deletion; (b) Genetic Algorithm; and (c) Simulated Annealing. For the

300×200×2.5mm plate, the three methods were in agreement for 10 sensor placements at best. The Simulated Annealing method found a 4-sensor placement to be the best, which according to the authors had a 99.5% probability of damage detection or identification. For the used structure, it was observed that the genetic algorithm and simulated annealing methods gave the most promising results.

Kirkegaard and Brincker [86] carried out an information based analysis for the sensor placement problem by using the parametric identification problem for a linear system. The system considered was a simply supported vibrating beam under the application of transverse load. The analysis was carried out for two sensors and the estimated parameters were expressed in terms of covariance matrix [C]. The covariance matrix [C] was the inverse of Fisher information matrix [F] which was depended on the experimental conditions. Maximizing the determinant of the Fisher information matrix would therefore minimize the covariance matrix providing the optimal locations of the sensors. A surface plot was drawn of the objective function over the plane that specified the sensor position along the beam. The sensitivity of the method was also studied and it was found that by increasing the number of sensors, the sensitivity of the optimal locations of the sensor become less sensitive. Singh and Joshi [87] proposed a sensor layout optimization using complete damage detection for evaluating objective function. The objective function was formulated based on the mean square error (MSE) and genetic algorithm was used for pattern identification. A cantilever beam with a fixed damage at mid-span was considered and responses from static strain sensors were used as

the inputs to damage detection algorithm (DDA). An artificial neural network (ANN) was trained with predefined data and the DDA worked by establishing essentially a correlation matrix, between strain pattern and damage status. A single optimization framework was able to optimize the number of sensors as well as their positions. Hemez and Farhat [88] extended the study of effective independence (EI) concept to allow the sensor placement based on the strain energy distribution. Instead of maximizing the Fisher Matrix, the algorithm placed the sensors along the critical load path of the structure. An eight bay truss structure was considered for this case and the conventional EI and the new algorithms were used for damage detection using FE updating. Both methods were effective for damage identification but the update based EI also showed damage in other areas. However, it was also found that the energy based sensor placement algorithm was highly sensitive to location and orientation of sensors.

Gao and Rose [89] proposed a covariance matrix adaptation evolutionary strategy (CMAES) for quantitative sensor placement optimization. A damage detection probability model for 12 sensors was developed for ultrasonic guided wave sensor network and it was found that the probability model achieved up to 11% improvement for damage detection compared to random sensor network configuration. Two cases were taken into account: one was for a structure with irregular damage detection probability and another for an aircraft wing section. A parametric study was also carried out to find out the reliability, quality and the efficiency of the algorithm and it was found that CMAES over-performed compared to the classical evolutionary algorithm both in the

searching converging speed and solution quality. Guo et al. [90] presented an improved genetic algorithm (IGA) for sensor placement optimization. The improvement was done using improved crossover, two-gene mutation and convergence criterion. A two dimensional truss structure, consisting of 31 elements, 14 nodes and 28 degrees of freedom, was used for the case study and finite element analysis was used. The analytical results obtained from IGA were compared to penalty function method and forced mutation method. It was found that IGA provided faster results in terms of convergence speed and placement optimization than the other two methods.

2.5 Summary

The literature review carried out above details the various techniques utilized for crack/damage identification, using dynamic/static deformation measurement/analysis; in addition it also gives some details concerning the mechanics of crack development in structures considering the mechanics of initiation and propagation of cracking in structures. Even though the studies reviewed for rotating shafts and propeller shafts have been few and far in between, yet the essential knowledge development in these areas have been suitably reviewed. Since crack detection methodologies would involve optimum placement of sensors relevant studies published in this area have also been reviewed.

From the above review, it has been observed that the use of static measurements and analyses, for crack detection, has been of recent origin. In addition, the studies carried out on cracking of marine propeller shafts, carrying a propeller at the overhanging end, have been almost non-existent even though the cracking of shafts poses a serious problem for marine floating structures. The best crack detection procedure would also involve the most optimum placement of sensors to detect its location and size. In the subsequent chapters the numerical studies, using finite element methodology available in the software ABAQUS, have been carried out on an overhanging rotating shaft carrying an end propeller. The results have been analyzed and the salient findings obtained from these studies are summed up in the final chapter.

Chapter 3

IDENTIFICATION OF THE SIZE AND LOCATION OF A CRACK, USING STATICAL DEFORMATIONS OF A MARINE ROTOR SHAFT WITH A PROPELLER AT THE OVERHANGING END

Ridwan B. HOSSAIN[1], Rangaswamy SESHADRI[1] & Arisi S.J. SWAMIDAS[1]

[1]Faculty of Engineering & Applied Science, Memorial University of Newfoundland, St. John's, Canada. e-mail: rbh546@mun.ca, aswamidas@mun.ca, seshadri@mun.ca.

Preface

A version of this paper has been presented in *International Workshop on Smart Materials, Structures & SHM in Conjunction with NDT in Canada 2013 Conference & NDT for the Energy Industry, Calgary, Alberta, CANADA, 2013*. The principal author Ridwan, wrote the paper, carried out the finite element analysis by modeling the system and plotting necessary graphs. The co-authors Dr. Seshadri and Dr. Swamidas supervised the principal author with technical guidance and reviewing the manuscript. In this chapter the

manuscript is presented with altered figure numbers, table numbers and reference formats in order to match the thesis formatting guidelines set out by Memorial University. The paper presents measurements from locations which could be used for crack detection. To view measurements and the subsequent analyses, carried out for all locations, see Appendix A.

Abstract

In this study a simpler but effective method, based on static deformation and strain measurements, is proposed for crack identification in marine propeller shafts. The study proposes to identify the crack location and crack depth based on a combination of deflection and strain measurements, measured at a few locations. Finite element method has been used in the numerical analysis used in this study. Cracks have been located at different (pre-selected) locations and for each location the displacement and strain have been determined for a given crack depth ratio. The calculations have been repeated for different crack depth ratios (Ratio of crack length against diameter) varying from 0.05 to 0.6 at different locations. By using the responses associated with the crack depth ratios at identified crack locations, a new method is proposed for detecting crack location and depth for a single crack.

Keywords: Rotor shaft, Static measurements, Crack identification, Overhanging propeller

3.1 Introduction

The problem of detecting the location and extent of damage in structures has received much attention during the last two decades and a large number of studies has been published to solve the problem; most of these studies were based on the dynamic response of the structures with the presence of a crack or many cracks. The dynamic analysis for damage detection provides large amount of information and sometimes it is not feasible to measure all the required responses at critical locations. Static analysis procedure, on the other hand, is easily executable and provides easily measurable information for many types of structures. Furthermore, static analysis requires less theoretical underpinnings and hence provides easily comprehensible results and conclusions pertaining to damage detection. Compared to dynamic analysis, little attention has been paid to the static analysis in damage detection so far.

Di Paola [1] showed that by superimposed strain, the variation in the stiffness of the structure can always be defined. This superimposed strain is a function of the stress distribution of the structure itself. Using this concept, Di Paola and Bilello [2] proposed a damage identification procedure for Euler-Bernouli beams. In case of non-redundant beams, the variation in the stiffness due to the presence of the damage was modeled as a superimposed curvature. The governing equation for damaged structure was reduced to a

Fredholm integral of second kind in terms of bending moment. The proposed method suggested that the integral can be solved in an iterative manner or in an exact form using the properties of its kernel. Buda and Caddemi [3] tried to identify concentrated damage in Euler-Bernouli beams using static response and the linear behaviour of the beam. Due to the presence of a crack, there exis an 'ineffective' zone adjacent to the crack. This ineffective zone, due to its low stress level reduces the flexural stiffness in case of straight beams. By avoiding closing or propagation of cracks, i.e., assuming the behavior of the beam to be linear, Buda and Caddemi [3] modeled the flexural stiffness as an internal hinge restrained by a rotational spring whose 'equivalent' stiffness was dependent on amount of damage and severity of damage at the crack location. The combination of the equilibrium, compatibility and constitutive equations generated a fourth order differential equation in terms of deflection parameter. Caddemi and Morassi [4] applied induced damage principle to identify cracks in straight elastic beams. Their aim was to look for an explicit expression in static deflection measurement which would uniquely indicated the crack position and severity in case of beam bending. They were able to formulate a closed form expression for identification of crack position and severity for different measurement positions. However, in practice, the measurement positions were not known with respect to the crack size, since a procedure for damage localization had to be formalized. This damage localization procedure was based on the knowledge of deflection profile along the beam length and the successive application of different closed form solutions.

Umesha et al [5] proposed a new method for locating and quantifying damage by using the static deflection profile as an input signal for wavelet (Symlet) analysis. This method emphasized on measuring the deflection at a particular point since in real life it is often very difficult to measure deflection at several points due to the requirement of large amount of instrumentation. They used a fixed beam with single damage to demonstrate the method. The damage was modeled as a reduced stiffness element in finite element analysis. Based on the work of Poudel et al [6] the stiffness of the damaged beam was modeled and an equation of deflection for concentrated load on that beam was obtained. The measured or calculated deflections were then treated as spatial distributed signals in wavelet analysis. For that signal, the continuous wavelet transform was obtained and wavelet coefficients were computed. When the wavelet coefficients were plotted against the length of the beam, it showed a sudden change or peak at the locations of the damage, sensor location and supports. By eliminating the location of the sensor and support, the location of the damage was determined. A generalized curve was then plotted with all maximum wavelet coefficients of the deflection response at the damaged point. The severity of the damage was then obtained by mapping the calculated wavelet co-efficient in the generalized curve.

In the present study a simpler but effective method, based on static deflection and strain measurements, is proposed for crack identification in marine propeller shafts. The shaft is fixed at one end and carries the propeller at the other end. The shaft is 1,300 mm long, and at 1000mm from the fixed support, there is an intermediate support which makes the

propeller shaft to act as an overhanging shaft. A preliminary analysis carried out earlier on rectangular overhanging beams has shown that the percentage changes in the statical displacements were more than that shown by the dynamic frequency parameters obtained from an earlier study carried out by Tlaisi et al [7]. Based on that, a combination of strain and displacement measurements have been carried out to identify the crack location and depth. To measure the statical response, finite element analysis has been used and ABAQUS[1], a well-known finite element software package, was used to carry out the analysis. The cracks have been located at a number of locations as a "seam" crack in ABAQUS which allows the adjacent surfaces to displace from each other based on the amount of load or stress, at that location. However, since the proposed method is being developed for the overhanging shaft, only a general procedure for crack detection is given in this paper to identify the crack size and location. Further details of this procedure are being developed to uniquely identify the crack size and location, based on an earlier work by Yang et al [8].

3.2 Model Preparation and Pre-processing for Finite Element Analysis

The finite element model of the rotor shaft has four major components, viz., the shaft, fixed end support, intermediate support and the propeller. The CAD model for all the four components are generated in the computer software SOLIDWORKS[2]. The data file from SOLIDWORKS was imported into ABAQUS and pre-processed for finite element

modeling. The rotor shaft is 1300mm in length and 15.75mm in diameter and is made of mild steel having the Young's Modulus of elasticity of 200.0 GPa.

The propeller used in this analysis is a 4-blade propeller, shown in Figure 3.1, having a weight of 15.39N. Due to the 3D nature of the propeller blade profiles, the exact CAD model generation was a difficult task. To solve this problem, a 3D laser scanner has been used. The scanner used in this analysis was a high-speed Terrestrial Laser Scanner (TLS) which produced dense point clouds based on the actual shape. The propeller has been scanned on both sides and for each side, a point cloud was obtained. Both the point clouds were then merged and a single point cloud was generated, as in Figure 3.2. The combined point cloud was then exported into SOLIDWORKS and by following the location of the points the CAD model of the propeller has been generated.

Figure 3.1: Propeller Used in the Analysis

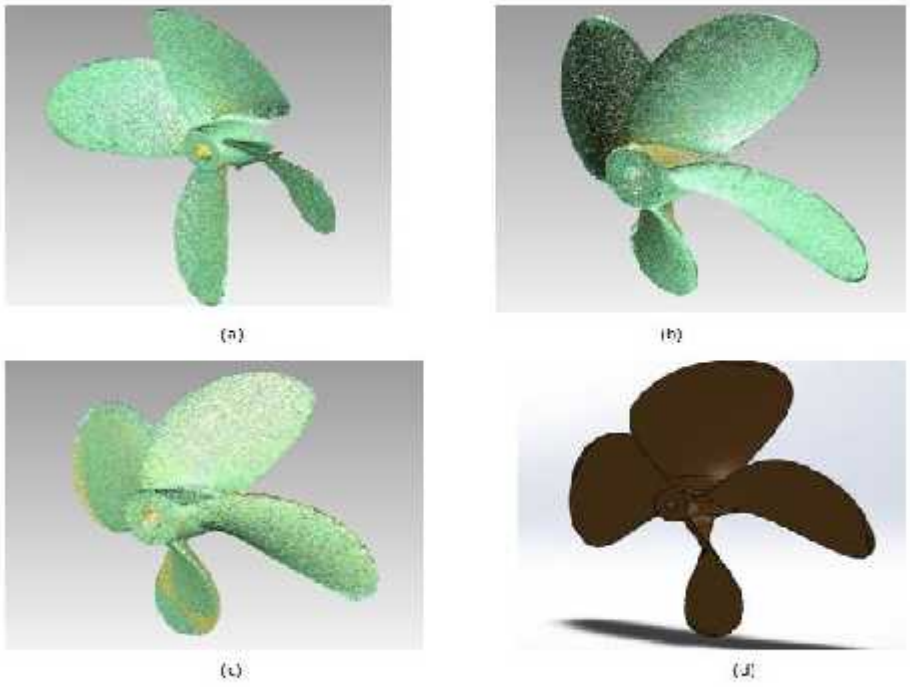

Figure 3.2: Propeller; (a) Scanned Point Cloud of Side 1; (b) Scanned Point Cloud of Side 2; (c) Combined Point Cloud; (d) CAD Model

The finite element analysis has been carried out using a well known finite element package ABAQUS. All the parts have been first assembled in SOLIDWORKS and the assembly was converted into a parasolid. The parasolid was then imported into ABAQUS graphic user interface (GUI); in the GUI the number of data points to be used for the analysis was reduced from 200,000 to 40000. The section used in the whole model was solid homogeneous section. As shown in Figure 3.3, the rotor shaft-system has been partitioned at seven locations, viz., 300mm, 450mm, 600mm, 750mm, 900mm, 1100mm and 1180mm (from the fixed end), where the strains and displacements are to be monitored. Strain and displacement sensors are assumed to be located at these locations.

All of them have been located at the bottom surface of the shaft. Another partition has been created to define cracks and is varied between locations 200mm, 400mm, 600mm, 800mm, 950mm, 1100mm and 1185mm where the crack locations are assumed.

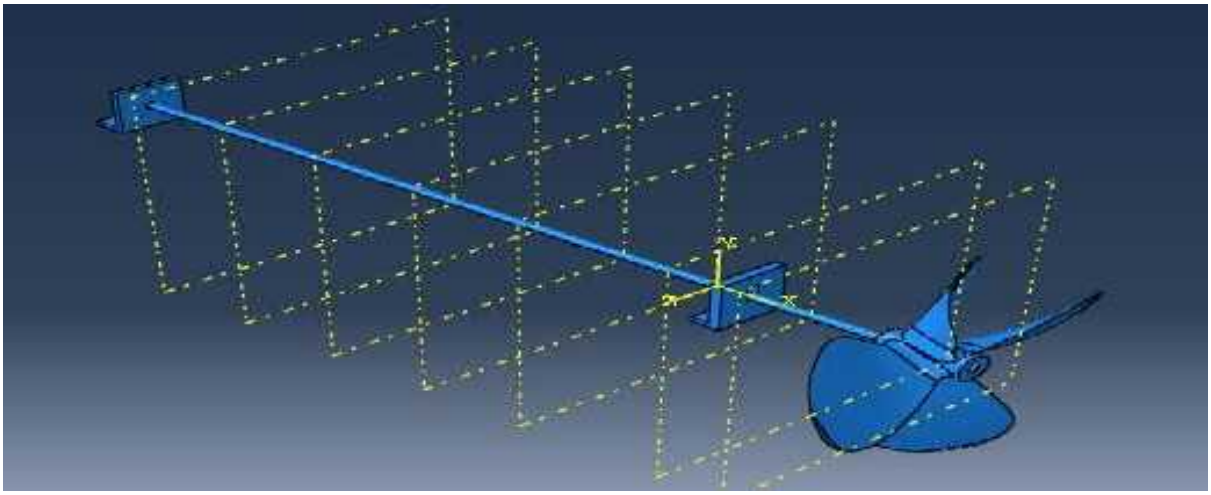

Figure 3.3: Model Assembly with Planes at Measuring Locations

Bending crack was considered in the analysis. A seam crack was used to represent the cracking section of the rotor shaft. The seam of the crack defines an edge or a face in the model that is originally closed but can open during analysis. To create the seam crack the shaft was cell-partitioned at the desired location. That cell partition was then defined as a seam crack, shown in Figure 3.4. Quadratic Tetrahedral elements (C3D10) have been used for the mesh generation. The element type belongs to the 3D stress family and the shape function is quadratic; the elements around the crack are clustered together to properly represent the singularity effect present at the crack tip.

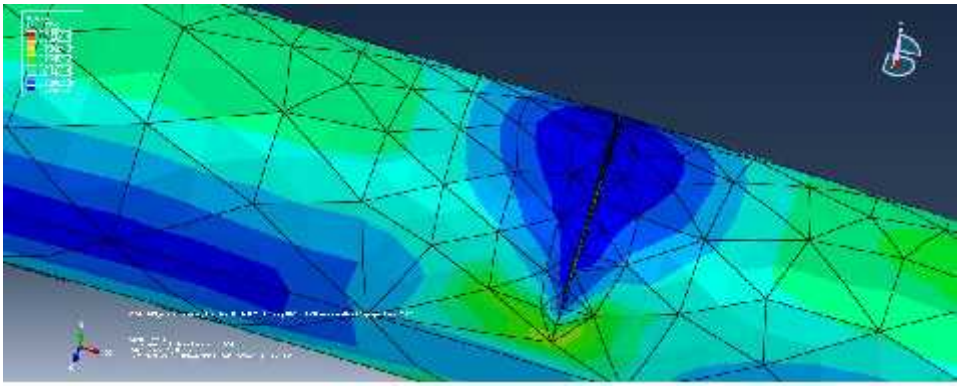

Figure 3.4: Seam Crack; Crack Location: at 800mm, Crack Depth Ratio: 0.4

3.3 Results & Discussion

3.3.1 Displacement Plots

The displacements were plotted as percentage of difference against the crack depth ratio. For each displacement sensor, a graph was plotted. Every graph shows the variation of data for different crack locations. The displacement plots show that with the increasing crack depth ratio, there is a significant amount of change in the displacements which is in agreement with the theory (Figures 3.5 & 3.6). The nature of the response depends upon the distance between the measuring locations and crack locations. Comparing our results with the work of Tlaisi et al (2012), it is found that the static deflection gives much better response for the presence of the crack than the frequency changes indicated in that paper. In that paper, the authors have shown that for a crack depth ratio of 0.6, the frequency change was around 6% only; whereas in the present study, the percentage change in

displacement at the propeller end is observed to be 17.5%, as shown in Figure 3.5 (when the sensor is located at 1300mm).

The displacement changes, even at other sensing locations (viz., 300 mm, 600 mm and 900 mm for cracks located at certain specific locations) seem to be much higher than 6% (for a crack depth ratio of 0.60). This indicates that the static displacement measurement changes give much higher changes than that observed in dynamic frequency measurements. Moreover Figures 3.5 and 3.6 indicate that even if the displacement changes are sensed at the proper location, it indicates about the crack presence (at possible crack locations) only when the crack depth ratio is much larger than 0.4; but if the crack is located in between 800 mm to 1100 mm from the fixed end, then the crack presence can be found even from a crack depth ratio of 0.3 (where the change is higher than 2%).

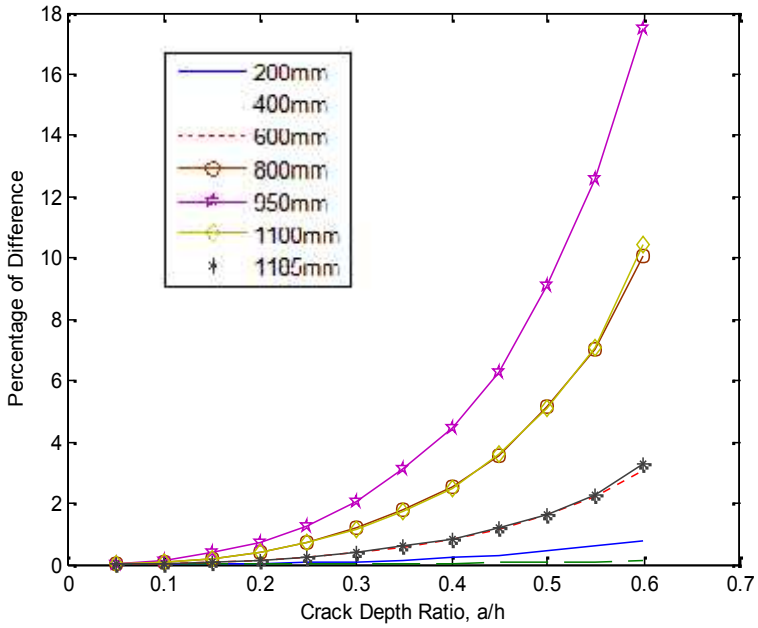

Figure 3.5: Percentage Change in Displacement against Crack Depth Ratio for Displacement Sensor Located at 1300mm from the Fixed End (Different Curves Show the Location of the Crack from Fixed End).

3.3.2 Strain Plots

Similar to the displacements, the percentage differences in strains have been plotted against crack depth ratios in Figures 3.7 and 3.9. It has been observed that only the first two strain sensors (located at 300mm and 450mm from fixed end) show appreciable changes with increasing crack depth ratios; moreover, it is observed that they show good response only if the crack is in between the supports of the rotor shaft (Figure 3.7). But the response changes they indicate are much higher than that shown for frequency measurements; in some cases they are even better than that obtained from deflection

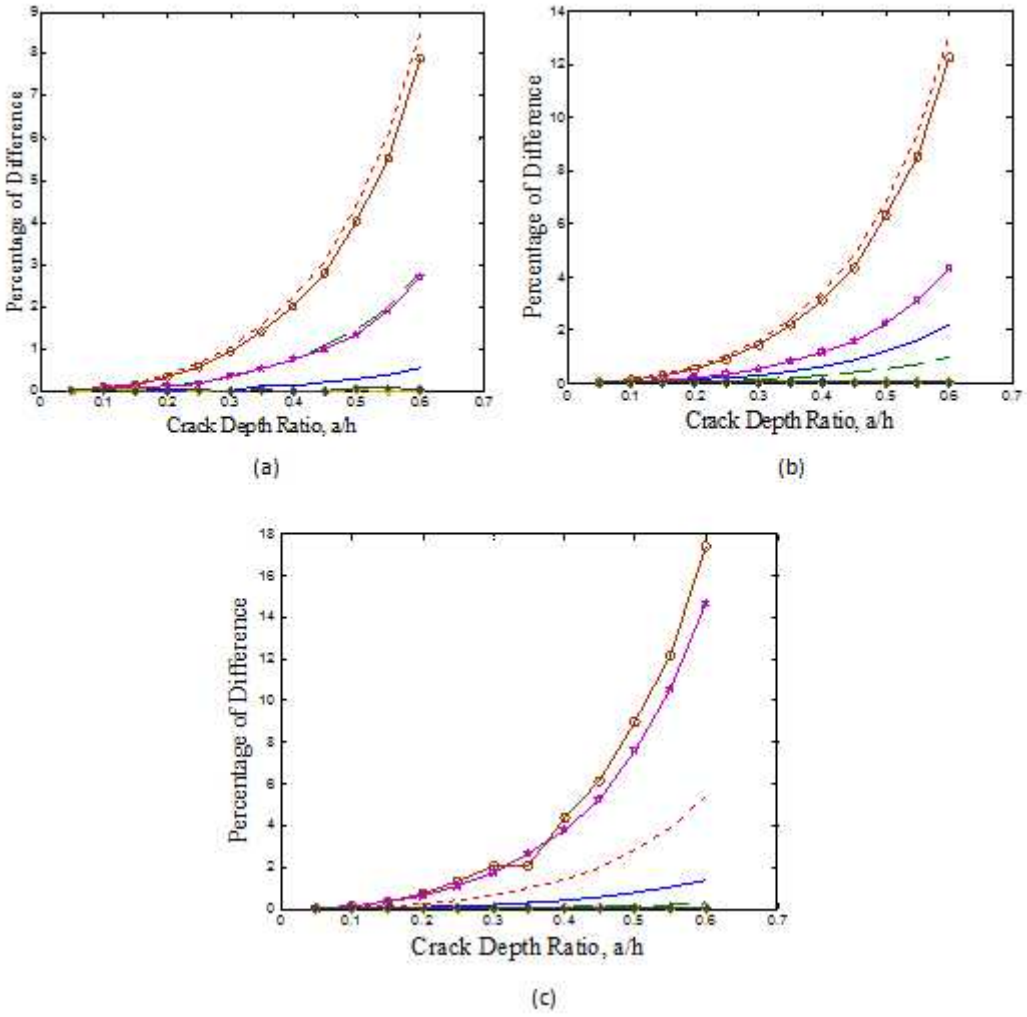

Figure 3.6: Percentage Change in Displacement Against Crack Depth Ratio for Various Crack Locations. Location of the Displacement Sensors are at: (a) 300mm; (b) 600mm; (c) 900mm.

measurements. The main reason behind this is the location of the point of contra-flexure (where the stress/strain shift occurs) within these two sensing points (see Figure 3.8). The maximum changes in strain for a crack (crack depth ratio of 0.6) for the crack located at 200mm, 600mm and 800mm (with the sensor located at 300 mm) are 37.75%, 40.4% and 37.59% respectively, as shown in Figure 3.7. For the same crack located at 200mm,

600mm and 800mm and the strain sensor located at 450mm, percentage changes are 11.34%, 12.63% and 10.19%, respectively. It is also found that strains are very sensitive to manual monitoring and hence even for a very small change of monitoring position they show a high amount of noise (Fig 3.7).

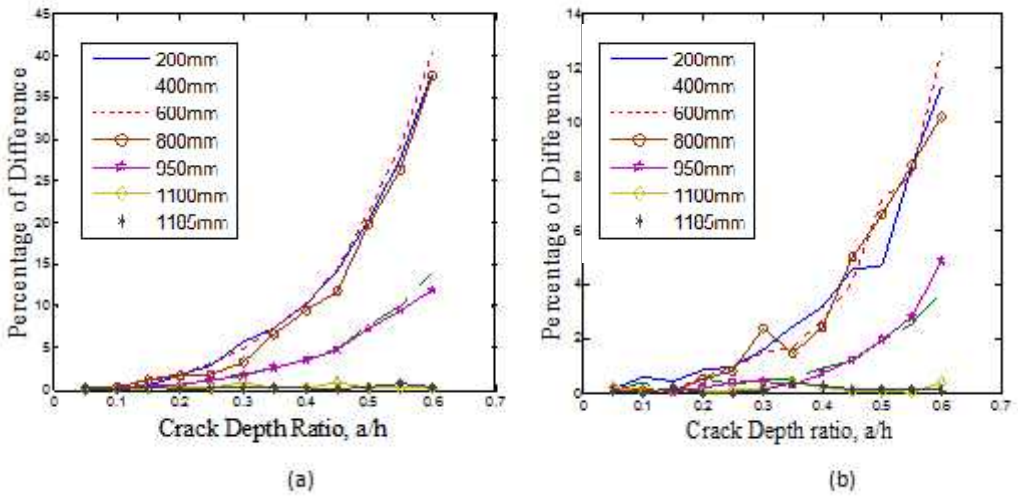

Figure 3.7: Percentage of Difference in Strain vs. the Crack Depth Ratio for Strain Gauges Located at (a) 300mm; (b) 450mm

The rest of the strain sensors show very high amount of change if they are located very near the location of the crack (Figure 3.9). For other cases, the changes they show are very insignificant. Once again it is seen that presence of the crack can be sensed from strain measurements only when the crack depth ratio is larger than 0.3.

For both the strain and displacement changes, if the rates of change of displacement/sensor (with respect to crack depth ratios) are plotted against the crack

depth ratios, it can be seen that crack presence can be sensed even from a crack depth ratio of 0.15 and higher. These results are not shown here (due to space limitation).

3.3.3 Procedure for Crack Detection

Based on the readings provided by the strain and displacement sensors for different crack locations and for crack positions, a crack detection procedure is formulated. The procedure is based on the logicality of the scenario presented below. Having the above plots, consider a scenario where the displacement sensor is located at 1300mm from the fixed end, for a crack depth ratio of 0.3 (from Figure 3.5). For this crack depth ratio, let us assume that the percentage difference in displacement is around 2%. For this difference, considering the plots shown in Figure 3.5, the crack could be anywhere between 800mm to 1100mm. Thereafter going to the strain plots at 300 mm [shown in Figure 3.7 (a)] if the strain sensor shows the percentage difference to be less than 1%, then the crack is outside the support, near 1100mm. If the percentage difference is in the range of 1-2.5%, the crack would be located in between 800mm to 950mm. Moreover considering the output of displacement sensor located at 600mm (see Figure 3.6), if it shows a percentage difference of nearly 1%, the crack is closer to 800mm and if the percentage difference is closer to 0.5, the crack is closer to 950mm. Thus we see that if we formalize a method to combine the outputs of the different sensors, then we can predict exactly where the crack is located for this crack depth ratio of 0.3.

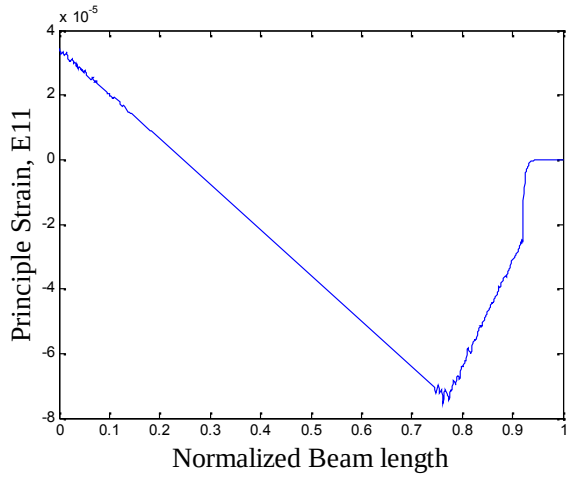

Figure 3.8: Variation of Principle Strain along the Length of the Beam for Uncracked Condition

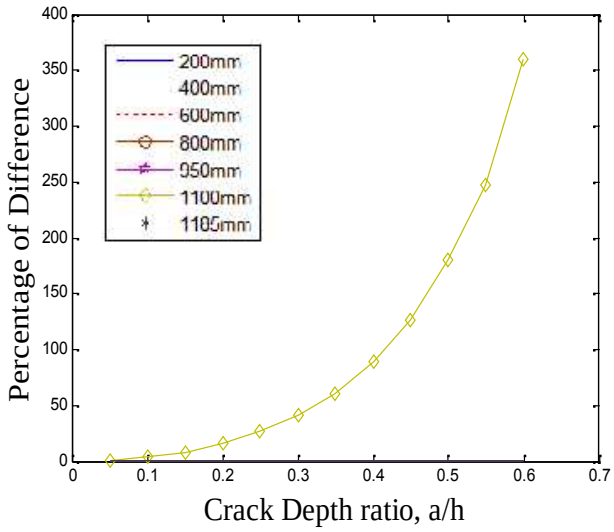

Figure 3.9: Percentage of Difference in Strain against Crack Depth Ratio for Strain Gauge Located at 1180mm

This procedure is formalized by plotting three dimensional plots for displacement/strain differences for different sensor locations, similar to the method illustrated in Yang et al [8] for different modes. The exact crack size and crack location can be identified for any experimentally measured percentage difference in displacement/strain ratios of difference sensor locations.

3.4 Conclusions

The method discussed above provides a simple procedure to identify tentatively the crack size and location in overhanging rotor shafts. The following conclusions are made from the above study:

(a) It can be clearly observed that both the displacement and strain monitoring show better percentage changes than that shown by dynamic frequency measurements.

(b) The displacement sensor located at the propeller end shows the maximum percentage difference for different positions. The change is 2.92 times that indicated from the frequency monitoring method (for a crack located at 950mm from the fixed end).

(c) The major changes in strain sensors are observed when they are located around the point of contra-flexure. At other locations the changes are marginal.

(d) The strain sensor located at 300 mm shows 6.73 times the differences observed in frequency monitoring method for a crack located around these regions. It is also 1.89 and

2.1 times more for cracks located faraway at 200mm to 600mm from the fixed end, respectively.

(e) Using the responses obtained from the above monitoring, a new crack detection method is being developed by using the statical measurements; this method is inferred to give much better results than the frequency measurements.

Appendix

[1]ABAQUS - A well known finite element software package to perform numerical simulation.

[2]SOLIDWORKS- A 3D mechanical Computer Aided Design software developed by Dassault Systèmes SolidWorks Corp.

References

[1] M. Di Paola. "Probabilistic analysis of truss structures with uncertain parameters (virtual distortion method approach)," *Prob. Eng. Mech. 19(4),* pp. 321-329. 2004. Available: http://dx.doi.org/10.1016/j.probengmech.2003.10.001. DOI: 10.1016/j.probengmech.2003.10.001.

[2] M. Di Paola and C. Bilello. "An integral equation for damage identification of Euler-Bernoulli beams under static loads," *J. Eng. Mech. 130(2),* pp. 225-234. 2004. Available: http://dx.doi.org/10.1061/(ASCE)0733-9399(2004)130:2(225). DOI: 10.1061/(ASCE)0733-9399(2004)130:2(225).

[3] G. Buda and S. Caddemi. "Identification of concentrated damages in euler-bernoulli beams under static loads," *J. Eng. Mech. 133(8),* pp. 942-956. 2007. Available: http://dx.doi.org/10.1061/(ASCE)0733-9399(2007)133:8(942). DOI: 10.1061/(ASCE)0733-9399(2007)133:8(942).

[4] S. Caddemi and A. Morassi. "Crack detection in elastic beams by static measurements," *Int. J. Solids Structures 44(16),* pp. 5301-5315. 2007. Available: http://dx.doi.org/10.1016/j.ijsolstr.2006.12.033. DOI: 10.1016/j.ijsolstr.2006.12.033.

[5] P. K. Umesha, R. Ravichandran and K. Sivasubramanian. "Crack detection and quantification in beams using wavelets," *Computer-Aided Civil and Infrastructure Engineering 24(8),* pp. 593-607. 2009. Available: http://dx.doi.org/10.1111/j.1467-8667.2009.00618.x. DOI: 10.1111/j.1467-8667.2009.00618.x.

[6] U. P. Poudel, G. Fu and J. Ye. "Wavelet transformation of mode shape difference function for structural damage location identification," *Earthquake Engineering and Structural Dynamics 36(8),* pp. 1089-1107. 2007. Available: http://dx.doi.org/10.1002/eqe.673. DOI: 10.1002/eqe.673.

[7] A. Tlaisi, A. S. J. Swamidas, A. Akinturk and M. R. Haddara, "Crack Detection in Shafts Using Mechanical Impedance Measurements," *Mechanical Engineering Research,* vol. 2, pp. 10-30, 2012.

[8] X. F. Yang, A. S. J. Swamidas and R. Seshadri. "Crack identification in vibrating beams using the energy method," *J. Sound Vibrat. 244(2),* pp. 339-357. 2001. Available: http://dx.doi.org/10.1006/jsvi.2000.3498. DOI: 10.1006/jsvi.2000.3498.

Chapter 4

IDENTIFICATION OF SIZE AND LOCATION OF A SINGLE BENDING CRACK IN A MARINE PROPELLER SHAFT USING STATIC PARAMETERS OF STRAIN AND DISPLACEMENT

Ridwan B. HOSSAIN[1] & Arisi S.J. SWAMIDAS[1]

[1]Faculty of Engineering & Applied Science, Memorial University of Newfoundland, St. John's, Canada. e-mail: rbh546@mun.ca, aswamidas@mun.ca.

Preface

A version of this paper has been submitted to *International Journal of Engineering Sciences and Management*. The principal author Ridwan, wrote the paper, carried out the finite element analysis by modeling the system and plotting necessary graphs. The co-author Dr. Swamidas supervised the principal author with technical guidance and reviewing of the manuscript. In this chapter the manuscript is presented with altered

figure numbers, table numbers and reference formats in order to match the thesis formatting guidelines set out by Memorial University.

Abstract

The study proposes a simpler but effective method for crack detection in a marine propeller shaft based on static displacement and strain. A small scale real life propeller shaft system used in an earlier analysis, at the Faculty of Engineering and Applied Science, Memorial University, St. John's, NL, has been used in this study; and only the weight of the system along with the added mass of the water has been considered for crack detection. A finite element analysis carried out by ABAQUS showed that cracking is possible under such loading conditions; hence a crack detection method has been proposed. The strains and displacements are measured at four different (previously identified critical) locations for un-cracked conditions and the same measurement is repeated for several pre-defined crack locations and crack depth ratios. Based on the changes in the above parameters, it is shown that crack sizes and locations can be properly identified in structures under such loading conditions, using this method.

Keywords: Rotor Shaft, Crack Detection, Finite Element Analysis, Static Measurement, Overhanging Propeller

4.1 Introduction

Shafts are the most common components used in all kinds of rotating machinery and mechanical equipment and in most high performance rotating devices. They are amongst components that are subjected to the most strenuous working conditions. Besides, the current trends among the machine users to utilize the machinery beyond the expected life period and the practice of run up and run down of machines twice or more per day are causing unexpected stress conditions on shaft's performance. Hence the number of shaft crack incidents has increased dramatically over the last few years. According to the technical bulletin of Bently-Nevada [1] one manufacturer has logged more than 28 incidents in North America over the past 10 years in the power generation industry alone. And the manufacturer indicates that this is a partial list only. Among the four basic failure mechanisms i.e. corrosion, wear, overload and fatigue, corrosion and wear almost never causes shaft failure (unless they act along with fatigue) and of the rest two, fatigue is more prominent than overload. The rapidly fluctuating nature of bending/shear stresses could be held responsible for this phenomenon of cracking along with rotating unbalance and accidental mass eccentricity.

Propeller and rotor shaft components are the key components of any marine propulsion system and the rotor shaft is placed within the stern tube bearing. The sheer purpose of the marine propeller shaft is to transfer the torque from the engine to propeller and the axial forces from the propeller to the thrust bearing. A schematic view of a marine

propulsion system is presented in Fig. 4.1. The combined bending and torsion with various degrees of stress concentration mainly causes cracks in such shafts. Other than that, the tribological wear at places where it co-acts with the seals and sleeves (along with the fluctuating fatigue loads) also leads to shaft failure [2].

Figure.4.1: Schematic View of Marine Propulsion System

Arisoy et al [3] carried out a failure analysis of a 17-4 PH stainless steel sailboat propeller shaft, which failed earlier than its normal usage life, using both macroscopic visual inspection and microscopic inspection with a light optical stereoscopic microscope (Fig 4.2); they stated that the failure was primarily due to torsional moments acting on the propeller. The striation marks shown in the above figure also indicate that bending was associated with the torsional fatigue in that case. Since failure in this case occurred at the location where the propeller was mounted to the shaft, it also indicates the presence of heavy bending and torsional moments (perpendicular and transverse to its rotating direction) on the rotating propeller blades. Fig. 4.3 provides a better illustration about the

crack initiation and propagation in a rotating shaft due to bending. The bending crack often moves along the plane, perpendicular to its longitudinal axis, and causes failure.

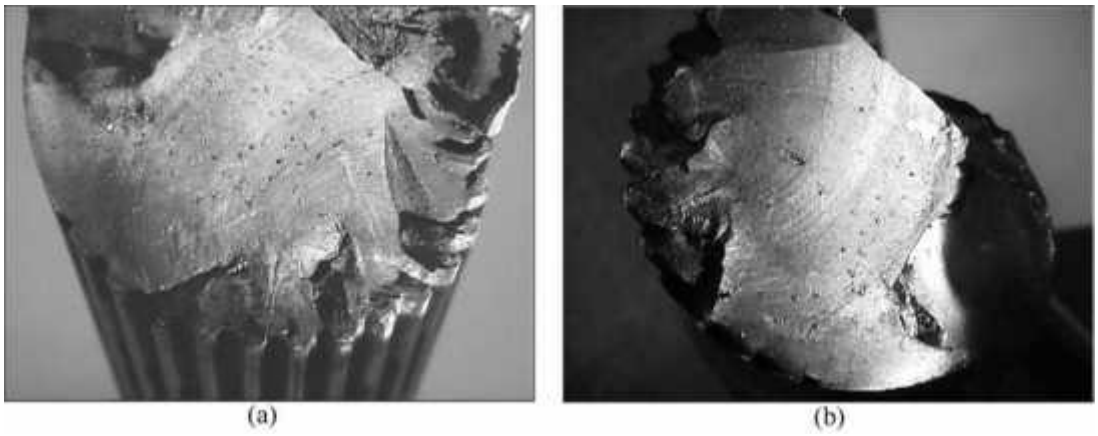

Figure. 4.2: (a) and (b) Show the Fractured Surface of the Failed Propeller Shaft Macroscopically [3]

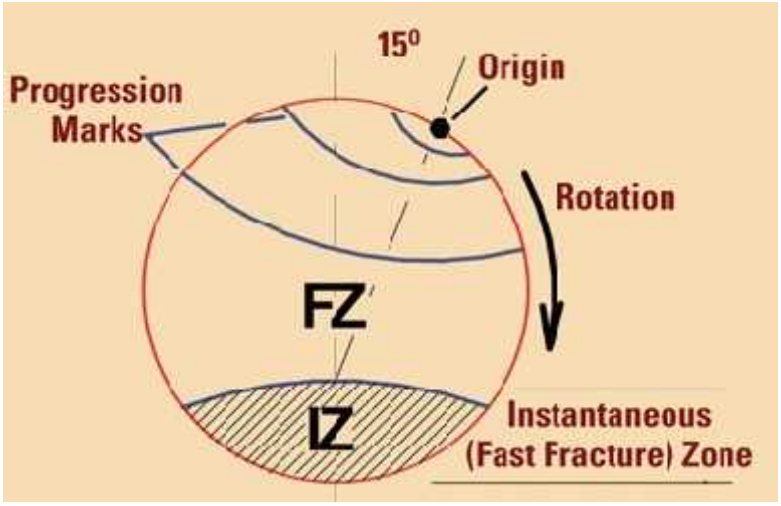

Figure. 4.3: Crack Initiation and Propagation due to Rotating Bending (*Source:[4]*)

In the present investigation, a single crack caused by bending of shaft due to the weight of rotor and propeller system is analyzed using finite element procedure for a marine propeller shaft. The possibility of crack initiation and propagation was validated by measuring the maximum strains (and the consequent stresses) caused by the weight of the rotor shaft and propeller system and added mass of the water. Based on the static response, a crack detection method (both location and extent) has been proposed following an earlier study carried out by Hossain et al [5].

4.2 Crack Detection Methodology

Most of the crack detection method in marine propeller shafts are based on visual inspection, as most of the propeller shafts are made of stainless steel and the surfaces of inspection are not uniform and smooth enough; hence ultrasound or eddy current measurements cannot be relied upon. The frequency response and the modal analysis provide large amount of information and sometimes it is not feasible to measure responses at critical locations. On the other hand, static analysis procedure is easily executable and provides easily measurable information for many types of structures. Furthermore, static analysis requires less theoretical underpinnings and hence provides easily comprehensible results and conclusions pertaining to damage detection. Compared to dynamic analysis, little attention has been paid to the use of static analysis in damage detection so far.

The static analysis is mostly done either by model based approach or finite element analysis. One of the difficulties of model based approach is finding an effective parameter estimation algorithm as the presence of noise and sparsity of data makes it difficult to identify damage. To overcome this problem, Hjelmstad and Shin [6] proposed an adaptive parametric grouping and a data perturbation scheme. Their proposed algorithm was based on the property change of the structure and, to identify the properties and assess the change in the properties, they used a parameterized finite element model along with the measurement obtained from a static test. Di Paola and Bilello [7] proposed a damage identification procedure for Euler-Bernouli beams by reducing the governing equation for damaged structure to a Fredholm integral of second kind in terms of bending moment. According to their literature, the solution of the integral depends explicitly on the variation of stiffness parameter caused by the presence of damage and hence it can be used in damage identification procedure by comparing the theoretical and measured response from the damaged and undamaged beams. Buda and Caddemi [8] modeled the flexural stiffness of an Euler-Bernouli beam as an internal hinge restrained by a rotational spring whose “equivalent” stiffness was dependent on damage extent at the crack location. By avoiding closing or propagation of cracks, i.e., assuming the behavior of the beam to be linear, they proposed of an 'ineffective zone' due to the presence of a concentrated damage and mentioned that due to the low stress level of such 'ineffective zone', it reduces the flexural stiffness adjacent to the crack. With this

approach they were able to generate a fourth order differential equation in terms of deflection by combining equilibrium, compatibility and constitutive equations.

Another proposed method of using static response as a damage identification parameter is Finite Element Analysis. Prabhakar et al [9] propose mechanical impedance as a potential parameter for crack detection by analyzing the influence of an open and breathing crack on the mechanical impedance of a rotor bearing system using FEM. They observed substantial change in the normalized mechanical impedance due to the presence of the crack and identified a definite trend depending upon the location and size of the crack. Kisa and Gurel [10] used a combination of finite element analysis and synthesis method (substructure technique) for non-propagating cracks in beams with circular cross section. Umesha et al [11] proposed a new method for locating and quantifying damage by using the static deflection profile as an input signal for wavelet (Symlet) analysis. This method emphasized on measuring the deflection at a particular point since in real life it is often very difficult to measure deflection at several points due to the requirement of large amount of instrumentation. They used a fixed beam with single damage to demonstrate the method. The damage was modeled as a reduced stiffness element in finite element analysis. Based on the work of Poudel et al [12] , the stiffness of the damaged beam was modeled and an equation of deflection for concentrated load on that beam was obtained. The measured or calculated deflections were then treated as spatial distributed signals in wavelet analysis. For that signal, the continuous wavelet transform was obtained and wavelet coefficients were computed. When the wavelet coefficients were plotted against

the length of the beam, it showed a sudden change or peak at the locations of the damage, sensor location and supports. By eliminating the location of the sensor and support, the location of the damage was determined. A generalized curve was then plotted with all maximum wavelet coefficients of the deflection response at the damaged point. The severity of the damage was then obtained by mapping the calculated wavelet co-efficient in the generalized curve.

Tlaisi et al [13] carried out experimental measurements (for impedance measurement) and numerical studies, using finite element procedure, to examine the crack development in rotating shafts. The experimental study was carried out using a modal analysis software, LMS test lab, and the numerical study was carried out using ANSYS software. Impedance and velocity frequency functions were used for crack detection and they were measured in the vertical direction for resonant and anti-resonant frequencies. These parameters showed significant variation for crack depths greater than 0.2 and 0.25 hence it was proposed as a tool for crack detection in such shafts.

The earlier work by Hossain et al [5] carried out a finite element analysis of an overhanging propeller shaft with a concentrated load at the end and concluded that percentage changes in deflection and strain provided much larger changes than frequencies obtained from the work of Tlaisi et al [13]. By measuring strain and displacement at a number of location, they were able to detect the optimum location for measuring strain and displacement where these two parameter show maximum variation

irrespective to the location and size of crack. Based on the outcome of the above study, they proposed a much–simpler crack detection method for this type of structures, using only two measurement sensors. In this study, a similar approach has been taken, by considering a more realistic scenario where the load considered will be only the weight of the shaft and the propeller, and the effect of the associated added mass of water has been reckoned for determining the possibility of cracking of propeller shaft.

4.3 Pre-Processing of the System Component

The finite element model of the rotor shaft has four major components, viz., the shaft, fixed end support, intermediate support and the propeller. The CAD model for all the four components were generated in the computer software SOLIDWORKS. The rotor shaft is 1300 mm in length and 15.75 mm in diameter and is made of mild steel; the center of the intermediate support is located at 1,000 mm from the fixed end.

The propeller considered in this analysis is a 4-bladed propeller (Fig. 4.4) used earlier by Tlaisi et al [13]for crack detection using mechanical impedance procedure. The propeller weighs 15.39N and is made of commercial bronze having a density of 8800kg/m^3. Since the weight of the system will be considered as the only load in analysis, it is very important to model the propeller exactly. Due to the 3D nature of the propeller blade profiles, the exact CAD model generation was a difficult task and to solve the problem, a 3D laser scanner was used. The scanner used in this analysis was a high-speed Terrestrial

Laser Scanner (TLS) which produced dense point clouds based on the actual shape. The propeller was scanned on both sides and for each side, a point cloud was obtained. Both the point clouds were then merged and a single point cloud was generated, as in Figure 4.5. The combined point cloud was then exported into SOLIDWORKS and by following the location of the points the CAD model of the propeller was generated. From SOLIDWORKS the weight was evaluated and was found to be in agreement with the actual measured weight.

Figure. 4.4: Propeller Used in the Analysis

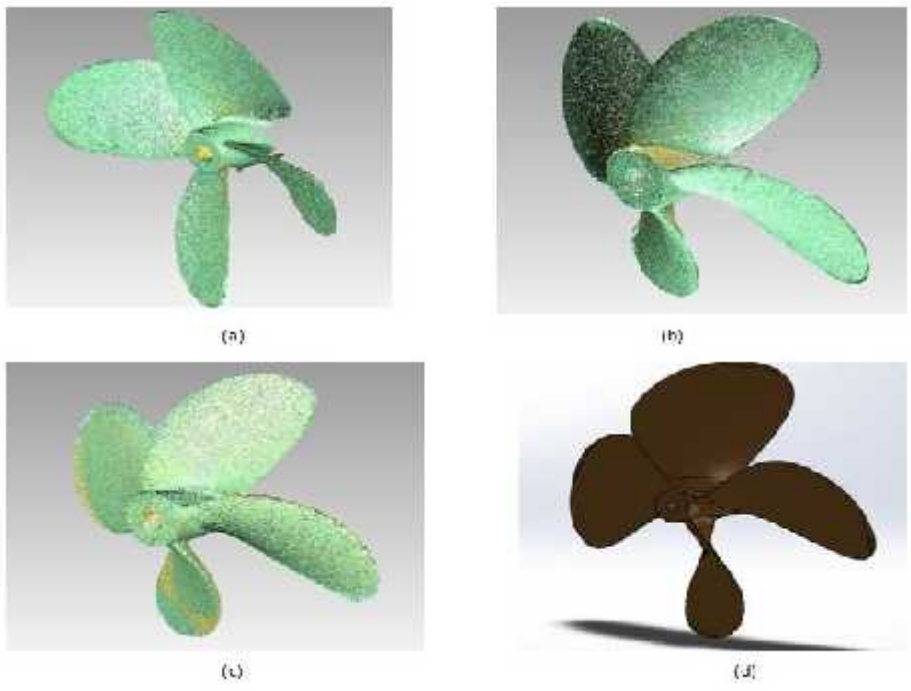

Figure. 4.5: Propeller; (a) Scanned Point Cloud of Side 1; (b) Scanned Point Cloud of Side 2; (c) Combined Point Cloud; (d) CAD Model

The finite element analysis was carried out using the well-known finite element package ABAQUS. All the parts were first assembled in SOLIDWORKS and the assembly was converted into a parasolid. The parasolid was then imported into ABAQUS graphic user interface (GUI); in the GUI the number of data points to be used for the analysis was reduced from 200,000 to 40000. The section used in the whole model was solid homogeneous section. The earlier analysis [5] showed that the surface strain change was only significant near the point of contra-flexure and in this study it was found to be located at 418mm from the fixed end. In addition, displacement changes were also found

to be prominent at the overhanging end and at-locations in between 700-800 mm from the fixed end. Consequently, the strain sensor locations were considered at 410mm and 530 mm from the fixed end and the displacement sensor locations were considered at 710 mm from the fixed end and at the overhanging end.

A seam crack was used to represent the cracking section of the rotor shaft. The seam of the crack defines an edge or a face in the model that is originally closed but can open during analysis. To create the seam crack the shaft was cell-partitioned at the desired location. That cell partition was then defined as a seam crack, shown in Figures 4.6. Quadratic Tetrahedral elements (C3D10) have been used for the mesh generation. The element type belongs to the 3D stress family and the shape functions are quadratic in nature; the elements around the crack are clustered together to properly represent the singularity effect present at the crack tip.

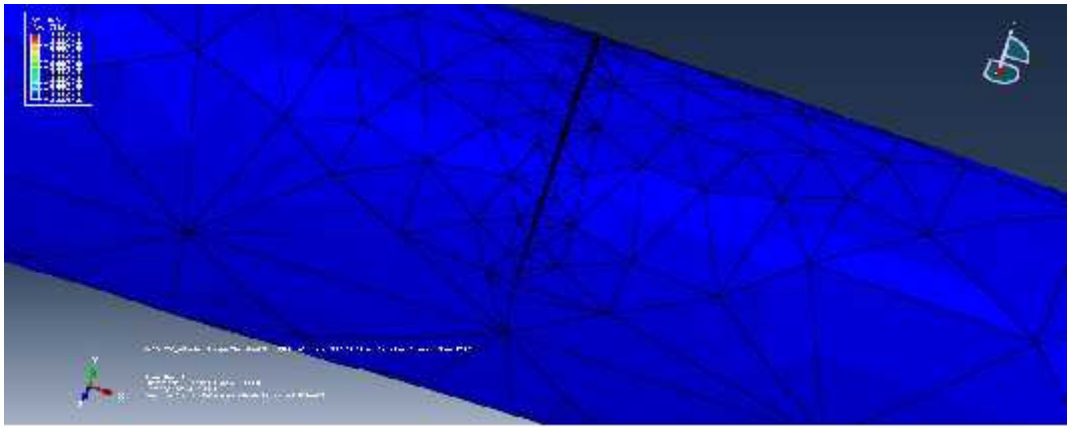

Figure. 4.6: Bending Seam Crack; Crack Location: at 750mm, Crack Depth Ratio: 0.4

4.4 Results & Discussion

4.4.1 Possibility of Cracking

The possibility of cracking was validated by computing the maximum strain (and the consequent stress) the shaft would experience during bending. Considering the added mass of water and the weight of the system, the maximum surface strain (over the intermediate support) obtained was 77 micro-strains. Since the shaft was executing a rotational motion, the strain range at the maximum strain location would be twice the static strain, viz., 154 με (equivalent stress would be 30.8 MPa). If we consider the expression used by Chattopadhyay [14] for crack threshold stress intensity factor:

$$a_{th} = \frac{1}{\pi}\left(\frac{\Delta K_{th}}{\Delta S}\right)^2$$

where, the threshold stress intensity factor ΔK_{th} was taken as $10\text{MPa}\sqrt{m}$ and threshold notch radius (for crack initiation) a_{th} = 5mm; then the nominal surface stress range ΔS obtained was 79.79 MPa. This would require a stress amplification factor of 2.591 (since the computed nominal stress range was 30.8 MPa) to initiate cracking in steel at the hotspot location. Considering that a run up and down operation would occur, during the start-up and slowing down of the rotating shaft and propeller, the excitation of natural frequencies during this operation would generate large dynamic strain amplifications; also the fretting wear caused by the tribological contact of rotating shaft with the hardened sleeve (of the bearing) would be locations for stress amplification in the rotor

shaft [2]. Moreover the blade bending caused during thrust generation in propeller will also cause additional bending stresses in the rotor shaft. As a consequence the required stress amplification of factor of 2.57 will be easily available to initiate cracking in the shaft. So the initiation and the propagation of crack under current loading scenario seem to be possible for the rotating propeller shaft.

4.4.2 Displacement Results

The displacements have been plotted as the percentage difference (between the cracked and un-cracked shaft) against crack depth ratio. For each sensor location individual plot represents the variation of displacement against crack depth ratio for different specified locations. For each location, the obtained result shows that the percentage change in displacements increases almost in an exponential manner as the crack grows larger (Figures 4.7 & 4.8). Comparing this result with the earlier work by Tlaisi et al [13] , it was found that the displacement changes provides much higher values than the frequency changes. It was found that the percentage difference for displacement was up to 21.5% (for the crack located at 750 mm) for the sensor located at 710mm (see Figure 4.7) and 22.6% (for crack located at 1030 mm) for the sensor located at 1300mm, whereas the frequency change was only 6% for 0.6 crack depth ratio. It should also be observed that the exponential percentage changes in displacements are noticeable only beyond a crack depth ratio of 0.3 to 0.4; hence the use of displacement changes as a crack predication parameter would not be sensitive enough if they are used below a crack depth ratio of 0.3.

It should be observed that the displacements are quite small and they need to be measured with proper devices to obtain correct results. This should not be held as a limitation of the method since in prototype situations, the displacements will be amplified by the scale ratio used in modelling the structure for small scale testing.

4.4.3 Strain Results

Similar to displacements, the percentage differences in strains have been plotted against the crack depth ratios in Figures 4.9 & 4.10. As observed earlier, the percentage differences were found to increase in an exponential manner with crack depth ratio and it showed larger changes than displacements, especially if the crack was within the intermediate support. The maximum percentage difference obtained at 410 mm was 33.3% when the crack was located at 400 mm; when the strain sensor was at 530 mm the change was 14.9%, when the crack was located at 750 mm (for a crack depth ratio of 0.6). Both of these values are much higher than frequency change (6%) and one of them was even higher than the displacement change as well. The limitation observed here is that for crack located beyond the intermediate support, strain changes did not provide significant variations. The same limitations given above for displacement changes, concerning detecting crack initiation, were also observed for strain changes. Hence displacement and strain changes do not seem to be sensitive enough for detecting crack initiation in rotating shafts. It can also be seen from Figure 4.9, that if the crack was

located at 400 mm, then the crack initiation can be detected even from a crack depth ratio of 0.15 (by the sensor located 410 mm).

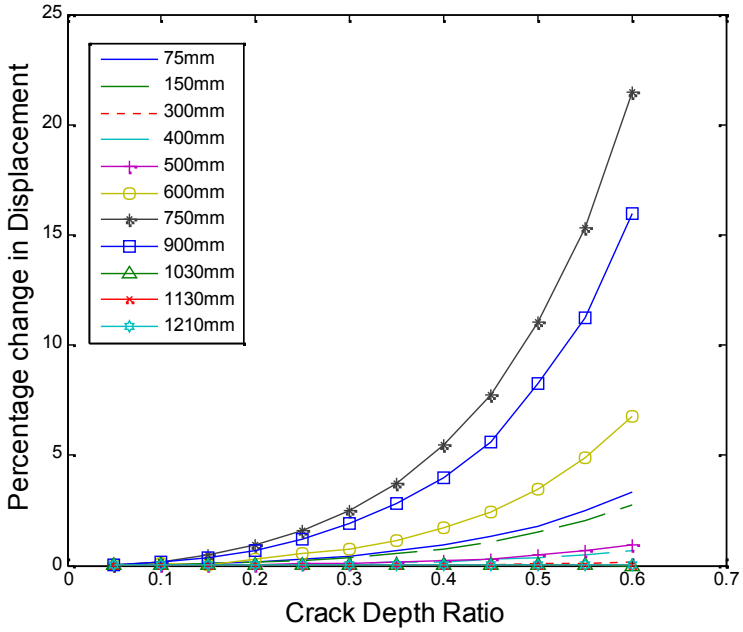

Figure 4.7: Percentage Change in Displacement against Crack Depth Ratio for Displacement Sensor Located at 710mm from the Fixed End (Different Curves Show the Location of the Crack from Fixed End).

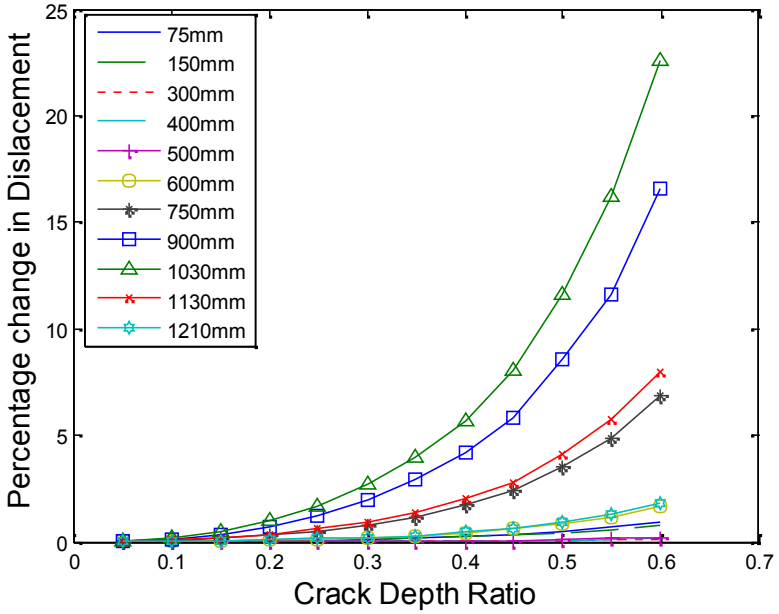

Figure 4.8. Percentage Change in Displacement against Crack Depth Ratio for Displacement Sensor Located at 1300mm from the Fixed End (Different Curves show the Location of the Crack from Fixed End)

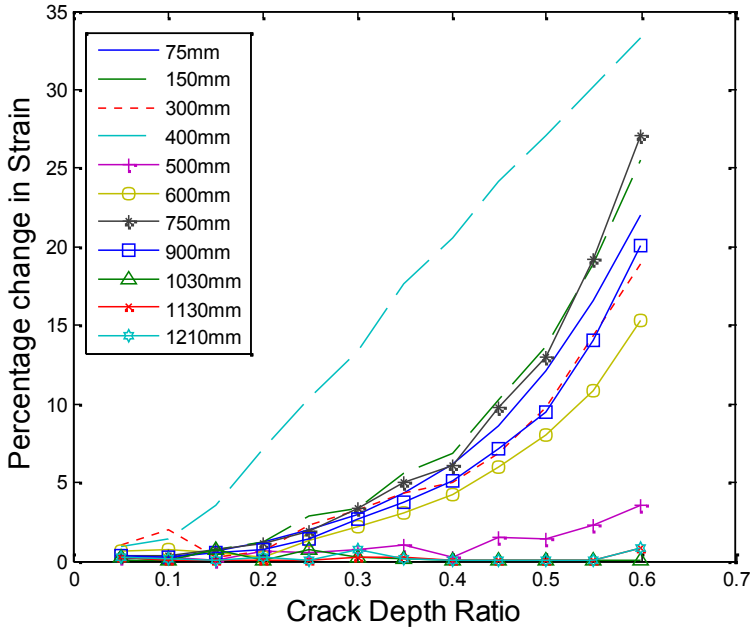

Figure 4.9: Percentage Change in Strain against Crack Depth Ratio for Strain Sensor Located at 410mm from the Fixed End (Different Curves Show the Location of the Crack from Fixed End)

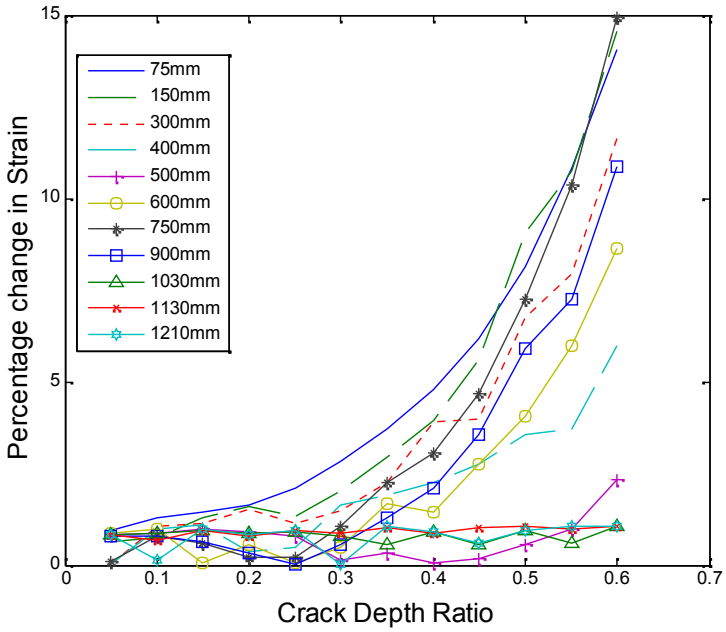

Figure 4.10: Percentage Change in Strain against Crack Depth Ratio for Strain Sensor Located at 530mm from the Fixed End (Different Curves Show the Location of the Crack from Fixed End)

4.4.4 Slopes of Percentage Differences in Displacements and Strains

Although the percentage changes, for both displacements and strains, are much higher than the frequency change (due to the exponential nature of the curves) they are not very sensitive for early crack detection. Hence, to overcome this deficiency in the crack detection proposed above, the slopes of each displacement/strain percentage difference curve were plotted against crack depth ratios in Figures 4.11, 4.12, 4.13, and 4.14. Most of the slope curves showed exponential increases against crack depth ratios. However, the first point in the crack depth growth (for a crack depth ratio of 0.05, in the numerical

computation) was not considered as it gave an unexpected high value. Since the strains were picked out manually using visual estimation, the raw plot of these slopes did not give a smooth curve; hence a five-point averaging procedure was carried out to reduce the variableness of the data. The maximum slope for strain (or percentage rate of change of strain as a function of crack depth increase) was found to be up to 176.6% and 112.1% at 410 mm and 530 mm respectively for the 0.6 crack depth ratio. For the same crack depth ratios, the maximum slope for displacement was found to increase to 124.2% and 127.9% at 710 mm and 1300 mm respectively. These plots could be used as effective tools for early crack detection as for most cases, even for the 0.1 crack depth ratio these plots provide significant amounts of change in the slope. So when over a period of measurement, significant changes in slopes occur (say from 5 to 8 or 10%) one can be sure that a crack has initiated in the rotor shaft, and the methodology given below can be used to detect the probable location and size of the crack.

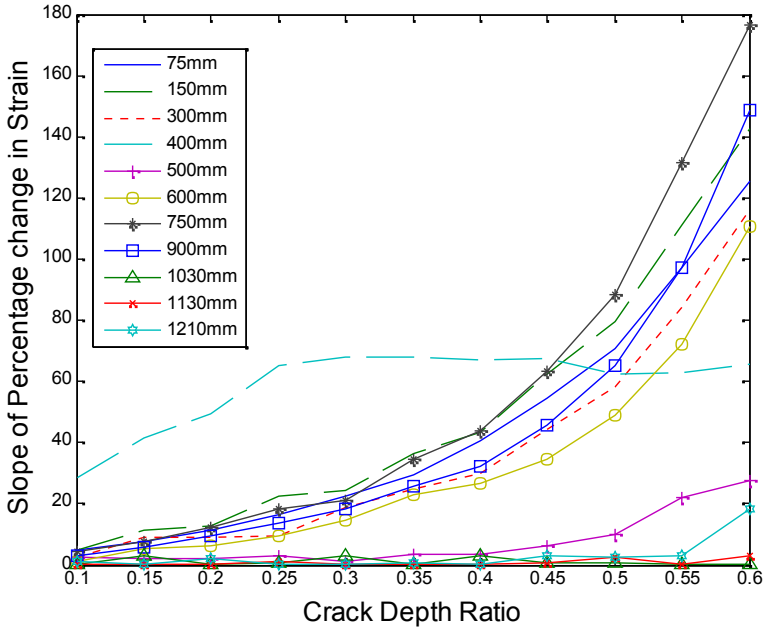

Figure 4.11: Slope of Percentage Change in Strain against Crack Depth Ratio for Strain Sensor Located at 410mm from the Fixed End (Different Curves Show the Location of the Crack from Fixed End)

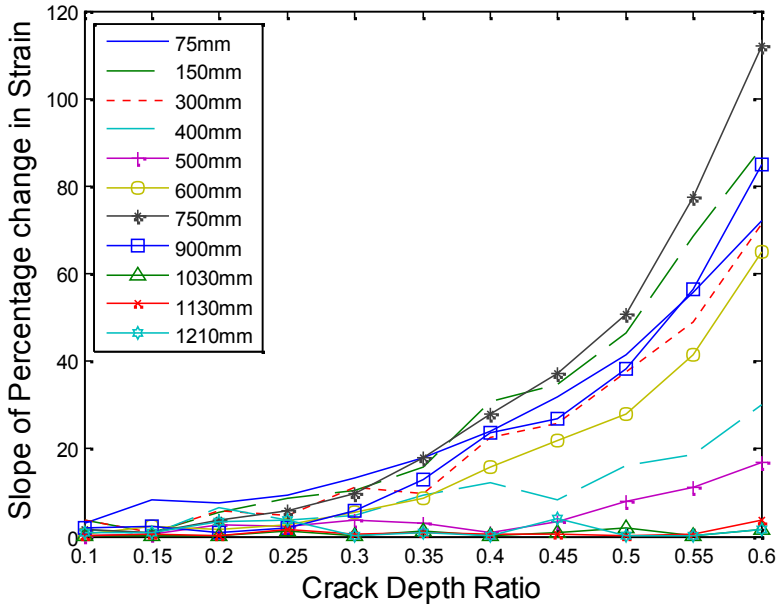

Figure 4.12: Slope of Percentage Change in Strain against Crack Depth Ratio for Strain Sensor Located at 530mm from the Fixed End (Different Curves Show the Location of the Crack from Fixed End)

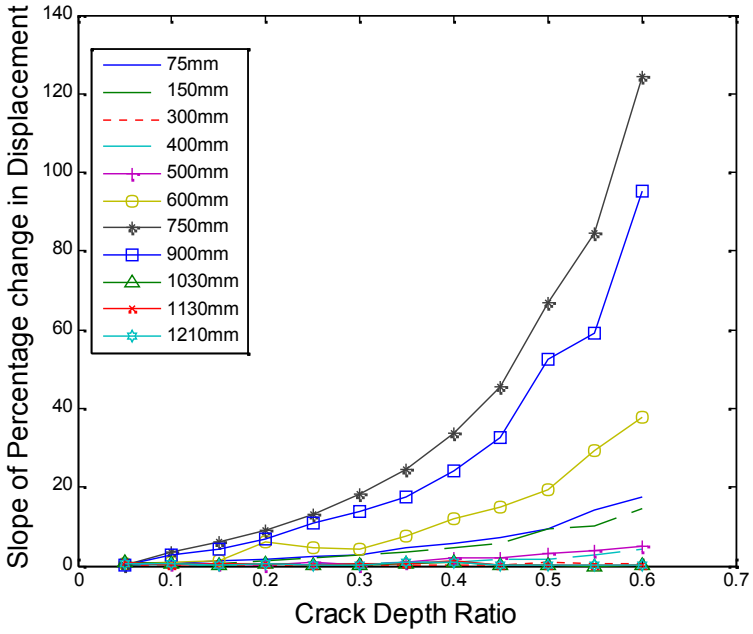

Figure 4.13: Slope of Percentage Change in Displacement against Crack Depth Ratio for Displacement Sensor Located at 710mm from the Fixed End (Different Curves Show the Location of the Crack from Fixed End)

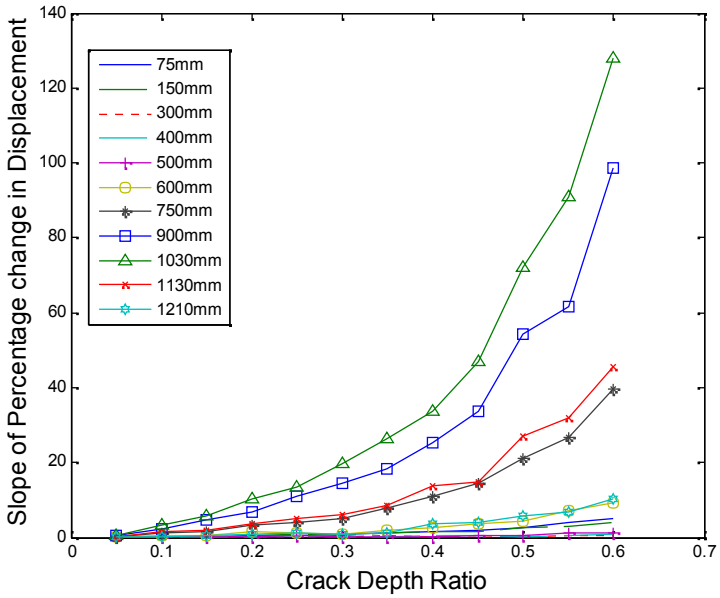

Figure 4.14: Slope of Percentage Change in Displacement against Crack Depth Ratio for Displacement Sensor Located at 1300mm from the Fixed End (Different Curves Show the Location of the Crack from Fixed End)

4.4.5 Procedure for Crack Detection

The earlier study by Hossain et al [5] considered the percentage differences that occurred in displacements and strains of the rotor shaft, as crack detection tool. But as discussed in the previous section, the slope of percentage difference provides an early indication of the crack initiation and presence than percentage difference; hence in this study the slope of percentage difference is used as the crack detection tool. Any two sensor values can be used to detect the initiation/presence of small cracks; it should be noted that the strains (as well as the differences and slopes) do not show much variation beyond intermediate support. Therefore it would be more practical to use either a combination of displacement and displacement or strain and displacement changes and slopes in crack detection.

The crack detection has been carried out with a Microsoft Excel macro enabled workbook. The responses stated above was first imported into the workbook and a macro has been developed using the built-in Visual Basic. When the macro is being run, it asks for the two responses. Based on the input it receives, it calculates the crack depth ratio for each of the above mentioned locations. The intermediate points are calculated using linear interpolation between the points. By plotting the calculated crack depth ratio against the crack location, the location and the size of the crack is detected.

4.4.5.1 Displacement-Displacement Sensors

Let's say we have obtained a value of 5 as slope of percentage difference in both the displacement sensors. After putting these values in input dialogue box, the macro calculates the crack depth ratio for each locations and puts them in some other part of the worksheet. Then the crack depth ratio is plotted against crack location using MATLAB. The two curves intersect at a location of 850mm and at a crack depth ratio of 0.2 (Figure 4.15) . This gives the location and size of the crack. These values have been verified to be proper by referring to the earlier computed values.

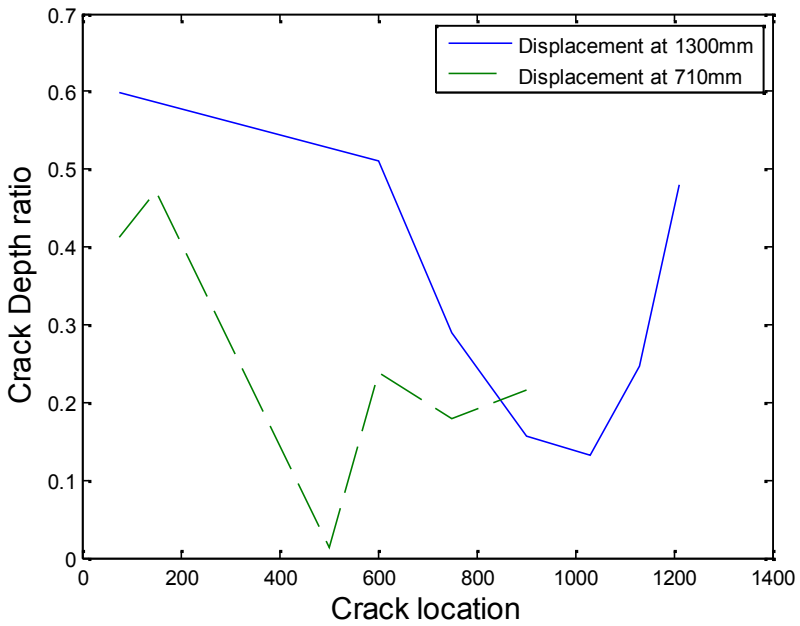

Figure 4.15: Computed Crack Depth Ratio against Crack Location; the Point of Intersection Gives the Size and Location of the Crack

4.4.5.2 Strain-Displacement Sensor

Similarly if we obtain a value of 5.5 as slope of percentage difference from the strain sensor at 410mm and a value of 4 as the slope of percentage change from the displacement sensor at 1300mm, the two curves intersect at a location of 885mm at a crack depth ratio of 0.14 (Figure 4.16). These values have also been determined to be the correct values by referring to the earlier computed values.

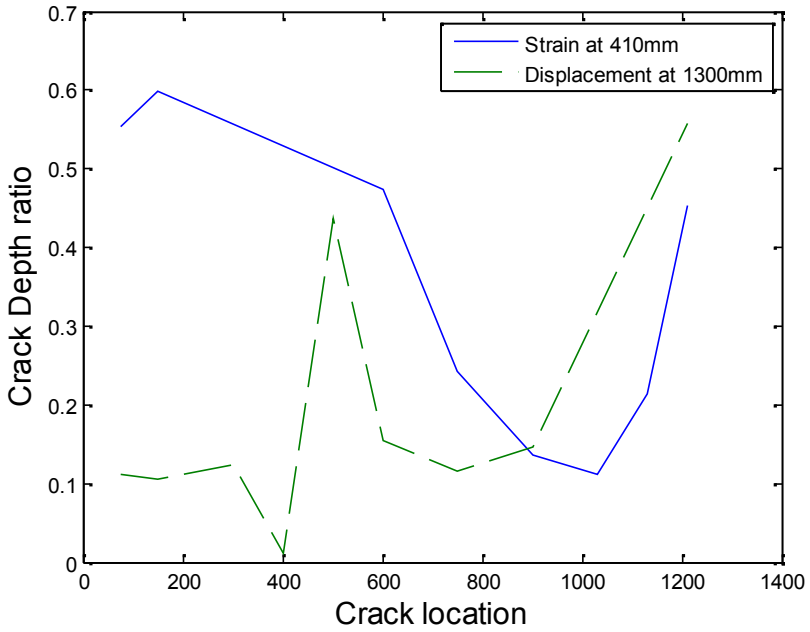

Figure 4.16: Computed Crack Depth Ratio against Crack Location; the Point of Intersection Gives the Size and Location of the Crack

4.5 Conclusions

The study outlines a simple but effective method to identify the probable location and size of the crack in a marine propeller shaft. The following conclusions can be made based on the outcome:

a) The load due to the weight of the marine propeller system causes sufficient stress to initiate and propagate cracks in the shaft.

b) Both the displacement and strain values show better percentage changes than frequency change and they can be used as effective tools for identifying crack propagation.

c) The slopes of percentage changes of displacements and strains show even higher changes and can be very useful for early crack detection. However, precision is required in measurement.

d) Since only large strain variations occur near the point of contra-flexure, they cannot detect crack presence beyond the intermediate support. Hence, a combination of results from strain-displacement sensors is required to use this method.

e) Cracks can be detected without disassembling the whole system which is more convenient than the current methods.

f) Only two sensors are required to identify crack location and size.

Acknowledgement

The authors would like to express their appreciation and thanks to Dr. R Seshadri, for his encouragement and financial support of this research. The authors would also like to thank the Faculty of Engineering and Applied Science for the facilities provided for experimental measurements and numerical analyses.

References

[1] Bently Nevada, "Early shaft crack detection on rotating machinery using vibration monitoring and diagnostics," Tech. Rep. 270, 1988.

[2] P. Bielawski, "Diagnostics of marine propeller shafts" *Journal of Polish CIMAC Selected Full Texts*, vol. 6, *(2)*, pp. 31-40, 2011.

[3] C. F. Arisoy, G. Basman and M. K. Sesen, "Failure of a 17-4 PH stainless steel sailboat propeller shaft" *Eng. Failure Anal.*, vol. 10, *(6)*, pp. 711-717, 2003. Available: http://dx.doi.org/10.1016/S1350-6307(03)00041-4. DOI: 10.1016/S1350-6307(03)00041-4.

[4] N. Sachs. (July, 2012). *Failure Analysis Of Machine Shafts, Maintenance Technology and Asset Performance*.

Available:http://www.maintenancetechnology.com/2012/07/failure-analysis-of-machine-shafts/.

[5] R. B. Hossain, R. Seshadri and A. S. Swamidas, "Identification of the size and location of A crack, using statical deformations of A marine rotor shaft with A propeller at the overhanging end," in *International Workshop on Smart Materials, Structures & SHM in Conjunction with NDT in Canada 2013 Conference & NDT for the Energy Industry*, Calgary, Alberta, CANADA, , 10 p, 2013.

[6] K. D. Hjelmstad and S. Shin, "Damage Detection and Assessment of Structures from Static Response" *J. Eng. Mech.*, vol. 123, *(6)*, pp. 568-576, 06/01; 2013/01, 1997. Available: http://dx.doi.org/10.1061/(ASCE)0733-9399(1997)123:6(568). DOI: 10.1061/(ASCE)0733-9399(1997)123:6(568).

[7] M. Di Paola and C. Bilello, "An integral equation for damage identification of Euler-Bernoulli beams under static loads" *J. Eng. Mech.*, vol. 130, *(2)*, pp. 225-234, 2004. Available: http://dx.doi.org/10.1061/(ASCE)0733-9399(2004)130:2(225). DOI: 10.1061/(ASCE)0733-9399(2004)130:2(225).

[8] G. Buda and S. Caddemi, "Identification of concentrated damages in euler-bernoulli beams under static loads" *J. Eng. Mech.*, vol. 133, *(8)*, pp. 942-956, 2007. Available: http://dx.doi.org/10.1061/(ASCE)0733-9399(2007)133:8(942). DOI: 10.1061/(ASCE)0733-9399(2007)133:8(942).

[9] S. Prabhakar, A. S. Sekhar and A. R. Mohanty, "Detection and monitoring of cracks using mechanical impedance of rotor-bearing system" *J. Acoust. Soc. Am.*, vol. 110, *(5)*, pp. 2351-2359, 2001. . DOI: http://dx.doi.org/10.1121/1.1412447.

[10] M. Kisa and M. Arif Gurel, "Free vibration analysis of uniform and stepped cracked beams with circular cross sections" *Int. J. Eng. Sci.*, vol. 45, *(2)*, pp. 364-380, 2007.

[11] P. K. Umesha, R. Ravichandran and K. Sivasubramanian, "Crack detection and quantification in beams using wavelets" *Computer-Aided Civil and Infrastructure Engineering*, vol. 24, *(8)*, pp. 593-607, 2009. Available: http://dx.doi.org/10.1111/j.1467-8667.2009.00618.x. DOI: 10.1111/j.1467-8667.2009.00618.x.

[12] U. P. Poudel, G. Fu and J. Ye, "Wavelet transformation of mode shape difference function for structural damage location identification" *Earthquake Engineering and Structural Dynamics*, vol. 36, *(8)*, pp. 1089-1107, 2007. Available: http://dx.doi.org/10.1002/eqe.673. DOI: 10.1002/eqe.673.

[13] A. Tlaisi, A. Swamidas, A. Akinturk and M. R. Haddara, "Crack detection in shafts using mechanical impedance measurements." *Mechanical Engineering Research*, vol. 2, *(2)*, pp. 10 - 30, 2012.

[14] S. Chattopadhyay, "Design fatigue curves based on small crack growth and crack closure" *Journal of Applied Science & Engineering Technology*, vol. 2, 2008.

Chapter 5

IDENTIFICATION OF SIZE AND LOCATION OF CIRCUMFERENTIAL HELICAL CRACK IN MARINE PROPELLER SHAFT USING STRAIN AND DISPLACEMENT MEASUREMENT

Ridwan B. HOSSAIN[1] & Arisi S.J. SWAMIDAS[1]

[1]Faculty of Engineering & Applied Science, Memorial University of Newfoundland, St. John's, Canada. e-mail: rbh546@mun.ca, aswamidas@mun.ca.

Preface

A version of this paper has been prepared for submission to *International Journal of Engineering Sciences and Management.* The principal author Ridwan, wrote the paper, carried out the finite element analysis by modeling the system and plotting necessary graphs. The co-author Dr. Swamidas supervised the principal author with technical guidance and reviewing of the manuscript. In this chapter the manuscript is presented with altered figure numbers, table numbers and reference formats in order to match the thesis formatting guidelines set out by Memorial University.

Abstract

The study discusses an approximated numerical method to identify and detect the presence and profile of circumferential helical cracks in a marine propeller shaft, subjected to the repeated cyclic loading effects of combined bending and torsion (Mode I + III) generated in rotating shafts. Part of such cracks remains always closed and hence conventional inspection method such as visual inspection or vibration measurement during the machine rotation fails to identify such cracks, even at very late stages of the shaft's total life. This study proposes a simple but effective method for identifying such cracks using strain and displacement measurements. The study was carried out using Finite Element Analysis on a small scale real life marine propeller shaft. It was found that due to the presence of the crack, both the percentage change and the percentage change of the slope of strains and displacements, show significant variations if measured at properly identified locations. Based on the changes in the above mentioned parameters (of strain and displacement) it is shown that the location and size of such cracks can be identified in this type of structure.

5.1 Introduction

Shafts are essential components for transmitting power in all kinds of rotational machinery and high performance rotating devices. Therefore, they are subjected to one of

the most strenuous working and repeated cyclic loading conditions and often fail due to fatigue cracking if not diagnosed at the appropriate time. According to Bachschmid et al [1], most often the information about the cracks and failure of rotor shafts are kept confidential by plant management and manufacturer. In this book the authors analyzed several rotor shaft failure cases from real life scenarios and found that early identification of damage is one of the key factors for failure prevention in shafts. Another technical report by Bently-Nevada [2] mentioned that one manufacturer had logged more than 28 incidents of shaft failure in North America for only power generation industries over the previous ten years and according to the manufacturer it was only a partial list. According to an EPRI report mentioned in that bulletin, one utility paid $6.2 million to replace power alone during an outage caused by shaft crack on turbine. The replacement cost was nearly $100,000; hence crack detection on shafts has received large attention over the past few decades. Moreover, it was also reported in that bulletin that under a specific situation, the presence of a crack was noted only when it was around 90 - 95% in crack depth, and it was stated to be a 400^0 spiral crack (see page 10 in reference [2]).

Propeller shaft is one of the key components of propulsion systems. It basically serves two purposes: (i) to transmit engine power to the propeller; (ii) to transfer the axial force to the thrust bearing. The main reason for cracking in such shafts is the stress concentration caused around discontinuities or hotspots during combined bending and torsion. So far, almost all of the work related to cracked shafts considered bending cracks only [1, 3-5]. In this study, the possibility of circumferential helical crack detection has

been discussed using an early crack detection method proposed in this study, based on variation of static parameters of strain and displacement.

5.2 Circumferential Helical Crack

Circumferential helical cracks are rare in ductile materials but they have been reported in brittle materials [6, 7]. The stable planar crack under bending (mode I) becomes inclined due to the superposition of shear stress parallel to the crack front (mode III). Under this mixed mode loading (mode I + III) condition, an initial micro crack might branch along the circumference if the probability of branching is equal everywhere along the circumference, such as in a rotor shaft under ideal conditions (without much cylindrical surface discontinuities). The combined mode I and mode III loading imposes an angle to the principal stress plane and therefore instead of being perpendicular to the principal axial plane, the crack propagates as a circumferential helical crack (see Fig 5.1-5.3). The technical bulletin of Bently-Nevada mentioned earlier [2] reported an incident of a shaft (probably constructed from a ductile metal) crack in a utility plant where they found a 400 degree spiral crack based on vibration measurement and subsequent examination after disassembly.

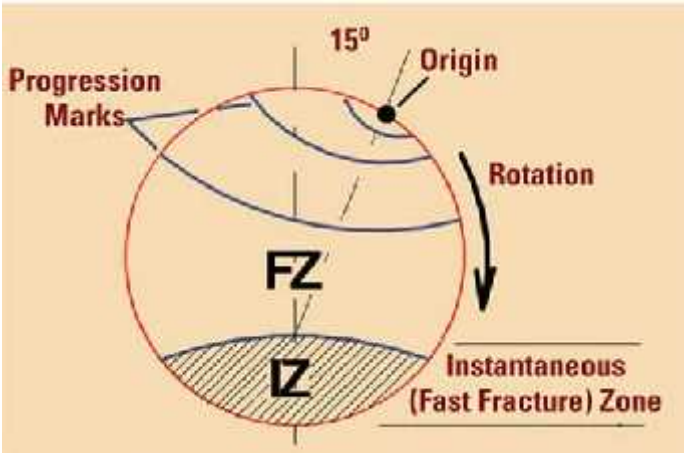

Figure 5.1: Effect of Rotating Bending (with a Heavy Bending Load) on Crack Origin [8]

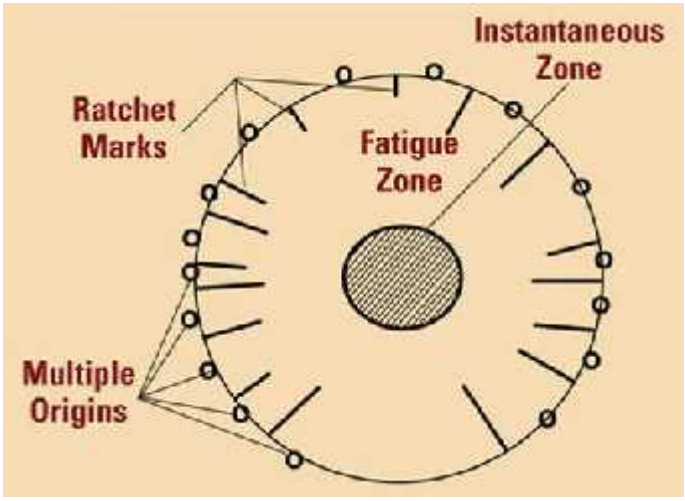

Figure 5.2: Schematic Diagram of Rotating Bending Failure (with a Lighter Bending Load) of Shafts Showing Multiple Crack Origin [8]

The major difficulty with identifying circumferential helical crack is that part of the crack remains closed, especially when the mode III loading dominates. Hence, it becomes difficult to identify such cracks at their early crack growth stage, especially with the

conventional methods such as visual inspection (using fiberscopes and magnifying glasses/mirrors). So far, the most common practice of identification method includes measurement of the super-synchronous 2X and 3X vibration components during machine rotation [2, 9] along with the 1X component. However, according to the report of Bently-Nevada [2], this methodology gives indication of crack only at a very late stage of crack growth development (in one analysis, it was found that there was already a 90-95% developed crack present in the rotating shaft, to show a significant change in 1X and 2X components of vibratory speed).

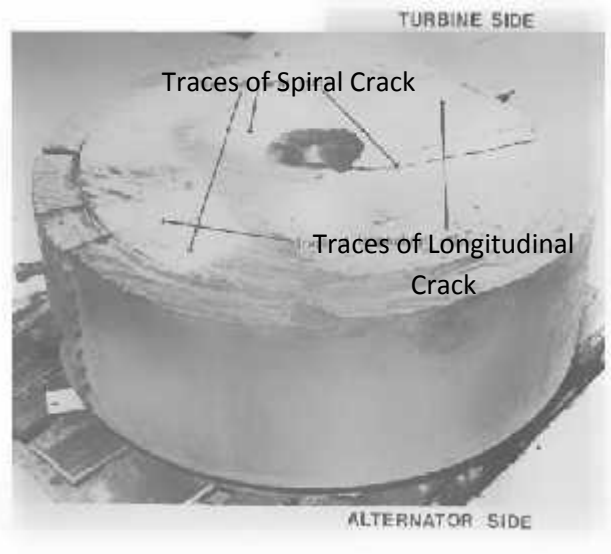

Figure 5.3: Circumferential Helical Crack on a 1.2m Diameter Hydraulic Turbine Shaft [10].

An earlier analysis carried out by Hossain et al [11] based on the use of static parameters (strain and displacement) for crack detection in rotating shafts was able to detect the presence of a bending crack at an early stage. The method was applied to a rotating

marine propeller shaft with a propeller attached to an overhanging end, where crack was initiated and propagated due to the bending effects of the propeller weight. Finite element analysis using ABAQUS was used to calculate the displacement and strain at several predefined locations. A sensor placement study was carried out to determine the most optimum placement that would give the maximum change in the measured parameters of strains and displacement. It was found that due to the presence of the propagating crack, variation of strain was high near the point of contra-flexure and variation of displacement was high near the free end. An inherent relationship was shown to exist between change in these magnitudes of strain and displacement and the crack location and crack depth, which could be used to identify the crack location and size. In this study, the same methodology has been applied to a helical circumferential crack in an overhanging marine propeller system under its weight and an identification method has been proposed for early crack detection.

5.3 Model Pre-processing and Load estimation

The propeller system considered for the analysis has four major components viz. a 4-bladed propeller, a 1.3 m steel shaft (15.75mm dia) having mounted the propeller at one end, a fixed support at the other end and an intermediate support located at 1000mm from the fixed end.

The 4 bladed propeller used in this analysis and earlier one ([11, 12]) was made of commercial bronze and weighed 15.39N having a density of 8800 kg/m^3 (Fig. 5.4). The exact modelling of the propeller was very important in this case as only the influence of its weight was considered for crack initiation and propagation. To measure and model the complex nature of the blades properly, a high-speed 3D Terrestrial Laser Scanner (TLS) manufactured by FARO was used which produced dense point clouds based on the actual shape. The propeller was scanned on both sides and point clouds were generated for each side. Both of the point clouds were then merged into a single point cloud and exported to SOLIDWORKS. Based on the location of the points, the propeller was generated using SOLIDWORKS drawing (Fig. 5.5). By defining the materials, the weight of the CAD model was evaluated and was found to be in agreement with weight measured for the actual model used in this study.

Figure 5.4: 4-bladed Propeller Used in the Analysis

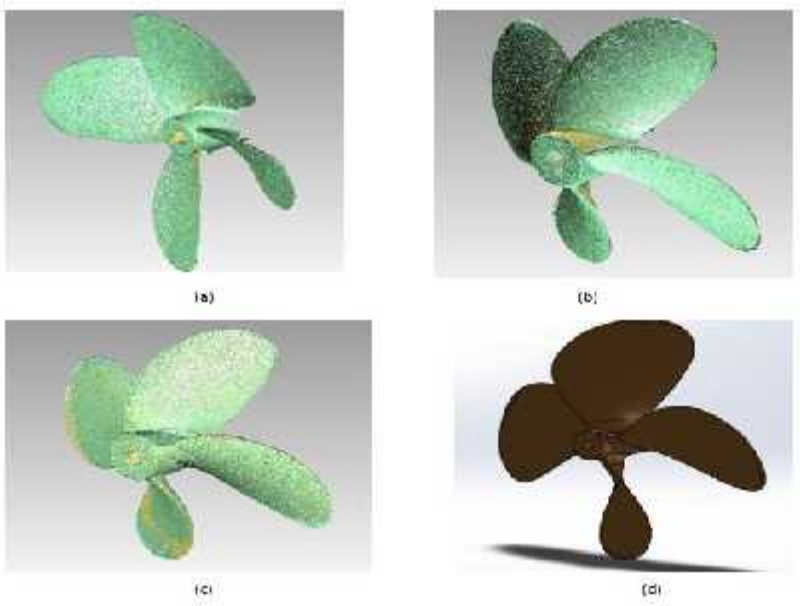

Figure 5.5: Propeller; (a) Scanned Point Cloud of side 1; (b) Scanned Point Cloud of Side 2; (c) Combined Point Cloud; (d) CAD Model

The other three propeller blade components were also modeled using SOLIDWORKS based on their dimensions and the four components were assembled. The assembly was then converted into a parasolid and exported to ABAQUS for finite element analysis. The density of the cloud of points was reduced from the laser-measured 200,000 points to 40000 points to make the data to be usable by the available computer space of the authors. In the earlier analysis carried out by Hossain et al [11], a number of locations was used to measure the strains and displacements throughout the shaft. It was found that only near the point of contra-flexure, the strain showed significant variations; and displacements showed significant variations at the free end and somewhere around the middle of the shaft, due to the presence of the crack. Therefore, in this study, to reduce

the number of the sensors to be located in actual measurement setup, strains were measured only at two locations (near the point of contra-flexure on either side (of the point of contra-flexure), i.e., 410mm and 530mm) and displacements were measured at the free end, i.e., at 1300mm and at 710 mm from the fixed end. The cracks were considered at 11 different locations from 75 mm to 1210 mm from the fixed end having crack depth ratios (depth of crack/radius of the shaft) ranging from 0.05 to 0.6 at each of the above locations.

The finite element model was meshed using a total number of 36,025 quadratic tetrahedral elements (C3D10). This type of element belongs to the 3D stress family having a quadratic shape function. The cracks used in the analysis were in nature seam cracks, which remain close initially but can open or close upon the application of appropriate load (Fig. 5.6). As it can be seen in Fig. 5.3 that the pitch of the helical crack is very small, therefore it can be considered that the crack is located in the same inclined plane, instead of being helical in nature. Smaller elements were used along the crack edges and measurement locations for ease in identification and better results. The elements around the crack are clustered together to properly represent the singularity effect present at the crack tip.

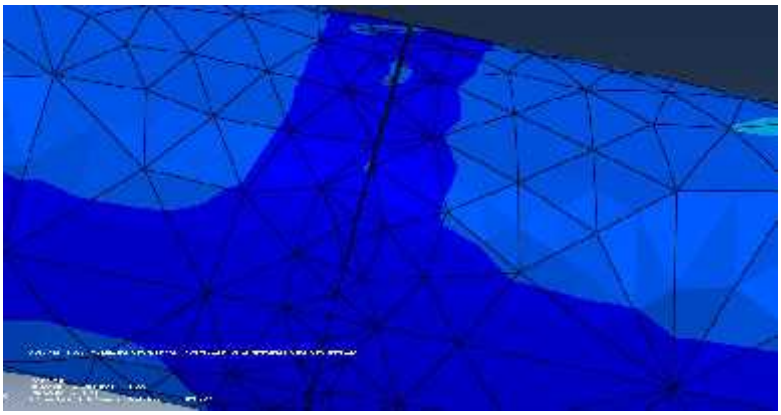

Figure 5.6: Circumferential Seam Crack; Crack location: 750mm, Crack Depth Ratio: 0.45

The bending load for the system was considered to be the weight of the components, participating in the rotary motion of the propeller shaft. The torsional load was calculated considering the study of Parsons et al [13] and then applying the similarity method proposed by Shumin et al [14]. The mass of the prototype model was 25,918.766 kg and the model ratio was calculated to be 0.0392. The total torsional load thus calculated was found to be 16.72N and considering the symmetry of the propeller blades, applied load on each blade was taken as 4.18N. These loads were applied as concentrated tangential (to the shaft circumference) forces at the centroid of each of the four blades, and were applied as a torsional couple, on the pair of opposite blades.

Moreover, the angle of the helix was obtained by measuring the inclination of principal stress plane and found to be 0.035 radians; hence the crack plane was modelled as an inclined plane at this angle. The strain and displacements, used in the subsequent crack computation, were obtained manually from the output database file. In real life, strains

gauge and laser technique might be implemented as the displacement change is sometimes small, especially for early cracks. A recent study by Kohut and Kurowski [15] has demonstrated how vision systems can be used to detect modal parameters. In addition the possibility of crack initiation was discussed in an earlier study carried out on bending crack development in marine propeller shafts [16].

5.4 Results & Discussion

5.4.1 Displacement Plots

Displacements were measured at both the locations (given earlier) for the uncracked condition at first. Then for every crack depth ratio at each location, they were monitored and the change computed; and the results were plotted as percentage change against crack depth ratio for each location (Figure 5.7 & 5.8). From both the figures it is clear that the percentage change in displacements increase rapidly with the crack depth ratio. For the same crack depth ratio, the percentage change differs from point to point, depending on the crack location, and it was found that for a 0.6 crack depth ratio, the maximum change (26.71%) obtained at first monitoring point (710 mm from fixed end) was for crack located at 750 mm from fixed end. For the same crack depth ratio, the maximum change (27.94%) obtained at the second measuring point (1300 mm from fixed end) was for crack located at 1030 mm from fixed end. Although only small changes were observed for crack depth ratios less than 0.3, they would definitely give better measurable results

for the prototype structure, due to scale model amplification ratios, if they were measured with suitable sensitive devices, under real life situations.

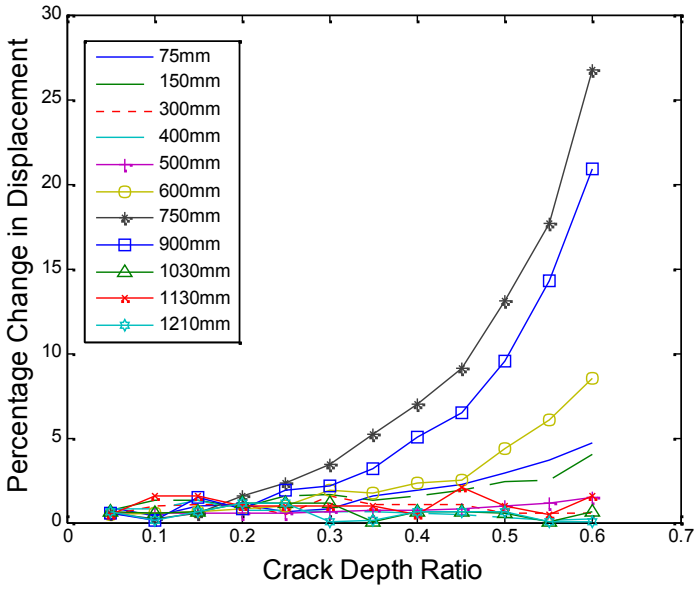

Figure 5.7: Percentage Change in Displacement against Crack Depth Ratio for the Displacement Sensor Located at 710mm from the Fixed End (Different Curves Show the Location of the Crack from Fixed End).

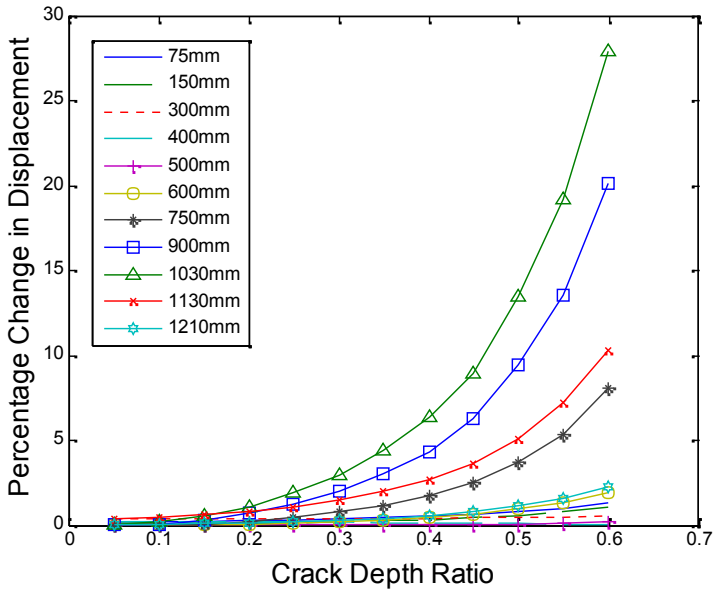

Figure 5.8: Percentage Change in Displacement against Crack Depth Ratio for the Displacement Sensor Located at 1300mm from the Fixed End (Different Curves Show the Location of the Crack from Fixed End)

5.4.2 Strain Plots

Similar to displacements, strains were also plotted as percentage difference against crack depth ratios (Figure 5.9 & 5.10). Both the plots show trends similar to displacements but the change is a little higher than displacements. For the first measuring point (410 mm from fixed end), the highest percentage change (31.31%) for crack depth ratio of 0.6 was obtained for the crack located at 750 mm from fixed end. For the second measuring point (530 mm from fixed end), the highest percentage change (22.05%) was for the crack located at same location as well. It is also clearly seen that although strain percentage

shows greater variation for location in between fixed and overhanging support, they show almost no variation for cracks located beyond the overhanging support, for both the locations. Hence it can be concluded that the strain measurements cannot be used for detecting cracks located on the overhanging end of the propeller. In addition, since the strain locations and nodal locations were manually identified from the data output obtained from the numerical computations, the improper identification of nodes and corresponding locations exist, which could have led to the fluctuations seen for the strain sensor located at 530 mm from the fixed end (see Figure 5.10).

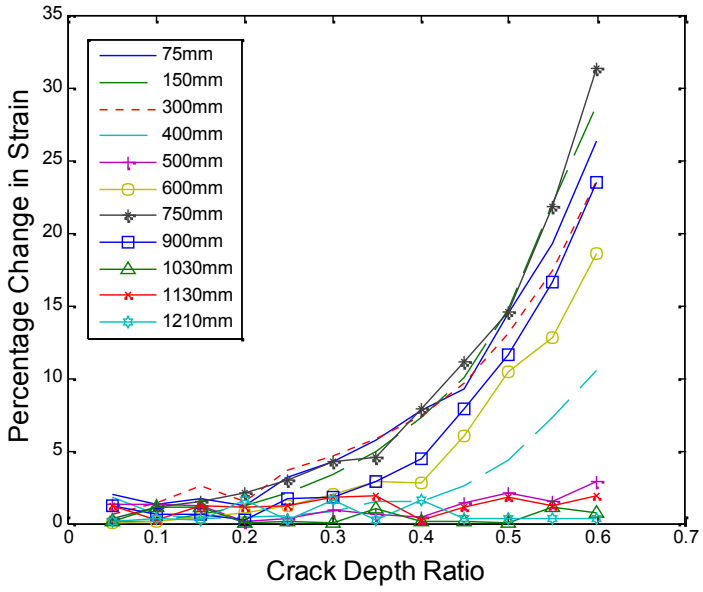

Figure 5.9: Percentage Change in Strain against Crack Depth Ratio for Strain Sensor Located at 410mm from the Fixed End (Different Curves Show the Location of the Crack from Fixed End)

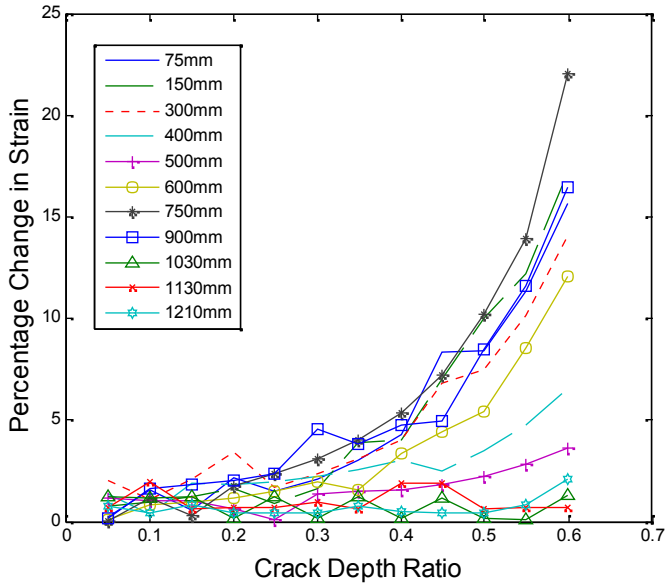

Figure 5.10: Percentage Change in Strain against Crack Depth Ratio for Strain Sensor Located at 530mm from the Fixed End (Different Curves Show the Location of the Crack from Fixed End)

5.4.3 Slope of Percentage Change in Displacement and Strain

Although, the percentage changes in displacement and strain show significant variations with crack size, for crack depth ratios below 0.3 their values are very close to each other. Even with the scale model amplification ratio, it will be difficult to identify the variation in actual prototype situations. To overcome this problem for crack identification in earlier crack growth stages, slopes of percentage changes for both displacements and strains were plotted against crack depth ratios (see Figures 5.11, 5.12, 5.13 & 5.14). Since large fluctuations were observed initially when slopes were computed from raw data, a 5-point average was done for all the values to reduce such fluctuations. The first value, viz., at a

crack depth ratio of 0.05 was not considered since the obtained initial change of slope value was very high. Thereafter all the values were considered since the computed average was the average of the five values, with two on either side of the assumed crack. The maximum slope for strain (or percentage change of slope of strain as a function of crack depth increase) was found to be up to 257.6% and 155.4%, at 410 mm and 530 mm respectively, for the 0.6 crack depth ratio. For the same crack depth ratios, the maximum slope for change of displacement was found to increase to 215.04% and 227.7%, at 710 mm and 1300 mm, respectively. These plots could be used as an effective tool for early crack detection as they provide a significant amount of change (5 - 10%) even for a very small crack depth ratio (0.1 - 0.15).

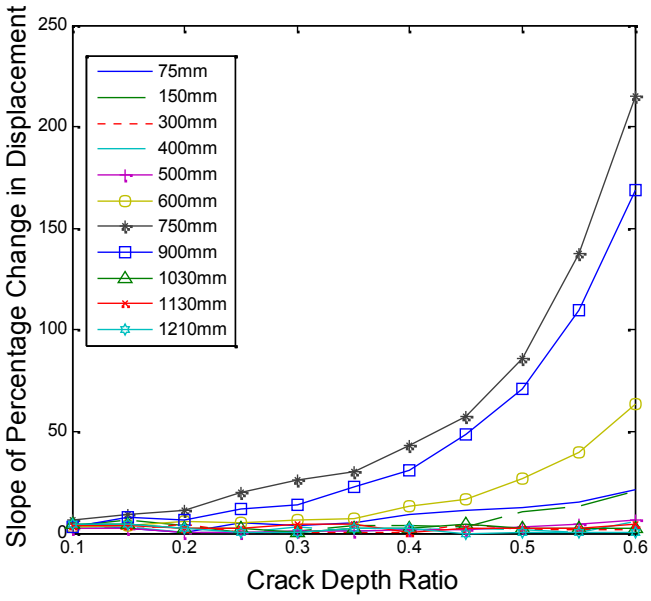

Figure 5.11: Slope of Percentage Change in Displacement against Crack Depth Ratio for Displacement Sensor Located at 710mm from the Fixed End (Different Curves Show the Location of the Crack from Fixed End)

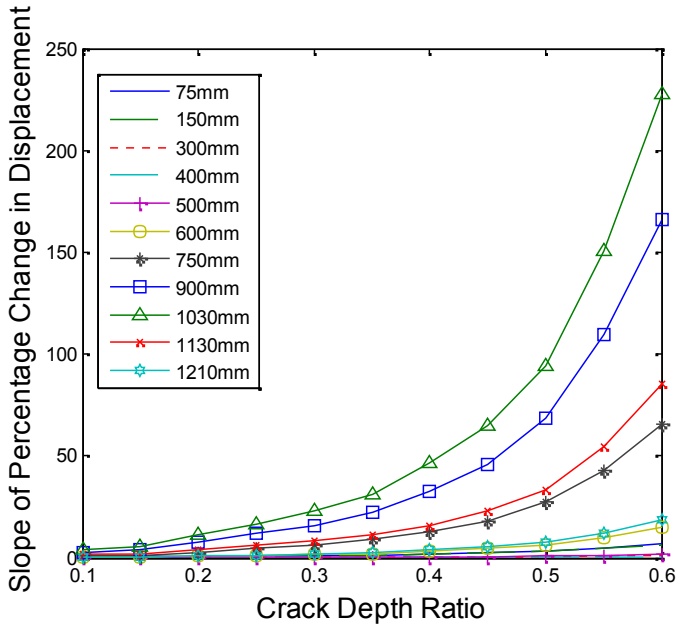

Figure 5.12: Slope of Percentage Change in Displacement against Crack Depth Ratio for Displacement Sensor Located at 1300mm from the Fixed End (Different Curves Show the Location of the Crack from Fixed End)

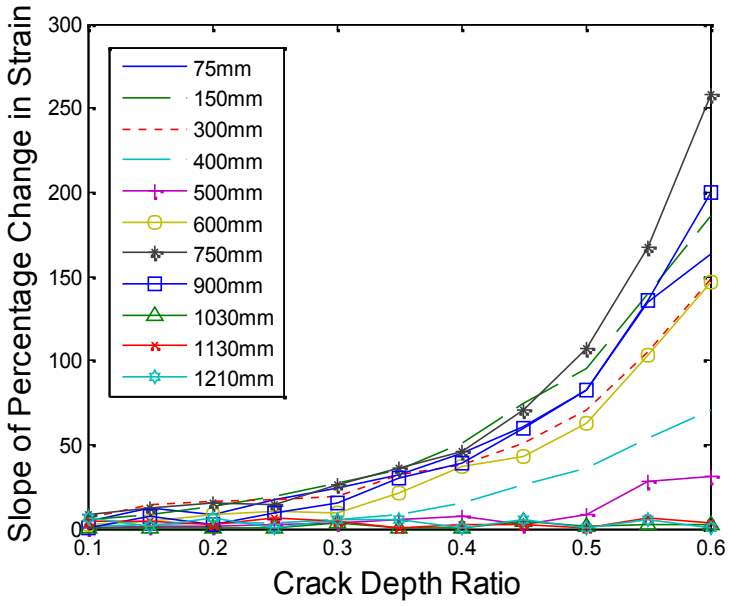

Figure 5.13:Slope of Percentage Change in Strain against Crack Depth Ratio for Strain Sensor Located at 410mm from the Fixed End (Different Curves Show the Location of the Crack from Fixed End)

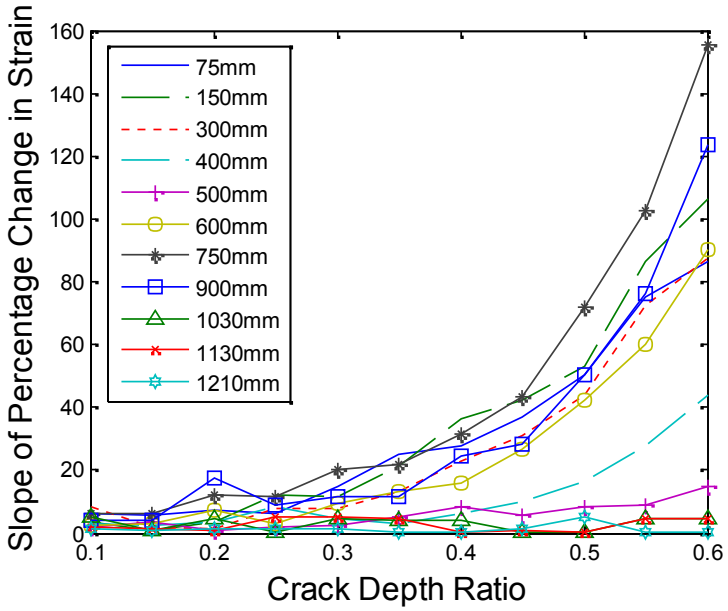

Figure 5.14: Slope of Percentage Change in Strain against Crack Depth Ratio for Strain Sensor Located at 530mm from the Fixed End (Different Curves Show the Location of the Crack from Fixed End)

It is also visualized that in real life crack growth scenarios, since the crack depth will not be known beforehand, and since the total crack growth life is analogous to the crack depth, the estimated total fatigue (or crack development) life of the specimen could be related to these percentage changes. An as alternate, instead of normalized crack depth or total fatigue life, even the total life (in terms of days or months) can be used to relate these changes in displacements and strains.

5. 4.4 Crack Detection Method

The earlier study by Hossain et al [11] showed that using the percentage differences of strains and displacements, a crack identification method (for both location and size) can be developed. It was also shown in that paper that the use of percentage of strain or displacement was able to detect crack depth ratio sizes greater than 0.30. But in the present study, it can be seen that slope of percentage differences provides much larger values than percentage difference and hence slope of percentage differences was used in this paper for crack detection. All the slope values (for percentage changes in displacement and strain) were saved in a Microsoft Excel workbook along with their corresponding crack location and size. A MATLAB script was then developed which read those values and asked for input parameters (defined – by the researcher - strain & displacement or displacement & displacement or strain & strain). The script interpolated the input values using spline interpolation and for the various specified crack locations, it calculated the crack depth ratios. The crack depth ratios beyond range (below 0.1 and above 0.6) were eliminated along with their locations and the rest were plotted against their corresponding locations. Two curves for the two given parameters (either strain & displacement or displacement & displacement) give a common point of intersection, which indicates the crack location and size. If multiple points of intersection are noted in one combination, then the other combination can be used to confirm the unique

intersection point. That means for most of cases in actual situation only two sensors would be good enough to identify both the crack location and size.

A few examples of identifying crack location and size has been illustrated below:

5.4.4.1 Strain-Displacement Plot

The first example explains the crack identification method using the slope of percentage change in difference for strain (measured at 410mm) and displacement (measured at 1300mm). Let's say both the strain and displacement sensors provide 5% change in slope value (in an actual measurement situation). By putting both the values as 5 in input dialogue box in MATLAB script, the plot shows a point of intersection having a Y value of 0.18 and X value of 910 (Figure 5.15). That means the crack is located at 910mm having a crack depth ratio of 0.18.

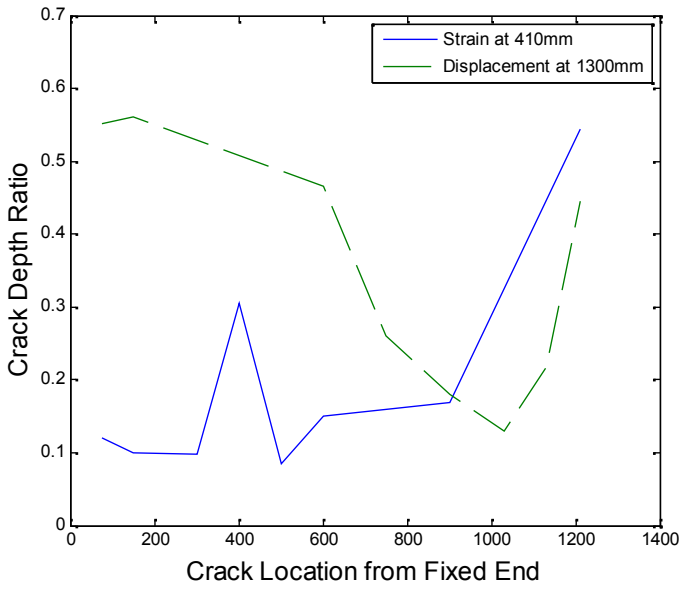

Figure 5.15: Computed Crack Depth Ratio against Crack Location; the Point of Intersection Gives the Size and Location of the Crack

5. 4.4.2 Displacement - Displacement Plot

Another way of crack identification is using the percentage change of displacement slope values (measured at 710mm and 1300mm) instead of strain changes. Now in this case let the % change values obtained (from actual measurements) be higher (for illustration), having a change of slope values of 15% at 710mm and 12% at 1300mm. The intersection shows a crack depth ratio of 0.29 to exist at 860mm (Figure 5.16).

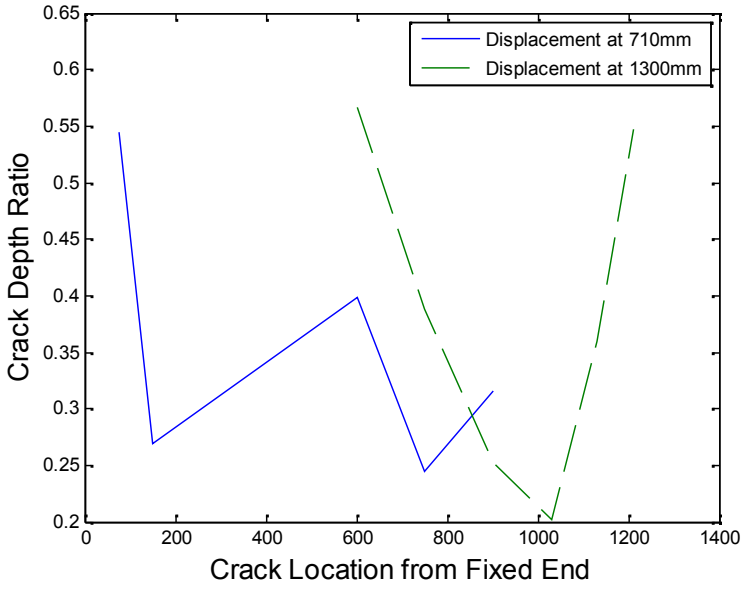

Figure 5.16: Computed Crack Depth Ratio against Crack Location; the Point of Intersection Gives the Size and Location of the Crack

5. 4.4.3 Strain-Strain Plot

Another plot was drawn using strain-strain combination having 5% change for slope values, at both the measured locations (viz., at 410 mm, and 530 mm, from the fixed end). The curves in this case showed two point of intersection; one near 400mm having a crack depth ratio of 0.3 and another is near 860mm having a crack depth ratio of 0.16 (Fig. 5.17). Such type of scenarios would require a third measurement location whose value would be used for cross-reference.

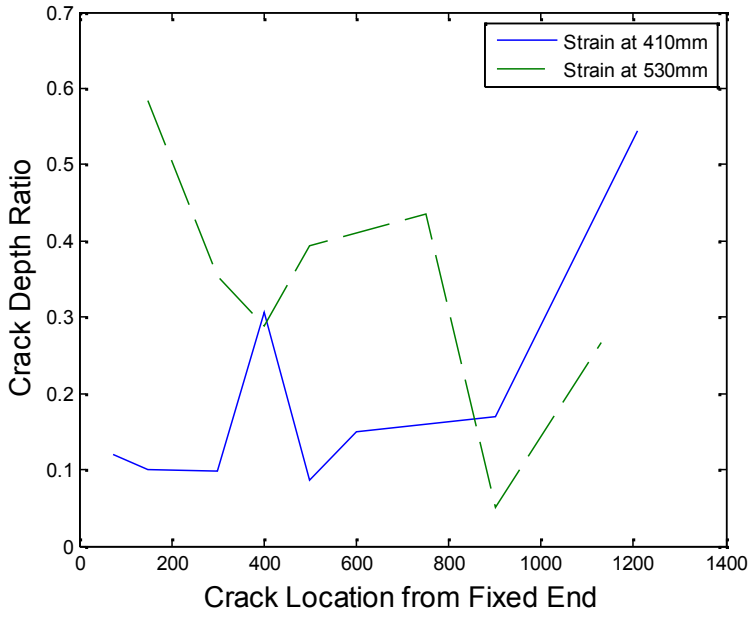

Figure 5.17: Computed Crack Depth Ratio against Crack Location; the Point of Intersection Gives the Size and Location of the Crack

5. 4.5 Difference between Bending and Circumferential Helical Crack Scenarios

A significance difference was found in the crack identification method for circumferential helical crack and bending crack (analyzed earlier by Hossain and Swamidas [16]). It was found that, both for displacement and strain, the slope showed higher percentage changes in case of an approximated helical crack. Fig. 5.18 shows an example, where strain measurements at 410mm were plotted for both type of cracks and it can be seen that the percentage change in slopes is much more rapid in the case of circumferential helical crack than bending crack, especially at high crack depth ratio.

Also, it was found that if the strain sensors were located near the crack location, in case of bending crack, it showed a higher percentage change. Fig.5.19 represents a scenario where strain sensors were located at 410mm for both type of crack at 400mm. It was found that percentage change for bending crack was up to 33.31% for a 0.60 bending crack depth ratio, whereas corresponding percentage change for a helical crack was up to 10.57%, only. Also it to be noted that if the displacements and strains were measured in the orthogonal horizontal direction, with the load also acting in the orthogonal (or horizontal) direction, then it will indicate the obvious difference between the presence of bending and approximated helical cracks. Thus a suitable combination of slope strain-displacement changes and strain-displacement changes could be used to differentiate between the existence of bending and axisymmetric approximated helical cracks, in the rotating shaft.

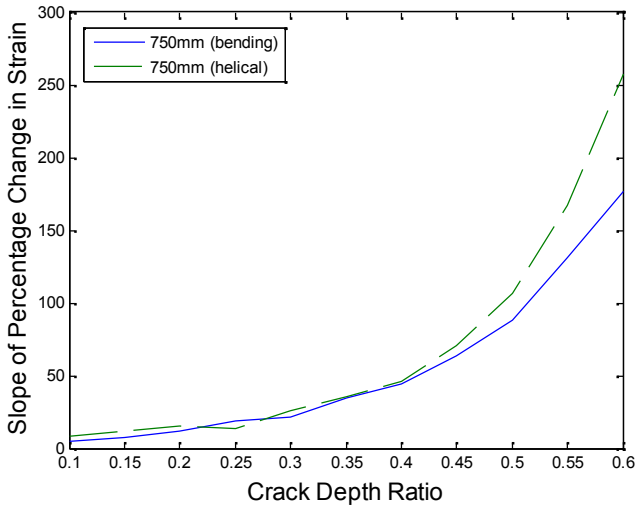

Figure 5.18: Slope of Percentage Change in Strain against Crack Depth Ratio at 750mm Location for both Crack Types (Strain Measured at 410mm).

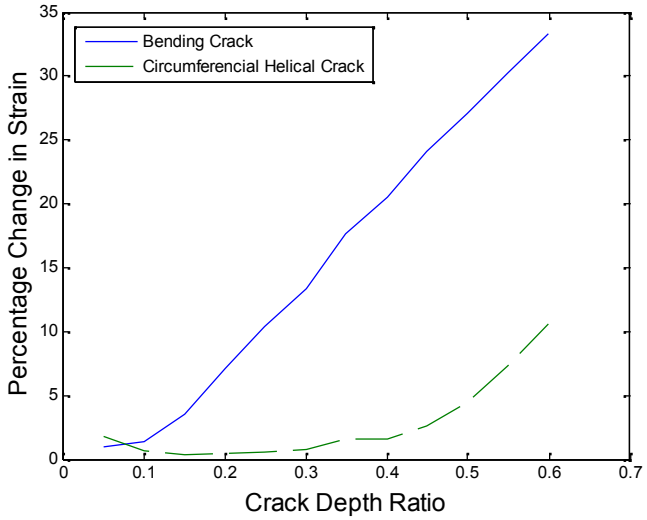

Figure 5.19: Percentage Change in Strain against Crack Depth Ratio at 400mm Location for both Crack Types (Strain Measured at 410mm)

5. 5 Conclusions

The study outlines a simple and effective method to identify the size and location of an approximated helical crack in a marine propeller shaft. The following conclusions can be made based on the outcome:

a) Circumferential helical crack can be caused in marine propeller shafts due to the rotating and bending nature of the shaft; moreover, it has also been observed from earlier research studies that even the combination of the 2X-components of the rotating shaft (at the super-synchronous speed) and/or visual inspection are not very effective in identifying such cracks as part of the crack remains always closed.

b) Both the percentage changes in strains and displacements show significant changes due to the presence of the crack and thus can be used to identify crack size and location. A change of 5% in the displacement and strain values are sufficient to detect crack around a crack depth ratio of 0.2

c) The slopes of percentage changes in strains and displacements are much higher than strains/displacements and show significant changes even during the earlier stage of crack growth; hence these changes can be used for early crack detection (as low as 0.10 – 0.15 crack depth ratio), but precision in measurement is required.

d) Although strains show much higher percentage changes than displacements these changes are negligible beyond the intermediate support; hence they should be combined with at least with one displacement measurement for identifying crack in the whole shaft.

e) Crack can be detected without disassembling the whole system and for most cases two sensors are sufficient to identify cracks.

References

[1] N. Bachschmid, P. Pennacchi and E. Tanzi, *Cracked Rotors: A Survey on Static and Dynamic Behaviour Including Modelling and Diagnosis.* Springer-Verlag, 2010.

[2] Bently Nevada, "Early shaft crack detection on rotating machinery using vibration monitoring and diagnostics," Tech. Rep. 270, 10p, 1988. Also see http//:pbadupws.nrc.gov/ ML0500/ML050060304.pdf.

[3] J. Wauer, "On the dynamics of cracked rotors: A literature survey" *Applied Mechanics Reviews,* vol. 43, *(1),* pp. 13-17, January 1, 1990.

[4] G. Sabnavis, R. G. Kirk, M. Kasarda and D. Quinn, "Cracked shaft detection and diagnostics: A literature review" *Shock Vib Dig,* vol. 36, *(4),* 2004.

[5] V. Rastogi and C. Kumar, "A brief review on dynamics of a cracked rotor" *International Journal of Rotating Machinery,* vol. vol. 2009, pp. 6 pages, 2009.

[6] A. J. Pons and A. Karma, "Helical crack-front instability in mixed-mode fracture" *Nature,* vol. 464, *(7285),* pp. 85-89, 2010.

[7] P. P. Milella, "Morphological aspects of fatigue crack growth and formation," in *Fatigue and Corrosion in Metals*, 1st ed.Springer, 2012, pp. 82.

[8] N. Sachs. (July, 2012). *Failure Analysis Of Machine Shafts, Maintenance Technology and Asset Performance*. Available: http://www.maintenancetechnology.com/2012/07/failure-analysis-of-machine-shafts/.

[9] A. Vania, P. Pennacchi and S. Chatterton, "Super-synchronous vibrations caused by transverse annular cracks in rotating machines," in *Proc. of International Conference on Surveillance-6, Acoustical and Vibratory Surveillance Methods and Diagnostic Techniques, session 2A,* Compiègne, France, 13p, 2011.

[10] P. Nguyen-Duy, "Failure analysis of a hydraulic turbine shaft," in *Fractography of Ceramic and Metal Failures*ASTM International, 1984, pp. 368.

[11] R. B. Hossain, R. Seshadri and A. S. Swamidas, "Identification of the size and location of A crack, using statical deformations of A marine rotor shaft with A propeller at the overhanging end," in *International Workshop on Smart Materials, Structures & SHM in Conjunction with NDT in Canada 2013 Conference & NDT for the Energy Industry,* Calgary, Alberta, CANADA, 10 p, 2013.

[12] A. Tlaisi, A. S. J. Swamidas, A. Akinturk and M. R. Haddara, "Crack Detection in Shafts Using Mechanical Impedance Measurements" *Mechanical Engineering Research,* vol. 2, *(2),* pp. 10 - 30, 2012.

[13] M. G. Parsons, W. S. Vorus and E. M. Richard. "Added mass and damping of vibrating propellers," PhD Thesis, University of Michigan. 1980.

[14] C. Shumin, A. Swamidas and J. Sharp, "Similarity method for modelling hydroelastic offshore platforms" *Ocean Eng.,* vol. 23, *(7),* pp. 575-595, 1996.

[15] P. Kohut and P. Kurowski, "Application of modal analysis supported by 3D vision-based measurements" *Journal of Theoretical and Applied Mechanics,* vol. 47, pp. 855-870, 2009.

[16] R. B. Hossain and A. S. Swamidas, "Identification of Size and Location a Single Bending Crack in a Mrine Propeller Shaft using Static Parameters of Strain and Displacement," *Int. J. Eng. Sci. & Mgmnt,* 2014. (submitted for publication)

Chapter 6

Summary, Findings, Conclusion & Recommendation

6.1 Summary

The study proposes a crack detection method for an overhanging marine propeller shaft with a propeller at the free end. The method is based on static strain and displacement measurements and therefore is simple and easy to implement. The analytical study was performed using a popular commercial finite element package - ABAQUS. The modeling of the whole propeller system was done mainly with SOLIDWORKS and then imported to ABAQUS. To model the exact nature of the propeller, the propeller was scanned with a 3D laser scanner and imported into SOLIDWORKS where it was modeled based on the point clouds and assembled with the rest of the rotating shaft components.

To identify the optimum locations for measurement, strain and displacements were computed at a number of locations, for a single bending crack placed in different locations. These computations showed that strain variations were significant near the point of contra-flexure whereas displacement variations were significant mainly at the free end. It was also found that if computations were made at these two locations, these two parameters of strain and displacement showed higher percentage changes than frequencies.

The study was carried out for the presence of a single bending crack and for a single circumferential approximated helical crack, in the rotating shaft. It was shown that under its rotatory motion conditions, the self-weight of the propeller system could cause cracking in the shaft. The cracks were modeled using 'seam' crack procedure, available in ABAQUS, in which the crack remained closed at the beginning of the analysis but the opening of crack was allowed after the application of load. The cracks were placed along the length of the shaft at 11 different locations. It was found that if both strain and displacement is monitored, significant variation due to the presence of crack in these tow parameters can be noted for all crack locations. The percentage change and slope of percentage change for both strain and displacement were calculated and it was found that both showed higher percentage changes than that obtained from frequency analysis and the use of 2X vibration components during synchronous speed.

Based on the analysis, a crack detection method was proposed using slope of percentage difference. The method required a script (either Visual Basic for Application (VBA) or MATLAB) which analyses the computed output data and calculates the crack depth ratio for the measured locations by interpolating the input value (given by user). The final script uses a spline interpolation and eliminates data that are beyond range. It then plots crack depth ratio against crack location and the two curves obtained from two sensor locations provide intersection point which defines the crack location and size.

6.2 Findings

The major findings of the thesis can be outlined as follows:

- Strain and displacement measurement show greater percentage change than frequency change due to the presence of the crack.
- Early crack detection is possible using slope of percentage change of computed strain and displacements
- Two sensors are sufficient to detect both crack location and size for single crack. In special cases, three sensors might be required.
- Both bending and circumferential helical crack can occur in a marine propeller shaft due to its own weight. Computed strains and displacements can identify both types of cracks at quite early stage.
- Due to the presence of the crack, significant strain variations occur near the point of contra-flexure whereas displacement is more sensitive at the free end.

6.3 Conclusions

The study proposes a simple but effective crack identification method for overhanging marine propeller shafts based on static strain and displacement computations. It was found that if computations were made at proper locations, strain and displacement changes showed higher percentage changes than frequency changes. The slope of percentage changes had a larger percentage increases with respect to crack size and

therefore could be used as an effective tool for identifying cracking at early stages of its growth. Based on the computed results, a crack detection method was proposed using MATLAB script which could identify crack location and size based on the measurement from two sensors. The study reduces the complexity and time consumption of dynamic analysis and therefore proposes an efficient technique for crack detection in marine propeller shafts which can be further extended to other types of rotating shafts as well.

6.4 Recommendation

The present work attempts to introduce a new method for identifying cracks in rotating shafts. Based on the findings and conclusions given above further extension of the work can be done to make the method applicable to different types of rotating shafts in various industrial machines and products:

- An experimental study should be carried out with the proposed setup to validate the computational findings given above. The experimental study would determine the feasibility of applying this method in practice and as well estimate the experimental errors which would provide a better and more appropriate procedure for crack identification.
- A more rigorous analytical model for strain and displacement variations along the length of the shaft with respect to crack location and size can be developed, using the classical theoretical developments. In addition the reason for higher

percentage change of strains near the point of contra-flexure could also be clarified in the model.

- In addition, relating the changes in displacements and strains to the total fatigue life (in terms of cycles of loading) or in terms of the length of days spent in crack development, would facilitate the easy application of these methods in industries.
- The method can be extended to other type of rotating shafts and structures.
- If the above technology could be further developed for online monitoring (during annual maintenance), a suitable monitoring method can be developed for crack detection in such type of structures; in addition custom-made instrumentation could be made available for such a maintenance procedure. The use of lesser numbers of sensors would be very helpful and as well prove to be economical and quick, since smaller amount of data would be required to process and predict the condition of the structure.

Bibliography

[1] C. E. Inglis, "Stresses in a plate due to the presence of cracks and sharp corners" *SPIE Milestone Series Ms*, vol. 137, pp. 3-17, 1997.

[2] K. Wieghardt, A. Sommerfeld and H. P. Rossmanith, "On splitting and cracking of elastic bodies" *Fatigue & Fracture of Engineering Materials & Structures*, vol. 18, *(12)*, pp. 1371-1405, 1995. Available: http://dx.doi.org/10.1111/j.1460-2695.1995.tb00864.x. DOI: 10.1111/j.1460-2695.1995.tb00864.x.

[3] A. Griffith, "VI. The Phenomena of Rupture and F low in Solids." *Phil.Trans.Roy.Soc.(Lon.) A*, vol. 221, pp. 163-198, 1920.

[4] A. A. Griffith, C. Biezeno and J. Burgers, "The theory of rupture" *SPIE Milestone Series Ms*, vol. 137, pp. 96-104, 1997.

[5] E. Orowan, "Fracture and strength of solids" *Reports on Progress in Physics*, vol. 12, *(1)*, pp. 185, 1949. Available: http://stacks.iop.org/0034-4885/12/i=1/a=309.

[6] G. Irwin, "Fracture dynamics," in *Fracturing of Metals, American Society for Metals*, Cleveland, OH, pp. 147-166, 1948, .

[7] G. R. Irwin, "Onset of fast crack propagation in high strength steel and aluminum alloys," in *Sagamore Research Conference Proceedings*, pp. 289-305, 1956, .

[8] G. R. Irwin, "Analysis of Stresses and Strains Near the End of a Crack Traversing a Plate" *Journal of Applied Mechanics*, vol. 24, pp. 361-364, 1957.

[9] A. A. Wells, "Unstable crack propagation in metals: Cleavage and fast fracture," in *Cranfield Crack Propagation Symposium*, pp. 210, 1961, .

[10] D. S. Dugdale, "Yielding of steel sheets containing slits" *J. Mech. Phys. Solids*, vol. 8, *(2)*, pp. 100, 1960.

Available: http://www.sciencedirect.com/science/article/pii/0022509660900132. DOI: http://dx.doi.org/10.1016/0022-5096(60)90013-2".

[11] F. M. Burdekin and D. Stone, "The crack opening displacement approach to fracture mechanics in yielding materials" *The Journal of Strain Analysis for Engineering Design*, vol. 1, *(2)*, pp. 145-153, 1966.

[12] P. Paris and F. Erdogan, "A critical analysis of crack propagation laws" *Journal of Basic Engineering*, vol. 85, *(4)*, pp. 528-533, 1963.

[13] R. G. Forman, V. Kearney and R. Engle, "Numerical analysis of crack propagation in cyclic-loaded structures" *Journal of Basic Engineering,* vol. 89, *(3),* pp. 459-463, 1967.

[14] M. Klesnil and Luk\'a\vs P, "Influence of strength and stress history on growth and stabilisation of fatigue cracks" *Eng. Fract. Mech.,* vol. 4, *(1),* pp. 77-92, 1972.

[15] R. J. Donahue, H. M. Clark, P. Atanmo, R. Kumble and A. J. McEvily, "Crack opening displacement and the rate of fatigue crack growth" *International Journal of Fracture Mechanics,* vol. 8, *(2),* pp. 209-219, 1972.

[16] R. G. Forman and S. R. Mettu, "Behavior of surface and corner cracks subjected to tensile and bending loads in ti – 6Al – 4V alloy," in *Fracture Mechanics: Twenty Second Symposium; ASTM STP 1131, American Society for Testing and Materials,* Philadelphia, PA, pp. 519-5461992, .

[17] N. Dowling and J. Begley, "Fatigue crack growth during gross plasticity and the J-integral" *Astm Stp,* vol. 590, pp. 82-103, 1976.

[18] J. Wauer, "On the dynamics of cracked rotors: A literature survey" *Applied Mechanics Reviews,* vol. 43, *(1),* pp. 13-17, January 1, 1990.

[19] R. Gasch, "Survey of the dynamic behaviour of a simple rotating shaft with a transverse crack" *J. Sound Vibrat.,* vol. 160, *(2),* pp. 313-332, 1993. Available: http://dx.doi.org/10.1006/jsvi.1993.1026. DOI: 10.1006/jsvi.1993.1026.

[20] V. Rastogi and C. Kumar, "A brief review on dynamics of a cracked rotor" *International Journal of Rotating Machinery,* vol. vol. 2009, pp. 6 pages, 2009.

[21] O. S. Salawu, "Detection of structural damage through changes in frequency: A review" *Eng. Struct.,* vol. 19, *(9),* pp. 718-723, 1997. Available: http://dx.doi.org/10.1016/S0141-0296(96)00149-6. DOI: 10.1016/S0141-0296(96)00149-6.

[22] S. W. Doebling, C. R. Farrar and M. B. Prime, "Summary review of vibration-based damage identification methods" *Shock Vib Dig,* vol. 30, *(2),* pp. 91-105, 1998.

[23] J. M. Lifshitz and A. Rotem, "Determination of reinforcement unbonding of composites by a vibration technique" *J. Composite Mater.,* vol. 3, *(3),* pp. 412-423, 1969.

[24] R. D. Adams, P. Cawley, C. J. Pye and B. J. Stone, "Vibration technique for non-destructively assessing the integrity of structures" vol. 20, *(2),* pp. 93-100, 1978.

[25] R. Adams, D. Walton, J. Flitcroft and D. Short, "Vibration testing as a nondestructive test tool for composite materials" *Composite Reliability*, vol. 580, pp. 159-175, 1975.

[26] P. F. Rizos, N. Aspragathos and A. D. Dimarogonas, "Identification of crack location and magnitude in a cantilever beam from the vibration modes" *J. Sound Vibrat.*, vol. 138, *(3)*, pp. 381-388, 1990. Available: http://dx.doi.org/10.1016/0022-460X(90)90593-O. DOI: 10.1016/0022-460X(90)90593-O.

[27] G. Hearn and R. Testa, "Modal Analysis for Damage Detection in Structures" *J. Struct. Eng.*, vol. 117, *(10)*, pp. 3042-3063, 1991. Available: http://ascelibrary.org/doi/abs/10.1061/%28ASCE%290733-9445%281991%29117%3A10%283042%29. DOI: 10.1061/(ASCE)0733-9445(1991)117:10(3042).

[28] M. Friswell, J. Penny and D. Wilson, "Using vibration data and statistical measures to locate damage in structures" *Modal Analysis: The International Journal of Analytical and Experimental Modal Analysis*, vol. 9, *(4)*, pp. 239-254, 1994.

[29] Y. Narkis, "Identification of crack location in vibrating simply supported beams" *J. Sound Vibrat.*, vol. 172, *(4)*, pp. 549-558, 1994. Available: http://dx.doi.org/10.1006/jsvi.1994.1195. DOI: 10.1006/jsvi.1994.1195.

[30] M. -. H. Shen and C. Pierre, "Natural modes of Bernoulli-Euler beams with symmetric cracks" *J. Sound Vibrat.*, vol. 138, *(1)*, pp. 115-134, 1990. Available: http://dx.doi.org/10.1016/0022-460X(90)90707-7. DOI: 10.1016/0022-460X(90)90707-7.

[31] B. S. Haisty and W. T. Springer, "General beam element for use in damage assessment of complex structures" *Journal of Vibration, Acoustics, Stress, and Reliability in Design*, vol. 110, *(3)*, pp. 389-394, 1988.

[32] F. Vestroni and D. Capecchi, "Damage evaluation in cracked vibrating beams using experimental frequencies and finite element models" *JVC/Journal of Vibration and Control*, vol. 2, *(1)*, pp. 69-86, 1996.

[33] D. Capecchi and F. Vestroni, "Identification of finite element models in structural dynamics" *Eng. Struct.*, vol. 15, *(1)*, pp. 21-30, 1993. Available: http://dx.doi.org/10.1016/0141-0296(93)90013-T. DOI: 10.1016/0141-0296(93)90013-T.

[34] P. G. Nikolakopoulos, D. E. Katsareas and C. A. Papadopoulos, "Crack identification in frame structures" *Computers and Structures*, vol. 64, *(1-4)*, pp. 389-406, 1997. Available: http://dx.doi.org/10.1016/S0045-7949(96)00120-4. DOI: 10.1016/S0045-7949(96)00120-4.

[35] D. R. Perchard and A. Swamidas. Crack detection in slender cantilever plates using modal analysis. Presented at Proceedings of the 12th International Modal Analysis Conference. pp. 1769-1777, 1994.

[36] D. Nwosu, A. Swamidas and J. Guigne , "Dynamic response of tubular T-joints under the influence of propagating cracks" *Journal of Offshore Mechanics and Arctic Engineering*, vol. 118, *(1)*, pp. 71-78, 1996.

[37] Y. Li, J. Guigne and A. Swamidas. Acoustical modal response of a submerged cantilever plate for non-contact fatigue crack detection application. Presented at Proceedings of SPIE, the International Society for Optical Engineering. pp. 1973-1979, 1997.

[38] S. Cheng, A. Swamidas, W. Wallace and X. Wu, "Nondestructive detection of cracks in tubular T-joints using vibration characteristics" *Journal of Offshore Mechanics and Arctic Engineering*, vol. 121, *(3)*, pp. 144-152, 1999.

[39] G. Owolabi, A. Swamidas and R. Seshadri, "Crack detection in beams using changes in frequencies and amplitudes of frequency response functions" *J. Sound Vibrat.*, vol. 265, *(1)*, pp. 1-22, 2003.

[40] X. F. Yang, A. S. J. Swamidas and R. Seshadri, "Crack identification in vibrating beams using the energy method" *J. Sound Vibrat.,* vol. 244, *(2),* pp. 339-357, 2001. Available: http://dx.doi.org/10.1006/jsvi.2000.3498. DOI: 10.1006/jsvi.2000.3498.

[41] X. Yang, I. Datta, A. S. Swamidas and R. Seshadri, "Coupled Bending-Torsional Vibration of a Cracked Hollow Beam Model in Water and Identification of Cracking" *Journal of Vibration and Acoustics,* vol. 127, *(6),* pp. 575-587, September 8, 2004. . DOI: 10.1115/1.1888587.

[42] T. D. Chaudhari and S. K. Maiti, "Study of vibration of geometrically segmented beams with and without crack" *Int. J. Solids Structures,* vol. 37, *(5),* pp. 761-779, 2000.

[43] S. Chinchalkar, "Determination of crack location in beams using natural frequencies" *J. Sound Vibrat.,* vol. 247, *(3),* pp. 417-429, 2001. Available: http://dx.doi.org/10.1006/jsvi.2001.3748. DOI: 10.1006/jsvi.2001.3748.

[44] A. Morassi, "Identification of a crack in a rod based on changes in a pair of natural frequencies" *J. Sound Vibrat.,* vol. 242, *(4),* pp. 577-596, 2001. Available: http://dx.doi.org/10.1006/jsvi.2000.3380. DOI: 10.1006/jsvi.2000.3380.

[45] D. Armon, Y. Ben-Haim and S. Braun, "Crack detection in beams by rankordering of eigenfrequency shifts" *Mechanical Systems and Signal Processing,* vol. 8, *(1),* pp. 81-91, 1, 1994. . DOI: 10.1006/mssp.1994.1006.

[46] Y. Lee and M. Chung, "Study on crack detection using eigenfrequency test data" *Computers and Structures*, vol. 77, *(3)*, pp. 327-342, 2000. Available: http://dx.doi.org/10.1016/S0045-7949(99)00194-7. DOI: 10.1016/S0045-7949(99)00194-7.

[47] P. Gudmundson, "Eigenfrequency changes of structures due to cracks, notches or other geometrical changes" *J. Mech. Phys. Solids*, vol. 30, *(5)*, pp. 339-353, 1982. Available: http://dx.doi.org/10.1016/0022-5096(82)90004-7. DOI: 10.1016/0022-5096(82)90004-7.

[48] F. K. Choy, R. Liang and P. Xu, "Fault identification of beams on elastic foundation" *Comput. Geotech.*, vol. 17, *(2)*, pp. 157-176, 1995. Available: http://www.sciencedirect.com/science/article/pii/0266352X9593867I. DOI: http://dx.doi.org/10.1016/0266-352X(95)93867-I.

[49] E. P. Carden and P. Fanning, "Vibration based condition monitoring: a review" *Structural Health Monitoring*, vol. 3, *(4)*, pp. 355-377, 2004.

[50] Y. Chen. "Crack detection in plated T-joints through vibration techniques," M.Eng. Thesis, Memorial University of Newfoundland. 135 pages, 1996.

[51] R. J. Allemang and D. L. Brown, "Correlation coefficient for modal vector analysis," in *Proceedings of the 1st International Modal Analysis Conference & Exhibit.* pp. 110-116, 1982.

[52] N. A. J. Lieven and D. J. Ewins, "Spatial correlationof modespaces: The coordinate modal assurance criterion (COMAC)," in *Proceedings of the 6th International Modal Analysis Conference*, Kissimmee, Florida, USA, pp. 1063-1070, 1988.

[53] A. Messina, E. J. Williams and T. Contursi, "Structural damage detection by a sensitivity and statistical-based method" *J. Sound Vibrat.,* vol. 216, *(5),* pp. 791-808, 1998. Available: http://dx.doi.org/10.1006/jsvi.1998.1728. DOI: 10.1006/jsvi.1998.1728.

[54] Z. Shi, S. Law and L. Zhang, "Damage Localization by Directly Using Incomplete Mode Shapes" *J. Eng. Mech.,* vol. 126, *(6),* pp. 656-660, 2000. Available: http://ascelibrary.org/doi/abs/10.1061/%28ASCE%290733-9399%282000%29126%3A6%28656%29. DOI: 10.1061/(ASCE)0733-9399(2000)126:6(656).

[55] A. Z. Khan, A. B. Stanbridge and D. J. Ewins, "Detecting damage in vibrating structures with a scanning LDV," in *Third International Conference on: Vibration Measurements by Laser Techniques: Advances and Applications, June 16, 1998 - June 19*, pp. 449-457, 1998.

[56] D. S. Araujo, C. M. M. Soares, C. A. Mota Soares and H. L. G. Pina, "Damage identification numerical model based on the sensitivity of orthogonality conditions and least squares techniques" *Computers and Structures,* vol. 78, *(1),* pp. 283-291, 2000. Available: http://dx.doi.org/10.1016/S0045-7949(00)00084-5. DOI: 10.1016/S0045-7949(00)00084-5.

[57] C. M. Mota Soares, M. M. de Freitas and A. L. Araujo, "Identification of material properties of composite plate specimens" *Composite Structures,* vol. 25, *(1-4),* pp. 277-285, 1993.

[58] C. P. Ratcliffe and W. J. Bagaria, "Vibration Technique for Locating Delamination in a Composite Beam" *AIAA J.*, vol. 36, *(6),* pp. 1074-1077, 06/01; 2013/01, 1998. Available: http://dx.doi.org/10.2514/2.482. DOI: 10.2514/2.482.

[59] W. Abdel M.M. and R. De G., "Damage detection in bridges using modal curvatures: Application to a real damage scenario" *J. Sound Vibrat.,* vol. 226, *(2),* pp. 217-235, 1999. Available: http://dx.doi.org/10.1006/jsvi.1999.2295. DOI: 10.1006/jsvi.1999.2295.

[60] B. H. Oh and B. S. Jung, "Structural damage assessment with combined data of static and modal tests" *Journal of Structural Engineering New York, N. Y.*, vol. 124, *(8),* pp. 956-965, 1998. Available: http://dx.doi.org/10.1061/(ASCE)0733-9445(1998)124:8(956). DOI: 10.1061/(ASCE)0733-9445(1998)124:8(956).

[61] K. D. Hjelmstad and S. Shin, "Damage Detection and Assessment of Structures from Static Response" *J. Eng. Mech.,* vol. 123, *(6),* pp. 568-576, 06/01; 2013/01, 1997. Available: http://dx.doi.org/10.1061/(ASCE)0733-9399(1997)123:6(568). DOI: 10.1061/(ASCE)0733-9399(1997)123:6(568).

[62] M. R. Banan, M. R. Banan and K. D. Hjelmstad, "Parameter estimation of structures from static response. I. Computational aspects" *Journal of Structural Engineering New York, N. Y.,* vol. 120, *(11),* pp. 3243-3258, 1994.

[63] M. Di Paola, "Probabilistic analysis of truss structures with uncertain parameters (virtual distortion method approach)" *Prob. Eng. Mech.,* vol. 19, *(4),* pp. 321-329, 2004. Available: http://dx.doi.org/10.1016/j.probengmech.2003.10.001. DOI: 10.1016/j.probengmech.2003.10.001.

[64] M. Di Paola and C. Bilello, "An integral equation for damage identification of Euler-Bernoulli beams under static loads" *J. Eng. Mech.,* vol. 130, *(2),* pp. 225-234, 2004. Available: http://dx.doi.org/10.1061/(ASCE)0733-9399(2004)130:2(225). DOI: 10.1061/(ASCE)0733-9399(2004)130:2(225).

[65] F. Vestroni and D. Capecchi, "Damage detection in beam structures based on frequency measurements" *J. Eng. Mech.,* vol. 126, *(7),* pp. 761-768, 2000. Available: http://dx.doi.org/10.1061/(ASCE)0733-9399(2000)126:7(761). DOI: 10.1061/(ASCE)0733-9399(2000)126:7(761).

[66] M. N. Cerri and F. Vestroni, "Detection of damage in beams subjected to diffused cracking" *J. Sound Vibrat.*, vol. 234, *(2)*, pp. 259-276, 2000. Available: http://dx.doi.org/10.1006/jsvi.1999.2887. DOI: 10.1006/jsvi.1999.2887.

[67] G. Buda and S. Caddemi, "Identification of concentrated damages in euler-bernoulli beams under static loads" *J. Eng. Mech.*, vol. 133, *(8)*, pp. 942-956, 2007. Available: http://dx.doi.org/10.1061/(ASCE)0733-9399(2007)133:8(942). DOI: 10.1061/(ASCE)0733-9399(2007)133:8(942).

[68] S. Caddemi and A. Morassi, "Crack detection in elastic beams by static measurements" *Int. J. Solids Structures*, vol. 44, *(16)*, pp. 5301-5315, 2007. Available: http://dx.doi.org/10.1016/j.ijsolstr.2006.12.033. DOI: 10.1016/j.ijsolstr.2006.12.033.

[69] P. K. Umesha, R. Ravichandran and K. Sivasubramanian, "Crack detection and quantification in beams using wavelets" *Computer-Aided Civil and Infrastructure Engineering*, vol. 24, *(8)*, pp. 593-607, 2009. Available: http://dx.doi.org/10.1111/j.1467-8667.2009.00618.x. DOI: 10.1111/j.1467-8667.2009.00618.x.

[70] U. P. Poudel, G. Fu and J. Ye, "Wavelet transformation of mode shape difference function for structural damage location identification" *Earthquake Engineering and Structural Dynamics*, vol. 36, *(8)*, pp. 1089-1107, 2007. Available: http://dx.doi.org/10.1002/eqe.673. DOI: 10.1002/eqe.673.

[71] Bently Nevada, "Early shaft crack detection on rotating machinery using vibration monitoring and diagnostics," Tech. Rep. 270, 10p, 1988. Also see http//:pbadupws.nrc.gov/ ML0500/ML050060304.pdf.

[72] K. R. Collins, J. Wauer and R. H. Plaut, "Detection of Cracks in Rotating Timoshenko Shafts Using Axial Impulses" *Journal of Vibration and Acoustics*, vol. 113, *(1)*, pp. 74-78, January 1, 1991. DOI: 10.1115/1.2930158.

[73] G. D. Gounaris and C. A. Papadopoulos, "Crack identification in rotating shafts by coupled response measurements" *Eng. Fract. Mech.*, vol. 69, *(3)*, pp. 339-352, 2002.

[74] S. Prabhakar, A. S. Sekhar and A. R. Mohanty, "Detection and monitoring of cracks using mechanical impedance of rotor-bearing system" *J. Acoust. Soc. Am.*, vol. 110, *(5)*, pp. 2351-2359, 2001. DOI: http://dx.doi.org/10.1121/1.1412447.

[75] W. R. Brook, T. P. Mannix, W. H. Miller and S. E. Thibault. Multiple axis transducer mounting collar. US Patent # 5520061 A, Publication Date, May 28, 1996. Available: http://www.google.ca/patents/US5520061.

[76] A. Sekhar and B. Srinivas, "Dynamics of cracked composite shafts" *J Reinf Plast Compos*, vol. 22, *(7)*, pp. 637-653, 2003.

[77] M. Kisa and M. Arif Gurel, "Free vibration analysis of uniform and stepped cracked beams with circular cross sections" *Int. J. Eng. Sci.*, vol. 45, *(2)*, pp. 364-380, 2007.

[78] W. C. Hurty, "Dynamic analysis of structural systems using component modes" *AIAA J.*, vol. 3, *(4)*, pp. 678-685, 1965.

[79] C. Lissenden, S. Tissot, M. Trethewey and K. Maynard, "Torsion response of a cracked stainless steel shaft" *Fatigue \& Fracture of Engineering Materials \& Structures*, vol. 30, *(8)*, pp. 734-747, 2007.

[80] C. F. Arisoy, G. Ba\csman and M. K. \cSe\csen, "Failure of a 17-4 PH stainless steel sailboat propeller shaft" *Eng. Failure Anal.*, vol. 10, *(6)*, pp. 711-717, 2003.

[81] P. Bielawski, "Diagnostics of marine propeller shafts" *Journal of Polish CIMAC*, vol. 6, pp. 31-40, 2011.

[82] A. Tlaisi, A. Swamidas, A. Akinturk and M. R. Haddara, "Crack detection in shafts using mechanical impedance measurements." *Mechanical Engineering Research*, vol. 2, *(2)*, pp. 10-30, 2012.

[83] T. K. Yu and J. H. Seinfeld, "Observability and optimal measurement location in linear distributed parameter systems " *Int J Control*, vol. 18, *(4)*, pp. 785-799, 1973.

[84] R. F. Guratzsch and S. Mahadevan. Sensor placement design for shm under uncertainty. Presented at Proc. 3rd European Workshop: Structural Health Monitoring. pp. 1168-1175, 2006.

[85] K. Worden and A. Burrows, "Optimal sensor placement for fault detection" *Eng. Struct.*, vol. 23, *(8)*, pp. 885-901, 2001.

[86] P. H. Kirkegaard and R. Brincker, "On the optimal location of sensors for parametric identification of linear structural systems" *Mechanical Systems and Signal Processing*, vol. 8, *(6)*, pp. 639-647, 1994.

[87] N. G. Singh and M. Joshi, "Optimization of location and number of sensors for structural health monitoring using genetic algorithm," in *Materials Forum*, pp. 359-367, 2009.

[88] F. M. Hemez and C. Farhat. An energy based optimum sensor placement criterion and its application to structural damage detection. Presented at Proceedings-SPIE the International Society for Optical Engineering. pp. 1568, 1994.

[89] H. Gao and J. L. Rose. Ultrasonic sensor placement optimization in structural health monitoring using evolutionary strategy. Presented at AIP Conference on Quantitative Nondestructive Evaluation. pp. 1687-1693, 2006.

[90] H. Guo, L. Zhang, L. Zhang and J. Zhou, "Optimal placement of sensors for structural health monitoring using improved genetic algorithms" *Smart Mater Struct*, vol. 13, *(3)*, pp. 528-534, 2004.

Appendices

Appendix A

This appendix includes all the computational results obtained using the setup mentioned in Chapter 3 i.e. bending crack caused by concentrated load at the end. The results show that significant changes in strain occur only near the point of contra-flexure and significant changes in displacement occur near locations of maximum positive and negative displacements, viz., at 710 mm from the fixed end and at the free end.

Table A1: Strains for crack located at 200mm from fixed end

Crack Depth Ratio	Strain at 300mm	Percentage of difference	Strain at 450mm	Percentage of difference	Strain at 600mm	Percentage of difference
uncracked	4.61E-06		-1.26E-05		-2.99E-05	
0.05	4.62E-06	0.245352	-1.26E-05	0.161301	-2.98E-05	0.368404
0.1	4.60E-06	0.095752	-1.27E-05	0.622159	-2.98E-05	0.248614
0.15	4.58E-06	0.51741	-1.26E-05	0.42113	-2.98E-05	0.272036
0.2	4.52E-06	1.798017	-1.27E-05	0.854973	-2.99E-05	0.09436
0.25	4.47E-06	2.946177	-1.27E-05	0.970982	-2.99E-05	0.011042
0.3	4.34E-06	5.679353	-1.28E-05	1.589168	-3.00E-05	0.398518
0.35	4.27E-06	7.299544	-1.29E-05	2.461622	-3.00E-05	0.311186
0.4	4.13E-06	10.24811	-1.30E-05	3.160856	-3.02E-05	0.970029
0.45	3.95E-06	14.25907	-1.32E-05	4.540254	-3.02E-05	0.957983
0.5	3.66E-06	20.43738	-1.32E-05	4.729365	-3.04E-05	1.555259
0.55	3.33E-06	27.69502	-1.36E-05	8.366971	-3.06E-05	2.421894
0.6	2.87E-06	37.75292	-1.40E-05	11.33951	-3.09E-05	3.308271

Table A1 (contd.)

Crack Depth Ratio	Strain at 750mm	Percentage of difference	Strain at 900mm	Percentage of difference	Strain at 1100mm	Percentage of difference
uncracked	-4.70E-05		-6.42E-05		-5.20E-05	
0.05	-4.70E-05	0.036985	-6.44E-05	0.363807	-5.22E-05	0.415051934
0.1	-4.70E-05	0.098839	-6.42E-05	0.010127	-5.21E-05	0.200887445
0.15	-4.70E-05	0.120094	-6.43E-05	0.150197	-5.20E-05	0.096980146
0.2	-4.72E-05	0.372187	-6.44E-05	0.325479	-5.21E-05	0.226671849
0.25	-4.71E-05	0.076308	-6.42E-05	0.037549	-5.21E-05	0.201657129
0.3	-4.71E-05	0.025082	-6.42E-05	0.00966	-5.20E-05	0.095440779
0.35	-4.71E-05	0.139862	-6.44E-05	0.413353	-5.20E-05	0.118338869
0.4	-4.72E-05	0.311608	-6.43E-05	0.215947	-5.21E-05	0.160479051
0.45	-4.75E-05	0.948215	-6.44E-05	0.329685	-5.20E-05	0.089090888
0.5	-4.73E-05	0.623854	-6.44E-05	0.382971	-5.20E-05	0.079277421
0.55	-4.75E-05	0.99604	-6.46E-05	0.588791	-5.20E-05	0.066000377
0.6	-4.77E-05	1.340169	-6.46E-05	0.705645	-5.20E-05	0.060227749

Table A1 (contd.)

Crack Depth Ratio	Strain at 1180mm	Percentage of difference
uncracked	-3.11E-05	
0.05	-3.10E-05	0.376287
0.1	-3.10E-05	0.458228
0.15	-3.10E-05	0.388176
0.2	-3.11E-05	0.085476
0.25	-3.11E-05	0.065874
0.3	-3.11E-05	0.008033
0.35	-3.11E-05	0.210476
0.4	-3.11E-05	0.101864
0.45	-3.13E-05	0.452122
0.5	-3.13E-05	0.533099
0.55	-3.13E-05	0.552058
0.6	-3.11E-05	0.189589

Table A2: Strains for crack located at 400mm from fixed end

Crack Depth Ratio	Strain at 300mm	Percentage of difference	Strain at 450mm	Percentage of difference	Strain at 600mm	Percentage of difference
uncracked	4.61E-06		-1.26E-05		-2.99E-05	
0.05	4.62E-06	0.284434	-1.26E-05	0.103296	-2.99E-05	0.012715
0.1	4.61E-06	0.094015	-1.26E-05	0.407622	-2.98E-05	0.289436
0.15	4.63E-06	0.622716	-1.26E-05	0.023043	-2.98E-05	0.410899
0.2	4.58E-06	0.520016	-1.27E-05	0.57369	-2.98E-05	0.329589
0.25	4.66E-06	1.238701	-1.25E-05	0.323396	-2.98E-05	0.237572
0.3	4.69E-06	1.798668	-1.25E-05	0.467215	-2.98E-05	0.33695
0.35	4.73E-06	2.643938	-1.25E-05	0.557798	-2.98E-05	0.314532
0.4	4.77E-06	3.579098	-1.25E-05	0.921718	-2.98E-05	0.40956
0.45	4.83E-06	4.899655	-1.24E-05	1.199822	-2.97E-05	0.754541
0.5	4.96E-06	7.69645	-1.23E-05	1.941964	-2.97E-05	0.573518
0.55	5.07E-06	10.01839	-1.23E-05	2.556177	-2.96E-05	0.789675
0.6	5.25E-06	14.01524	-1.21E-05	3.714681	-2.95E-05	1.164437

Table A2 (contd.)

Crack Depth Ratio	Strain at 750mm	Percentage of difference	Strain at 900mm	Percentage of difference	Strain at 1100mm	Percentage of difference
uncracked	-4.70E-05		-6.42E-05		-5.20E-05	
0.05	-4.70E-05	0.039748	-6.45E-05	0.463055	-5.23E-05	0.655771
0.1	-4.70E-05	0.005101	-6.42E-05	0.0832	-5.22E-05	0.375028
0.15	-4.70E-05	0.1405	-6.43E-05	0.165154	-5.21E-05	0.177797
0.2	-4.73E-05	0.614714	-6.43E-05	0.228879	-5.20E-05	0.020204
0.25	-4.70E-05	0.180886	-6.42E-05	0.004363	-5.20E-05	0.11045
0.3	-4.70E-05	0.128597	-6.42E-05	0.032563	-5.21E-05	0.196269
0.35	-4.69E-05	0.292053	-6.45E-05	0.511044	-5.21E-05	0.191459
0.4	-4.70E-05	0.192789	-6.43E-05	0.167491	-5.20E-05	0.106986
0.45	-4.71E-05	0.095225	-6.43E-05	0.110466	-5.22E-05	0.46181
0.5	-4.70E-05	0.095013	-6.42E-05	0.00779	-5.20E-05	0.005388
0.55	-4.69E-05	0.260594	-6.42E-05	0.020878	-5.20E-05	0.01828
0.6	-4.69E-05	0.275048	-6.42E-05	0.025552	-5.20E-05	0.013854

Table A2 (contd.)

Crack Depth Ratio	Strain at 1180mm	Percentage of difference
uncracked	-3.11E-05	
0.05	-3.10E-05	0.270566
0.1	-3.11E-05	0.002249
0.15	-3.11E-05	0.06491
0.2	-3.11E-05	0.116324
0.25	-3.11E-05	0.113111
0.3	-3.12E-05	0.099936
0.35	-3.10E-05	0.244217
0.4	-3.12E-05	0.225258
0.45	-3.12E-05	0.109576
0.5	-3.11E-05	0.093831
0.55	-3.11E-05	0.037597
0.6	-3.11E-05	0.036633

Table A3: Strains for crack located at 600mm from fixed end

Crack Depth Ratio	Strain at 300mm	Percentage of difference	Strain at 450mm	Percentage of difference	Strain at 600mm	Percentage of difference
uncracked	4.61E-06		-1.26E-05		-2.99E-05	
0.05	4.61E-06	0.065138	-1.26E-05	0.215332	-3.01E-05	0.61066
0.1	4.62E-06	0.326557	-1.26E-05	0.125544	-3.06E-05	2.529973
0.15	4.66E-06	1.275396	-1.26E-05	0.162095	-3.22E-05	7.603637
0.2	4.69E-06	1.852298	-1.25E-05	0.564155	-3.44E-05	15.03629
0.25	4.75E-06	3.115969	-1.25E-05	0.959858	-3.77E-05	26.24232
0.3	4.83E-06	4.918328	-1.24E-05	1.483489	-4.20E-05	40.54916
0.35	4.95E-06	7.397902	-1.24E-05	1.663065	-4.82E-05	61.12656
0.4	5.09E-06	10.49954	-1.22E-05	2.73178	-5.56E-05	85.89258
0.45	5.27E-06	14.47229	-1.21E-05	4.08893	-6.53E-05	118.5206
0.5	5.59E-06	21.39903	-1.17E-05	7.171122	-8.13E-05	171.927
0.55	5.95E-06	29.16474	-1.16E-05	8.027683	-9.98E-05	233.8259
0.6	6.47E-06	40.39773	-1.10E-05	12.62594	-1.28E-04	329.3659

Table A3 (contd.)

Crack Depth Ratio	Strain at 750mm	Percentage of difference	Strain at 900mm	Percentage of difference	Strain at 1100mm	Percentage of difference
uncracked	-4.70E-05		-6.42E-05		-5.20E-05	
0.05	-4.70E-05	0.017855	-6.34E-05	1.215442	-5.23E-05	0.696756
0.1	-4.71E-05	0.011903	-6.43E-05	0.133214	-5.22E-05	0.412166
0.15	-4.70E-05	0.144964	-6.43E-05	0.140693	-5.21E-05	0.188188
0.2	-4.73E-05	0.574753	-6.43E-05	0.210026	-5.20E-05	0.009044
0.25	-4.70E-05	0.183011	-6.41E-05	0.066841	-5.22E-05	0.421402
0.3	-4.69E-05	0.312033	-6.42E-05	0.009972	-5.21E-05	0.162018
0.35	-4.68E-05	0.430002	-6.45E-05	0.443891	-5.21E-05	0.166829
0.4	-4.69E-05	0.403007	-6.42E-05	0.080084	-5.20E-05	0.101213
0.45	-4.71E-05	0.015092	-6.42E-05	0.02711	-5.22E-05	0.457769
0.5	-4.68E-05	0.627892	-6.34E-05	1.257354	-5.20E-05	0.071965
0.55	-4.66E-05	0.897839	-6.41E-05	0.186811	-5.20E-05	0.091208
0.6	-4.64E-05	1.297658	-6.40E-05	0.301485	-5.20E-05	0.118339

Table A3 (contd.)

Crack Depth Ratio	Strain at 1180mm	Percentage of difference
uncracked	-3.11E-05	
0.05	-3.10E-05	0.285348
0.1	-3.10E-05	0.251607
0.15	-3.12E-05	0.100257
0.2	-3.11E-05	0.103792
0.25	-3.11E-05	0.115039
0.3	-3.12E-05	0.102828
0.35	-3.10E-05	0.260926
0.4	-3.12E-05	0.218188
0.45	-3.11E-05	0.030527
0.5	-3.13E-05	0.481685
0.55	-3.13E-05	0.479757
0.6	-3.13E-05	0.467546

Table A4: Strains for crack located at 800mm from fixed end

Crack Depth Ratio	Strain at 300mm	Percentage of difference	Strain at 450mm	Percentage of difference	Strain at 600mm	Percentage of difference
uncracked	4.61E-06		-1.26E-05		-2.99E-05	
0.05	4.61E-06	0.131795	-1.26E-05	0.201824	-2.99E-05	0.09369
0.1	4.62E-06	0.350658	-1.26E-05	0.111242	-2.98E-05	0.309513
0.15	4.66E-06	1.132744	-1.26E-05	0.074691	-2.98E-05	0.400191
0.2	4.68E-06	1.6482	-1.25E-05	0.522836	-2.97E-05	0.514627
0.25	4.69E-06	1.825592	-1.25E-05	0.820011	-2.93E-05	2.004972
0.3	4.76E-06	3.366749	-1.23E-05	2.371039	-2.97E-05	0.700335
0.35	4.91E-06	6.653161	-1.24E-05	1.487461	-2.97E-05	0.757218
0.4	5.04E-06	9.435408	-1.23E-05	2.415536	-2.96E-05	1.053681
0.45	5.15E-06	11.80295	-1.20E-05	5.00588	-2.95E-05	1.438481
0.5	5.52E-06	19.85114	-1.18E-05	6.580746	-2.93E-05	1.825622
0.55	5.82E-06	26.38857	-1.15E-05	8.39796	-2.92E-05	2.410852
0.6	6.34E-06	37.58552	-1.13E-05	10.18736	-2.89E-05	3.415011

Table A4 (contd.)

Crack Depth Ratio	Strain at 750mm	Percentage of difference	Strain at 900mm	Percentage of difference	Strain at 1100mm	Percentage of difference
uncracked	-4.70E-05		-6.42E-05		-5.20E-05	
0.05	-4.71E-05	0.09225	-6.44E-05	0.348694	-5.23E-05	0.69233
0.1	-4.71E-05	0.064192	-6.43E-05	0.113583	-5.22E-05	0.39504
0.15	-4.70E-05	0.124983	-6.43E-05	0.147392	-5.21E-05	0.195307
0.2	-4.72E-05	0.430002	-6.43E-05	0.190862	-5.20E-05	0.03733
0.25	-4.71E-05	0.083747	-6.41E-05	0.051728	-5.20E-05	0.062922
0.3	-4.64E-05	1.424129	-6.35E-05	1.075217	-5.21E-05	0.183954
0.35	-4.70E-05	0.140712	-6.44E-05	0.288085	-5.20E-05	0.146047
0.4	-4.69E-05	0.260382	-6.42E-05	0.075254	-5.20E-05	0.078123
0.45	-4.70E-05	0.103728	-6.42E-05	0.039419	-5.22E-05	0.448533
0.5	-4.67E-05	0.736296	-6.41E-05	0.082421	-5.22E-05	0.529735
0.55	-4.66E-05	0.910805	-6.41E-05	0.129475	-5.23E-05	0.582073
0.6	-4.64E-05	1.307648	-6.40E-05	0.238539	-5.23E-05	0.585344

Table A4 (contd.)

Crack Depth Ratio	Strain at 1180mm	Percentage of difference
uncracked	-3.11E-05	
0.05	-3.10E-05	0.257392
0.1	-3.11E-05	0.133355
0.15	-3.10E-05	0.27378
0.2	-3.11E-05	0.153278
0.25	-3.11E-05	0.063304
0.3	-3.12E-05	0.104756
0.35	-3.10E-05	0.23297
0.4	-3.12E-05	0.237147
0.45	-3.10E-05	0.260926
0.5	-3.10E-05	0.230721
0.55	-3.11E-05	0.125
0.6	-3.10E-05	0.275386

Table A5: Strains for crack located at 950mm from fixed end

Crack Depth Ratio	Strain at 300mm	Percentage of difference	Strain at 450mm	Percentage of difference	Strain at 600mm	Percentage of difference
uncracked	4.61E-06		-1.26E-05		-2.99E-05	
0.05	4.61E-06	0.01433	-1.26E-05	0.167657	-2.99E-05	0.017065
0.1	4.62E-06	0.231022	-1.26E-05	0.005562	-2.98E-05	0.337954
0.15	4.63E-06	0.598832	-1.26E-05	0.079458	-2.98E-05	0.282409
0.2	4.63E-06	0.607734	-1.26E-05	0.202619	-2.98E-05	0.407218
0.25	4.66E-06	1.207869	-1.25E-05	0.414773	-2.98E-05	0.329924
0.3	4.68E-06	1.653845	-1.25E-05	0.436227	-2.99E-05	0.167639
0.35	4.73E-06	2.595085	-1.25E-05	0.294791	-2.98E-05	0.409895
0.4	4.77E-06	3.608193	-1.25E-05	0.712742	-2.97E-05	0.598949
0.45	4.83E-06	4.765038	-1.24E-05	1.238757	-2.97E-05	0.704016
0.5	4.94E-06	7.316263	-1.23E-05	1.989639	-2.97E-05	0.630402
0.55	5.04E-06	9.498809	-1.22E-05	2.786606	-2.95E-05	1.155402
0.6	5.15E-06	11.92019	-1.20E-05	4.866033	-2.94E-05	1.52481

Table A5 (contd.)

Crack Depth Ratio	Strain at 750mm	Percentage of difference	Strain at 900mm	Percentage of difference	Strain at 1100mm	Percentage of difference
uncracked	-4.70E-05		-6.42E-05		-5.20E-05	
0.05	-4.71E-05	0.053352	-6.45E-05	0.472559	-5.23E-05	0.559368
0.1	-4.70E-05	0.099264	-6.42E-05	0.018073	-5.21E-05	0.244375
0.15	-4.70E-05	0.061216	-6.43E-05	0.179956	-5.21E-05	0.183762
0.2	-4.70E-05	0.013179	-6.42E-05	0.009037	-5.20E-05	0.024053
0.25	-4.70E-05	0.159205	-6.43E-05	0.15565	-5.22E-05	0.431408
0.3	-4.70E-05	0.106491	-6.43E-05	0.189772	-5.20E-05	0.123919
0.35	-4.70E-05	0.113718	-6.46E-05	0.668252	-5.20E-05	0.130461
0.4	-4.70E-05	0.203842	-6.42E-05	0.052507	-5.20E-05	0.121418
0.45	-4.72E-05	0.278024	-6.42E-05	0.03677	-5.22E-05	0.474895
0.5	-4.69E-05	0.398331	-6.41E-05	0.066997	-5.20E-05	0.074467
0.55	-4.68E-05	0.451258	-6.41E-05	0.089744	-5.20E-05	0.114683
0.6	-4.68E-05	0.555623	-6.41E-05	0.133993	-5.20E-05	0.045604

Table A5 (contd.)

Crack Depth Ratio	Strain at 1180mm	Percentage of difference
uncracked	-3.11E-05	
0.05	-3.11E-05	0.177057
0.1	-3.11E-05	0.075836
0.15	-3.11E-05	0.032134
0.2	-3.10E-05	0.232327
0.25	-3.11E-05	0.007712
0.3	-3.12E-05	0.123394
0.35	-3.12E-05	0.146209
0.4	-3.12E-05	0.219795
0.45	-3.11E-05	0.018638
0.5	-3.13E-05	0.550773
0.55	-3.11E-05	0.006748
0.6	-3.13E-05	0.570053

Table A6: Strains for crack located at 1100mm from fixed end

Crack Depth Ratio	Strain at 300mm	Percentage of difference	Strain at 450mm	Percentage of difference	Strain at 600mm	Percentage of difference
uncracked	4.61E-06		-1.26E-05		-2.99E-05	
0.05	4.61E-06	0.056887	-1.26E-05	0.224867	-2.99E-05	0.084321
0.1	4.61E-06	0.049722	-1.26E-05	0.034962	-2.98E-05	0.228203
0.15	4.62E-06	0.210395	-1.26E-05	0.155738	-2.98E-05	0.374761
0.2	4.61E-06	0.144171	-1.26E-05	0.061978	-2.98E-05	0.312524
0.25	4.61E-06	0.137223	-1.26E-05	0.116009	-2.98E-05	0.211472
0.3	4.57E-06	0.835065	-1.26E-05	0.127133	-2.98E-05	0.332935
0.35	4.62E-06	0.248175	-1.26E-05	0.386962	-2.98E-05	0.194073
0.4	4.62E-06	0.204315	-1.26E-05	0.23917	-2.99E-05	0.031788
0.45	4.56E-06	0.9306	-1.26E-05	0.082637	-2.98E-05	0.276721
0.5	4.61E-06	0.187596	-1.26E-05	0.059594	-2.98E-05	0.239914
0.55	4.61E-06	0.138526	-1.26E-05	0.03814	-2.98E-05	0.348996
0.6	4.61E-06	0.145691	-1.26E-05	0.380606	-2.98E-05	0.210803

Table A6 (contd.)

Crack Depth Ratio	Strain at 750mm	Percentage of difference	Strain at 900mm	Percentage of difference	Strain at 1100mm	Percentage of difference
uncracked	-4.70E-05		-6.42E-05		-5.20E-05	
0.05	-4.71E-05	0.014879	-6.44E-05	0.343241	-5.23E-05	0.632295
0.1	-4.70E-05	0.069506	-6.42E-05	0.066529	-5.39E-05	3.682936
0.15	-4.70E-05	0.047613	-6.43E-05	0.141939	-5.63E-05	8.260053
0.2	-4.65E-05	1.165235	-6.45E-05	0.432985	-6.02E-05	15.87242
0.25	-4.70E-05	0.112442	-6.42E-05	0.009348	-6.62E-05	27.35783
0.3	-4.70E-05	0.171746	-6.42E-05	0.007167	-7.35E-05	41.51866
0.35	-4.70E-05	0.055477	-6.36E-05	0.954467	-8.32E-05	60.13077
0.4	-4.71E-05	0.193001	-6.42E-05	0.040354	-9.82E-05	88.97159
0.45	-4.73E-05	0.457634	-6.42E-05	0.011218	-1.18E-04	126.1042
0.5	-4.70E-05	0.075245	-6.42E-05	0.06762	-1.45E-04	179.6877
0.55	-4.70E-05	0.161968	-6.42E-05	0.099248	-1.81E-04	247.5738
0.6	-4.72E-05	0.383877	-6.42E-05	0.089744	-2.39E-04	360.065

Table A6 (contd.)

Crack Depth Ratio	Strain at 1180mm	Percentage of difference
uncracked	-3.11E-05	
0.05	-3.10E-05	0.300129
0.1	-3.11E-05	0.001607
0.15	-3.11E-05	0.070052
0.2	-3.11E-05	0.145245
0.25	-3.10E-05	0.29788
0.3	-3.11E-05	0.122751
0.35	-3.11E-05	0.166132
0.4	-3.12E-05	0.197623
0.45	-3.11E-05	0.032776
0.5	-3.12E-05	0.285669
0.55	-3.11E-05	0.043702
0.6	-3.12E-05	0.276029

Table A7: Strains for crack located at 1185mm from fixed end

Crack Depth Ratio	Strain at 300mm	Percentage of difference	Strain at 450mm	Percentage of difference	Strain at 600mm	Percentage of difference
uncracked	4.61E-06		-1.26E-05		-2.99E-05	
0.05	4.61E-06	0.181951	-1.26E-05	0.110447	-2.99E-05	0.015392
0.1	4.61E-06	0.051242	-1.26E-05	0.015892	-2.98E-05	0.241587
0.15	4.62E-06	0.340019	-1.26E-05	0.193084	-2.98E-05	0.317878
0.2	4.61E-06	0.085547	-1.26E-05	0.016686	-2.98E-05	0.347323
0.25	4.62E-06	0.242312	-1.26E-05	0.034167	-2.98E-05	0.242591
0.3	4.61E-06	0.167838	-1.26E-05	0.118393	-2.98E-05	0.325908
0.35	4.62E-06	0.244701	-1.26E-05	0.395703	-2.98E-05	0.177677
0.4	4.62E-06	0.253386	-1.26E-05	0.255856	-2.98E-05	0.302151
0.45	4.61E-06	0.083159	-1.26E-05	0.129517	-2.98E-05	0.293117
0.5	4.62E-06	0.395386	-1.26E-05	0.162095	-2.98E-05	0.275048
0.55	4.57E-06	0.804884	-1.26E-05	0.131901	-2.98E-05	0.261664
0.6	4.62E-06	0.389306	-1.26E-05	0.112036	-2.98E-05	0.280736

Table A7 (contd.)

Crack Depth Ratio	Strain at 750mm	Percentage of difference	Strain at 900mm	Percentage of difference	Strain at 1100mm	Percentage of difference
uncracked	-4.70E-05		-6.42E-05		-5.20E-05	
0.05	-4.71E-05	0.040386	-6.45E-05	0.460251	-5.23E-05	0.6398
0.1	-4.70E-05	0.102665	-6.42E-05	0.02602	-5.21E-05	0.191074
0.15	-4.70E-05	0.075883	-6.43E-05	0.22031	-5.21E-05	0.32192
0.2	-4.70E-05	0.014879	-6.45E-05	0.462432	-5.21E-05	0.231098
0.25	-4.70E-05	0.089274	-6.42E-05	0.010751	-5.20E-05	0.127383
0.3	-4.70E-05	0.162393	-6.42E-05	0.010439	-5.20E-05	0.147394
0.35	-4.70E-05	0.002763	-6.42E-05	0.032096	-5.23E-05	0.660773
0.4	-4.70E-05	0.059728	-6.36E-05	0.983136	-5.20E-05	0.035021
0.45	-4.73E-05	0.458485	-6.42E-05	0.02415	-5.21E-05	0.345588
0.5	-4.73E-05	0.571352	-6.42E-05	0.102832	-5.20E-05	0.143931
0.55	-4.73E-05	0.608549	-6.43E-05	0.127138	-5.20E-05	0.140082
0.6	-4.73E-05	0.608549	-6.42E-05	0.104857	-5.20E-05	0.103138

Table A7 (contd.)

Crack Depth Ratio	Strain at 1180mm	Percentage of difference
uncracked	-3.11E-05	
0.05	-3.12E-05	0.383677
0.1	-3.18E-05	2.067487
0.15	-3.26E-05	4.780864
0.2	-3.44E-05	10.53474
0.25	-3.63E-05	16.70957
0.3	-3.90E-05	25.21088
0.35	-4.28E-05	37.39279
0.4	-4.67E-05	50.15569
0.45	-5.28E-05	69.72998
0.5	-5.99E-05	92.42318
0.55	-6.82E-05	119.2433
0.6	-7.87E-05	153.0182

Table A8: Displacements for crack located at 200mm from fixed end (mm)

Crack Depth Ratio	Disp. at 300mm	% of Diff.	Disp. at 600mm	% of Diff.	Disp. at 900mm	% of Diff.	Disp. at 1300mm	% of Diff.
uncracked	0.1474		0.3474		0.2061		-0.9800	
0.05	0.1473	0.0292	0.3474	0.0069	0.2061	0.0034	-0.9799	0.0090
0.1	0.1473	0.0448	0.3474	0.0017	0.2061	0.0112	-0.9799	0.0068
0.15	0.1474	0.0387	0.3476	0.0671	0.2062	0.0471	-0.9801	0.0104
0.2	0.1475	0.0713	0.3478	0.1304	0.2062	0.0820	-0.9804	0.0487
0.25	0.1474	0.0387	0.3480	0.1871	0.2063	0.1262	-0.9807	0.0765
0.3	0.1473	0.0183	0.3483	0.2591	0.2064	0.1737	-0.9809	0.0946
0.35	0.1475	0.1317	0.3489	0.4344	0.2066	0.2761	-0.9815	0.1599
0.4	0.1475	0.1289	0.3495	0.6054	0.2069	0.3868	-0.9822	0.2297
0.45	0.1477	0.2287	0.3503	0.8512	0.2072	0.5411	-0.9831	0.3181
0.5	0.1478	0.2891	0.3515	1.1866	0.2076	0.7527	-0.9843	0.4377
0.55	0.1480	0.4058	0.3530	1.6069	0.2082	1.0220	-0.9858	0.5941
0.6	0.1482	0.5497	0.3550	2.1837	0.2089	1.3787	-0.9878	0.7963

Table A9: Displacements for crack located at 400mm from fixed end (mm)

Crack Depth Ratio	Disp. at 300mm	% of Diff.	Disp. at 600mm	% of Diff.	Disp. at 900mm	% of Diff.	Disp. at 1300mm	% of Diff.
uncracked	0.1474		0.3474		0.2061		-0.9800	
0.05	0.1473	0.0489	0.3473	0.0135	0.2061	0.0015	-0.9800	0.0014
0.1	0.1475	0.0699	0.3475	0.0294	0.2061	0.0180	-0.9800	0.0004
0.15	0.1474	0.0604	0.3475	0.0213	0.2061	0.0204	-0.9800	0.0011
0.2	0.1475	0.1276	0.3475	0.0429	0.2061	0.0112	-0.9800	0.0018
0.25	0.1477	0.2063	0.3476	0.0639	0.2061	0.0199	-0.9800	0.0009
0.3	0.1479	0.3570	0.3478	0.1264	0.2062	0.0485	-0.9802	0.0272
0.35	0.1482	0.5443	0.3480	0.1906	0.2062	0.0675	-0.9803	0.0379
0.4	0.1485	0.7553	0.3483	0.2671	0.2063	0.0927	-0.9805	0.0513
0.45	0.1490	1.0974	0.3487	0.3820	0.2063	0.1218	-0.9806	0.0653
0.5	0.1495	1.4767	0.3491	0.5072	0.2064	0.1558	-0.9808	0.0794
0.55	0.1503	1.9864	0.3497	0.6722	0.2065	0.1878	-0.9809	0.0961
0.6	0.1515	2.8259	0.3507	0.9658	0.2067	0.2863	-0.9815	0.1534

Table A10: Displacements for crack located at 600mm from fixed end (mm)

Crack Depth Ratio	Disp. at 300mm	% of Diff.	Disp. at 600mm	% of Diff.	Disp. at 900mm	% of Diff.	Disp. at 1300mm	% of Diff.
uncracked	0.1474		0.3474		0.2061		-0.9800	
0.05	0.1474	0.0217	0.3475	0.0311	0.2061	0.0218	-0.9801	0.0088
0.1	0.1475	0.1113	0.3478	0.1261	0.2062	0.0665	-0.9802	0.0251
0.15	0.1476	0.1921	0.3484	0.2977	0.2063	0.1242	-0.9806	0.0666
0.2	0.1479	0.3990	0.3494	0.5898	0.2066	0.2392	-0.9812	0.1244
0.25	0.1484	0.6786	0.3509	1.0208	0.2069	0.4217	-0.9822	0.2310
0.3	0.1489	1.0383	0.3529	1.5945	0.2074	0.6672	-0.9837	0.3851
0.35	0.1497	1.5968	0.3558	2.4126	0.2081	1.0026	-0.9856	0.5760
0.4	0.1507	2.2416	0.3593	3.4400	0.2090	1.4272	-0.9880	0.8239
0.45	0.1519	3.0905	0.3640	4.7817	0.2101	1.9663	-0.9911	1.1328
0.5	0.1539	4.4241	0.3711	6.8157	0.2118	2.8034	-0.9957	1.6061
0.55	0.1563	6.1030	0.3800	9.3852	0.2140	3.8603	-1.0017	2.2141
0.6	0.1599	8.5088	0.3929	13.1128	0.2172	5.3860	-1.0103	3.0978

Table A11: Displacements for crack located at 800mm from fixed end (mm)

Crack Depth Ratio	Disp. at 300mm	% of Diff.	Disp. at 600mm	% of Diff.	Disp. at 900mm	% of Diff.	Disp. at 1300mm	% of Diff.
uncracked	0.1474		0.3474		0.2061		-0.9800	
0.05	0.1474	0.0007	0.3475	0.0190	0.2061	0.0340	-0.9801	0.0106
0.1	0.1475	0.1052	0.3478	0.1203	0.2064	0.1529	-0.9808	0.0813
0.15	0.1476	0.1595	0.3483	0.2568	0.2068	0.3703	-0.9820	0.2077
0.2	0.1478	0.3346	0.3492	0.5147	0.2076	0.7289	-0.9841	0.4161
0.25	0.1482	0.5782	0.3505	0.9065	0.2087	1.2913	-0.9872	0.7366
0.3	0.1487	0.9331	0.3524	1.4465	0.2103	2.0537	-0.9916	1.1898
0.35	0.1494	1.4190	0.3549	2.1682	0.2103	2.0537	-0.9974	1.7823
0.4	0.1503	2.0088	0.3582	3.1023	0.2151	4.3927	-1.0049	2.5448
0.45	0.1515	2.7960	0.3624	4.3323	0.2187	6.1372	-1.0148	3.5570
0.5	0.1533	4.0427	0.3693	6.3016	0.2245	8.9503	-1.0307	5.1765
0.55	0.1555	5.5174	0.3771	8.5412	0.2310	12.1196	-1.0488	7.0214
0.6	0.1590	7.8899	0.3899	12.2486	0.2419	17.3896	-1.0787	10.0756

Table A12: Displacements for crack located at 950mm from fixed end (mm)

Crack Depth Ratio	Disp. at 300mm	% of Diff.	Disp. at 600mm	% of Diff.	Disp. at 900mm	% of Diff.	Disp. at 1300mm	% of Diff.
uncracked	0.1474		0.3474		0.2061		-0.9800	
0.05	0.1474	0.0244	0.3475	0.0225	0.2061	0.0364	-0.9802	0.0208
0.1	0.1475	0.0719	0.3476	0.0619	0.2063	0.1344	-0.9814	0.1418
0.15	0.1475	0.0767	0.3478	0.1051	0.2068	0.3295	-0.9837	0.3798
0.2	0.1475	0.1208	0.3480	0.1776	0.2073	0.6042	-0.9870	0.7155
0.25	0.1476	0.1832	0.3485	0.3166	0.2083	1.0822	-0.9925	1.2769
0.3	0.1479	0.3617	0.3492	0.5346	0.2097	1.7411	-1.0003	2.0723
0.35	0.1482	0.5443	0.3502	0.8092	0.2115	2.6462	-1.0108	3.1427
0.4	0.1484	0.7418	0.3513	1.1276	0.2138	3.7545	-1.0239	4.4816
0.45	0.1489	1.0166	0.3529	1.5752	0.2169	5.2487	-1.0413	6.2571
0.5	0.1494	1.3559	0.3551	2.2232	0.2217	7.6032	-1.0691	9.0909
0.55	0.1502	1.9314	0.3582	3.1046	0.2278	10.5231	-1.1031	12.5675
0.6	0.1514	2.7139	0.3624	4.3289	0.2363	14.6479	-1.1515	17.5034

Table A13: Displacements for crack located at 1100mm from fixed end (mm)

Crack Depth Ratio	Disp. at 300mm	% of Diff.	Disp. at 600mm	% of Diff.	Disp. at 900mm	% of Diff.	Disp. at 1300mm	% of Diff.
uncracked	0.1474		0.3474		0.2061		-0.9800	
0.05	0.1473	0.0034	0.3474	0.0055	0.2061	0.0126	-0.9801	0.0149
0.1	0.1474	0.0441	0.3475	0.0245	0.2061	0.0199	-0.9808	0.0816
0.15	0.1474	0.0407	0.3475	0.0213	0.2061	0.0180	-0.9820	0.2091
0.2	0.1473	0.0183	0.3474	0.0104	0.2061	0.0049	-0.9841	0.4217
0.25	0.1473	0.0156	0.3474	0.0037	0.2061	0.0044	-0.9872	0.7391
0.3	0.1474	0.0061	0.3474	0.0124	0.2061	0.0218	-0.9915	1.1748
0.35	0.1474	0.0339	0.3475	0.0204	0.2061	0.0175	-0.9971	1.7521
0.4	0.1474	0.0075	0.3474	0.0127	0.2061	0.0175	-1.0043	2.4866
0.45	0.1474	0.0014	0.3474	0.0069	0.2061	0.0136	-1.0153	3.6050
0.5	0.1473	0.0278	0.3473	0.0178	0.2061	0.0102	-1.0299	5.0918
0.55	0.1473	0.0129	0.3474	0.0078	0.2061	0.0044	-1.0494	7.0816
0.6	0.1473	0.0081	0.3474	0.0014	0.2061	0.0024	-1.0821	10.4236

Table A14: Displacements for crack located at 1185mm from fixed end (mm)

Crack Depth Ratio	Disp. at 300mm	% of Diff.	Disp. at 600mm	% of Diff.	Disp. at 900mm	% of Diff.	Disp. at 1300mm	% of Diff.
uncracked	0.1474		0.3474		0.2061		-0.9800	
0.05	0.1473	0.0434	0.3474	0.0101	0.2061	0.0092	-0.9801	0.0170
0.1	0.1474	0.0380	0.3475	0.0210	0.2061	0.0082	-0.9802	0.0282
0.15	0.1473	0.0054	0.3474	0.0020	0.2061	0.0010	-0.9807	0.0713
0.2	0.1474	0.0109	0.3474	0.0060	0.2061	0.0131	-0.9814	0.1435
0.25	0.1473	0.0258	0.3473	0.0167	0.2060	0.0146	-0.9822	0.2306
0.3	0.1474	0.0081	0.3474	0.0124	0.2061	0.0146	-0.9837	0.3835
0.35	0.1474	0.0319	0.3475	0.0207	0.2061	0.0189	-0.9858	0.5927
0.4	0.1474	0.0095	0.3474	0.0098	0.2061	0.0092	-0.9880	0.8203
0.45	0.1474	0.0061	0.3474	0.0092	0.2061	0.0155	-0.9916	1.1851
0.5	0.1472	0.0767	0.3473	0.0320	0.2060	0.0180	-0.9962	1.6528
0.55	0.1472	0.0740	0.3473	0.0273	0.2060	0.0131	-1.0020	2.2488
0.6	0.1473	0.0645	0.3473	0.0204	0.2061	0.0034	-1.0120	3.2703

Appendix B

This appendix includes computational values of strains and displacement at a number of locations for different crack locations for the setup used in Chapter 4 i.e. bending crack caused by the weight of the system. The results were used to identify the optimum measurement locations for strain and displacement measurement. For every case, only 0.6 crack depth ratios are tabulated here; as it can be seen from the results in appendix A that both strains and displacements will increase similarly, with respect to crack depth ratios, for any location.

Table A15: Strains for 0.6 Crack Depth Ratio at Different Locations for Bending Crack Under Self Weight

Crack Location	Strain at 50mm	Strain at 110mm	Strain at 170mm	Strain at 230mm	Strain at 290mm	Strain at 350mm	Strain at 410mm
uncracked	-5.49E-06	-6.73E-06	-7.36E-06	-7.29E-06	-6.48E-06	-4.97E-06	2.74E-06
75	-4.53E-06	-5.90E-06	-6.48E-06	-6.44E-06	-5.75E-06	-4.30E-06	2.15E-06
300	-4.67E-06	-6.03E-06	-6.60E-06	-6.55E-06	-7.71E-06	-4.39E-06	2.24E-06
500	-5.67E-06	-6.96E-06	-7.52E-06	-7.43E-06	-6.60E-06	-5.08E-06	2.87E-06
700	-6.59E-06	-7.83E-06	-8.32E-06	-8.15E-06	-7.29E-06	-5.70E-06	3.44E-06

Table A15 (contd.)

Crack Location	Strain at 470mm	Strain at 530mm	Strain at 590mm	Strain at 650mm	Strain at 710mm	Strain at 770mm	Strain at 830mm
uncracked	-1.59E-07	-3.77E-06	-8.09E-06	-1.31E-05	-1.88E-05	-2.51E-05	-3.23E-05
75	-6.91E-07	-4.24E-06	-8.50E-06	-1.35E-05	-1.91E-05	-2.54E-05	-3.25E-05
300	-6.14E-07	-4.17E-06	-8.43E-06	-1.34E-05	-1.90E-05	-2.53E-05	-3.24E-05
500	-5.48E-08	-3.67E-06	-8.00E-06	-1.30E-05	-1.87E-05	-2.51E-05	-3.23E-05
700	4.59E-07	-3.22E-06	-7.58E-06	-1.27E-05	-2.42E-05	-2.49E-05	-3.21E-05

Table A15 (contd.)

Crack Location	Strain at 890mm	Strain at 950mm	Strain at 1020mm	Strain at 1080mm	Strain at 1140mm	Strain at 1200mm
uncracked	-4.01E-05	-4.85E-05	-5.41E-05	-4.01E-05	-2.69E-05	-1.45E-05
75	-4.03E-05	-4.88E-05	-5.40E-05	-4.02E-05	-2.70E-05	-1.45E-05
300	-4.02E-05	-4.87E-05	-5.40E-05	-4.01E-05	-2.70E-05	-1.45E-05
500	-4.00E-05	-4.86E-05	-5.40E-05	-4.01E-05	-2.69E-05	-1.45E-05
700	-3.99E-05	-4.86E-05	-5.40E-05	-4.01E-05	-2.69E-05	-1.45E-05

Table A16: Displacements for 0.6 Crack Depth Ratio at Different Locations for Bending Crack Under Self Weight

Crack Location	Disp. at 50mm	Disp. at 110mm	Disp. at 170mm	Disp. at 230mm	Disp. at 290mm	Disp. at 350mm	Disp. at 410mm
uncracked	9.18E-04	4.38E-03	1.09E-02	2.08E-02	3.40E-02	5.01E-02	6.84E-02
75	7.08E-04	5.16E-03	1.35E-02	2.48E-02	3.90E-02	5.58E-02	7.46E-02
300	7.38E-04	3.63E-03	9.26E-03	1.79E-02	2.95E-02	4.65E-02	6.60E-02
500	9.58E-04	4.54E-03	1.13E-02	2.14E-02	3.50E-02	5.15E-02	7.03E-02
700	1.16E-03	5.38E-03	1.32E-02	2.47E-02	4.00E-02	5.85E-02	7.97E-02

Table A16 (contd.)

Crack Location	Disp. at 470mm	Disp. at 530mm	Disp. at 590mm	Disp. at 650mm	Disp. at 710mm	Disp. at 770mm	Disp. at 830mm
uncracked	8.80E-02	1.08E-01	1.25E-01	1.39E-01	1.47E-01	1.47E-01	1.35E-01
75	9.43E-02	1.14E-01	1.31E-01	1.45E-01	1.52E-01	1.51E-01	1.38E-01
300	8.65E-02	1.07E-01	1.25E-01	1.39E-01	1.48E-01	1.47E-01	1.35E-01
500	9.04E-02	1.10E-01	1.27E-01	1.41E-01	1.49E-01	1.48E-01	1.35E-01
700	1.02E-01	1.25E-01	1.47E-01	1.65E-01	1.75E-01	1.69E-01	1.51E-01

Table A16 (contd.)

Crack Location	Disp. at 890mm	Disp. at 950mm	Disp. at 1020mm	Disp. at 1080mm	Disp. at 1140mm	Disp. at 1200mm
uncracked	1.08E-01	6.25E-02	-1.87E-02	-1.14E-01	-2.28E-01	-3.54E-01
75	1.10E-01	6.35E-02	-1.89E-02	-1.15E-01	-2.30E-01	-3.58E-01
300	1.08E-01	6.26E-02	-1.87E-02	-1.14E-01	-2.28E-01	-3.54E-01
500	1.08E-01	6.27E-02	-1.87E-02	-1.14E-01	-2.28E-01	-3.55E-01
700	1.18E-01	6.76E-02	-1.99E-02	-1.21E-01	-2.40E-01	-3.72E-01

Appendix C

This appendix includes computational values of strains and displacement at a number of locations for different crack locations for the setup used in Chapter 5 i.e. circumferential helical crack caused by the weight of the system and the calculated torsional load. The results were used to identify the optimum measurement locations for strain and displacement measurement. For every case, only 0.6 crack depth ratios are tabulated here; as it can be seen from the results in appendix A that both strains and displacements will increase similarly, with respect to crack depth ratios, for any location.

Table A17: Strains for 0.6 Crack Depth Ratio at Different Location for Circumferential Helical Crack Under Self Weight & Torsional Load

Crack Location	Strain at 50mm	Strain at 110mm	Strain at 170mm	Strain at 230mm	Strain at 290mm	Strain at 350mm	Strain at 410mm
uncracked	-5.50E-06	-6.74E-06	-7.42E-06	-7.26E-06	-6.46E-06	-4.94E-06	2.73E-06
75	-4.15E-06	-5.54E-06	-6.26E-06	-6.20E-06	-5.55E-06	-4.17E-06	2.05E-06
300	-4.29E-06	-5.67E-06	-6.38E-06	-6.32E-06	-5.52E-06	-4.28E-06	2.13E-06
500	-5.53E-06	-6.85E-06	-7.48E-06	-7.39E-06	-6.62E-06	-5.07E-06	2.92E-06
700	-6.72E-06	-7.98E-06	-8.50E-06	-8.37E-06	-7.51E-06	-5.92E-06	3.66E-06

Table A17 (contd.)

Crack Location	Strain at 470mm	Strain at 530mm	Strain at 590mm	Strain at 650mm	Strain at 710mm	Strain at 770mm	Strain at 830mm
uncracked	-1.88E-07	-3.73E-06	-8.02E-06	-1.30E-05	-1.84E-05	-2.50E-05	-3.16E-05
75	-7.22E-07	-4.11E-06	-8.24E-06	-1.30E-05	-1.84E-05	-2.46E-05	-3.15E-05
300	-6.43E-07	-4.12E-06	-8.30E-06	-1.32E-05	-1.87E-05	-2.49E-05	-3.19E-05
500	6.14E-08	-3.44E-06	-7.75E-06	-1.25E-05	-1.83E-05	-2.44E-05	-3.12E-05

700	7.19E-07	-2.93E-06	-7.24E-06	-1.22E-05	-1.83E-05	-2.44E-05	-3.11E-05

Table A17 (contd.)

Crack Location	Strain at 890mm	Strain at 950mm	Strain at 1020mm	Strain at 1080mm	Strain at 1140mm	Strain at 1200mm
uncracked	-3.98E-05	-4.75E-05	-5.34E-05	-3.94E-05	-2.64E-05	-1.42E-05
75	-3.90E-05	-4.70E-05	-5.12E-05	-3.87E-05	-2.64E-05	-1.38E-05
300	-3.89E-05	-4.70E-05	-5.27E-05	-3.94E-05	-2.64E-05	-1.34E-05
500	-3.88E-05	-4.58E-05	-5.15E-05	-3.87E-05	-2.63E-05	-1.38E-05
700	-3.92E-05	-4.77E-05	-5.27E-05	-3.93E-05	-2.63E-05	-1.41E-05

Table A18: Displacements for 0.6 Crack Depth Ratio at Different Location for Circumferential Helical Crack Under Self Weight & Torsional Load

Crack Location	Disp. at 50mm	Disp. at 110mm	Disp. at 170mm	Disp. at 230mm	Disp. at 290mm	Disp. at 350mm	Disp. at 410mm
uncracked	9.46E-04	4.58E-03	1.10E-02	2.10E-02	3.42E-02	5.04E-02	6.77E-02
75	5.92E-04	5.52E-03	1.39E-02	2.60E-02	4.00E-02	5.68E-02	7.43E-02
300	6.27E-04	3.36E-03	8.60E-03	1.70E-02	2.81E-02	4.50E-02	6.34E-02
500	9.60E-04	4.50E-03	1.12E-02	2.12E-02	3.46E-02	5.15E-02	6.87E-02
700	1.27E-03	5.69E-03	1.37E-02	2.53E-02	4.14E-02	6.05E-02	8.12E-02

Table A18 (contd.)

Crack Location	Disp. at 470mm	Disp. at 530mm	Disp. at 590mm	Disp. at 650mm	Disp. at 710mm	Disp. at 770mm	Disp. at 830mm
uncracked	8.72E-02	1.07E-01	1.24E-01	1.38E-01	1.45E-01	1.45E-01	1.32E-01
75	9.38E-02	1.12E-01	1.29E-01	1.43E-01	1.50E-01	1.48E-01	1.35E-01
300	8.39E-02	1.04E-01	1.22E-01	1.37E-01	1.45E-01	1.45E-01	1.33E-01
500	8.85E-02	1.07E-01	1.25E-01	1.37E-01	1.46E-01	1.44E-01	1.32E-01
700	1.04E-01	1.29E-01	1.50E-01	1.69E-01	1.80E-01	1.72E-01	1.52E-01

Table A18 (contd.)

Crack Location	Disp. at 890mm	Disp. at 950mm	Disp. at 1020mm	Disp. at 1080mm	Disp. at 1140mm	Disp. at 1200mm
uncracked	1.06E-01	5.94E-02	-2.07E-02	-1.17E-01	-2.32E-01	-3.58E-01
75	1.07E-01	6.10E-02	-2.24E-02	-1.18E-01	-2.32E-01	-3.60E-01
300	1.05E-01	5.99E-02	-2.07E-02	-1.15E-01	-2.29E-01	-3.58E-01
500	1.05E-01	5.87E-02	-2.21E-02	-1.16E-01	-2.29E-01	-3.56E-01
700	1.19E-01	6.77E-02	-2.22E-02	-1.23E-01	-2.44E-01	-3.76E-01